

Optimization of Photocatalytic Processes: Catalyst Design, Kinetics and Reaction Engineering

Von der Naturwissenschaftlichen Fakultät
der Gottfried Wilhelm Leibniz Universität Hannover
zur Erlangung der Lehrbefugnis (*venia legendi*)

im Fachgebiet
Technische Chemie

angenommene

kumulative Habilitationsschrift

von

Dr. rer. nat. Jonathan Zacharias Bloh

geboren am 17.09.1983 in Neustadt am Rübenberge, Ortsteil Vesbeck

2021

“On the arid lands there will spring up industrial colonies without smoke and without smokestacks; forests of glass tubes will extend over the plains and glass buildings will rise everywhere; inside of these will take place the photochemical processes that hitherto have been the guarded secret of the plants, but that will have been mastered by human industry which will know how to make them bear even more abundant fruit than nature, for nature is not in a hurry and mankind is. And if in a distant future the supply of coal becomes completely exhausted, civilization will not be checked by that, for life and civilization will continue as long as the sun shines! If our black and nervous civilization, based on coal, shall be followed by a quieter civilization based on the utilization of solar energy, that will not be harmful to progress and to human happiness.”

— Giacomo Ciamician,
The Photochemistry of the Future, *Science*, 1912

Abstract

The use of light energy to drive chemical reactions has gained increasing interest for a variety of applications in the last decades. This habilitation thesis comprises a selected number of original papers from the author's own research in this field, particularly concerning semiconductor photocatalysis. Semiconductor photocatalysis has so far been explored for two main applications: The decontamination of air, water or surfaces from unwanted pollutants and the synthesis of value-added chemical products. While in principle the design criteria and required properties of photocatalysts and devices for these two applications are quite different, they also share a number of fundamental aspects.

A universally important aspect is the design of efficient photocatalyst materials, which on the one hand absorb the light energy and convert it efficiently to usable chemical potential energy and on the other hand exhibit good catalytic properties so that this energy can be effectively transferred to the target molecules. Modification with metals and metal ions is a very prominent and powerful tool to improve the catalyst properties. This procedure may improve the catalyst's activity and selectivity to certain products or even alter the spectrum of usable light. However, the induced properties are very sensitive to the concentration and location of the added metals. Therefore, a fundamental model was developed that is able to predict the optimal metal concentration for a given system with good precision.

Photocatalysis can be used to degrade and thereby remove harmful pollutants such as nitrogen oxides from the air. Of particular interest in the optimization of this application is the selectivity of the photocatalytic reaction. Unlike in chemical synthesis where unwanted side-products are mainly a nuisance for product isolation and purification, potentially toxic intermediates and side-products may pose severe risks in environmental applications where the population may be directly exposed to them. However, as shown herein, modification with metal ions as co-catalysts is a very effective way to engineer the selectivity and suppress the formation of side-products.

Being a light-driven process, the photocatalyst's activity is dynamic with respect to the locally absorbed photon flux, which due to its exponential decay often varies by several orders of magnitude throughout the studied system. This highly inhomogeneous distribution in catalyst activity adds another layer of complexity to the process and requires specific approaches to model the kinetics and optimize these processes. Herein, a new holistic approach for this problem is presented and evaluated on the basis of two exemplary cases. Furthermore, the integration of photocatalytic reactions into combined reaction cascades with traditional chemical or biocatalytic reaction steps is discussed and kinetically analyzed.

As a consequence of the exponential decay of light intensity, photocatalytic processes cannot be performed efficiently in traditional reactor types, particularly at larger scales. Herein, the fundamental challenges and basic design criteria for photoreactors are discussed. Also, a new concept for powering photocatalytic reactions based on internal illumination with wirelessly powered light sources is presented.

Contents

1	Introduction	1
2	Optimization of photocatalyst materials by modification with metals	5
2.1	Fundamental aspects of metal-ion doping and prediction of the optimal doping ratio	5
2.2	Refined model of the optimal doping ratio: surface grafting versus doping	6
2.3	Advantages of metal-grafted materials	8
3	Air pollutant degradation using photocatalysis	10
3.1	Mechanism of photocatalytic NO _x oxidation	10
3.2	Catalyst materials	12
3.3	Optimization of the selectivity and activity using metal co-catalysts	14
3.4	Photocatalytic ozone decomposition	18
3.5	Efficacy and limitations of the technology	20
4	Kinetic modeling and optimization of photocatalytic processes	21
4.1	Kinetic analysis of the photocatalytic reduction of molecular oxygen to hydrogen peroxide	21
4.2	The effect of sacrificial electron donors on the kinetics of photocatalytic reactions	25
4.3	A holistic approach for kinetic modeling of photocatalytic reactions	28
4.4	Applications of the new kinetic model	33
4.5	Modeling and optimization of photoenzymatic cascade reactions	36
5	Reactor concepts for efficient photocatalytic processes	40
5.1	General considerations	40
5.2	Suitable light sources	41
5.3	Energetic aspects and efficiency	42
5.4	Internal illumination with wireless light emitters	43
5.5	Future prospects	46
6	Publications	47
7	References	49
8	About the author	69
8.1	Curriculum Vitae	69
8.2	List of teaching activities	70
8.3	List of publications	71
8.3.1	Peer-reviewed articles	71
8.3.2	Other articles	73
8.3.3	Patents filed	73
9	Publication reprints	75
P1	Refined Model for the Optimal Metal Content in Semiconductor Photocatalysts	76

P2	Grafted iron(III) ions significantly enhance NO ₂ oxidation rate and selectivity of TiO ₂ for photocatalytic NOx abatement	84
P3	Photocatalytic NOx abatement: Why the selectivity matters	96
P4	On the underlying mechanisms of the low observed nitrate selectivity in photocatalytic NOx abatement and the importance of the oxygen reduction reaction	105
P5	Efficiency of Solar-Light-Driven TiO ₂ Photocatalysis at Different Latitudes and Seasons. Where and When Does TiO ₂ Really Work?	114
P6	Photogenerated Charge Carriers and Paramagnetic Species in (W,N)-Codoped TiO ₂ Photocatalysts under Visible-Light Irradiation: An EPR Study	117
P7	Adjusting Nitrogen Doping Level in Titanium Dioxide by Codoping with Tungsten: Properties and Band Structure of the Resulting Materials	124
P8	Properties and photochemistry of valence-induced-Ti ³⁺ enriched (Nb,N)-codoped anatase TiO ₂ semiconductors	136
P9	Improving the Selectivity of Photocatalytic NOx Abatement through Improved O ₂ Reduction Pathways Using Ti _{0.909} W _{0.091} O ₂ N _x Semiconductor Nanoparticles	141
P10	Band structure and charge carrier dynamics in (W,N)-codoped TiO ₂ resolved by electrochemical impedance spectroscopy combined with UV-vis and EPR spectroscopies	153
P11	Improved photocatalytic ozone abatement over transition metal-grafted titanium dioxide	159
P12	Cascading g-C ₃ N ₄ and Peroxygenases for Selective Oxyfunctionalization Reactions	169
P13	Selective Activation of C-H Bonds in a Cascade Process Combining Photochemistry and Biocatalysis	178
P14	Photoenzymatic Hydroxylation of Ethylbenzene Catalyzed by Unspecific Peroxygenase: Origin of Enzyme Inactivation and the Impact of Light Intensity and Temperature	183
P15	Modeling and Optimization of the Photocatalytic Reduction of Molecular Oxygen to Hydrogen Peroxide over Titanium Dioxide	191
P16	Kinetic effects and oxidation pathways of sacrificial electron donors on the example of the photocatalytic reduction of molecular oxygen to hydrogen peroxide over illuminated titanium dioxide	204
P17	Model-Based Analysis of the Photocatalytic HCl Oxidation Kinetics over TiO ₂ .	215
P18	Hydrogen peroxide driven biocatalysis	241
P19	A Holistic Approach to Model the Kinetics of Photocatalytic Reactions	259
P20	Kinetics and Optimization of the Photocatalytic Reduction of Nitrobenzene . .	272
P21	Hydrocarbon Synthesis via Photoenzymatic Decarboxylation of Carboxylic Acids	282
P22	Heterogeneous Photoredox Catalysis: Reactions, Materials, and Reaction Engineering	287
P23	Completely integrated wirelessly-powered photocatalyst-coated spheres as a novel means to perform heterogeneous photocatalytic reactions	297

1 Introduction

Driven by the need for action to combat climate change and resource scarcity, modern industry is currently facing what probably amounts to the greatest fundamental transformation since industrialization itself - the transition into a carbon-neutral circular economy. Towards this goal, fossil-based power generation, fuels and feedstocks need to be substituted by carbon-neutral alternatives and waste-streams completely recycled. The majority of concepts on how this can be achieved are largely reliant on the widespread exploitation of renewable energy sources. Great potential is also seen in the optimization of current processes to reduce the overall amount of required resources and to prevent waste in the first place rather than recycling it.

With an annual supply of approximately 1.5×10^{18} kWh at the Earth's surface, the Sun is by far the most powerful energy source available to mankind and could theoretically provide about ten thousand times as much energy as is presently consumed by the entire human society. This energy can not only be used to generate electricity or heat but also to directly induce chemical transformations and synthesize chemical products. This has long been exploited by Nature to create chemical energy in the well-known photosynthesis process that takes place in plants and phototrophic microorganisms. The global magnitude of photosynthesis is estimated at 130 TW and it thereby constitutes the greatest chemical process on Earth. However, natural photosynthesis is rather inefficient, typically less than one percent of the sunlight is converted to chemical energy. Also, with the exception of using custom-engineered organisms, a plethora of products is generated, from which only a fraction is actually desired. Therefore, there is increasing interest to utilize light also in specifically engineered industrial processes, often termed artificial photosynthesis, which efficiently create specific chemical products.

The inside cover of this thesis features a quote from photochemistry pioneer Giacomo Ciamician who already envisioned a solar-driven chemical industry more than a century ago.^[1] His vision is also quite compatible with the more modern principles of green chemistry.^[2,3] Photochemical processes enable the use of renewable energy either directly through sunlight or by employing artificial lighting which is powered by renewable power supplies such as photovoltaics or wind power. Additionally, the unique reactivity of photocatalysts which often involves highly reactive radicals, enables completely new reaction pathways with potential shortcuts in many production routes.^[4-12] **[P22]** The substitution of often toxic and hazardous high energy reagents and reduction in process steps helps to reduce both the costs and the environmental footprint of the production processes.

However, the prospects of light energy utilization are not just limited to the industry. Another one of the great challenges of our time which solar energy can contribute to solving is the supply of clean water and air to allow for healthy living conditions everywhere. Photocatalysis can be used to activate water and oxygen, forming highly oxidizing compounds which can decompose almost all known pollutants in the water, air or on surfaces. On the one hand, this can be utilized for waste-water treatment, offering an alternative or addition to traditional methods which is environmentally friendly, particularly when sunlight is employed.^[13-15] On the other hand, photocatalysts can be incorporated into construction materials so that once built, our buildings can passively remove pollutants such as nitrogen oxides from the air using only sunlight.^[16-19] **[P3]**

Several challenges in the implementation of photocatalysis have so far prevented this vision from becoming reality, these can best be illustrated by first considering how photocatalysis works.

The fundamental principle of photocatalysis is based on the property of semiconductors to absorb photons with energy matching or exceeding the so-called band gap, which is the energy difference between the electronically filled valence band and the empty conduction band.^[20,21] During this process, the photon energy is transferred to one of the electrons in the valence band, exciting it into the conduction band. The absorber can also be a molecule, in this case the excitation happens from the HOMO to the LUMO orbital. As a result of the excitation, also a positively charged “hole” is left behind in the valence band, where the electron used to be. Together, these two charge-carriers, electron and hole, are the basis of the photocatalyst’s reactivity. They are extremely reactive since in comparison to the ground state their reduction and oxidation potentials, respectively, are offset by the band gap energy (typically 2 to 3.5 eV).^[22]

Since the formed charge carriers present a short-lived high-energy state that can readily fall back to its ground state through recombination, the catalyst needs to realize the reactions faster than the lifetime of the charge carriers. However, before any reactions can take place, the charge carriers first have to diffuse to the surface of the particle and there be transferred to the target substrates.^[23] This also outlines one of the primary design criteria for efficient photocatalysts. To facilitate productive energy transfer at the surfaces, the materials not only need a good charge carrier mobility but also small dimensions, *e.g.*, nanoparticles, so that the diffusion path to the surface is kept as short as possible. In addition, doping may be employed to facilitate charge carrier separation through trapping.

Once the charge carriers make it to the surface, they should not linger and must be transferred to the target substrates as fast as possible, lest they recombine while waiting. This highlights that the employed materials need to have good catalytic properties as well, *i.e.*, fast electron transfer kinetics. Noteworthy, this task may also be “outsourced” by using co-catalysts anchored on the surface of the semiconductor particles.^[24–26] Extensive research in the last decades has succeeded in producing fundamental insight into this issue and also in the development of better materials. However, the majority of currently reported processes are still suffering from poor overall quantum efficiency, *i.e.*, are only transferring a small fraction of the light energy into the products.

The kinetics of the surface reaction are also strongly influenced by the reaction conditions, *e.g.*, temperature and substrate concentration.^[P15,P19,P20] Consequently, the effect of the reaction conditions and the kinetics should be known and optimized together with the catalyst in a holistic approach. Particularly for the application in the chemical industry a detailed investigation of the kinetics is required anyway to allow for knowledge-based process optimization and scale-up. However, detailed kinetic analysis and modeling has so far been done only in select few cases and with great effort.^[27–31] The majority of current models are either strongly simplified and thereby imprecise or very time-consuming and difficult to apply. The reason for this is the complexity of modeling the light distribution, which is, however, extremely important as a photocatalyst’s activity is dynamic with respect to the locally absorbed photon flux.

Finally, the application of these reactions in the chemical industry requires suitable photoreactors in which they can be realized. Since usually this cannot be done in current standard equipment, specific solutions need to be developed. This is not a trivial task since in addition to all of the challenges associated with traditional chemical reaction engineering, the light required by the reactions needs to be efficiently introduced into the reaction medium which can be quite difficult given light penetration depths of typically only a few millimeters.^[32,33]

The following chapters describe the author’s own contributions to overcome the abovementioned challenges and pave the road for a future solar-driven chemical industry. Throughout this thesis, to distinguish references to the author’s own work they are marked by bold blue citations which feature the prefix “P” (*e.g.* [P1]). A complete list of these references is compiled in chapter 6 while the citations to the general literature can be found in chapter 7.

The first part of this thesis (chapter 2) describes the author’s work on improving photocatalyst materials by modification with metals. Metal modification may be useful to facilitate charge separation through the formation of electron or hole traps. Metals situated on the surface may also act as (co-)catalysts and thereby increase the materials effectiveness. In both cases, it has been shown that there exists an optimal metal concentration to achieve the maximum effect. In order to facilitate the process of material optimization and enable a knowledge-based catalyst design, the author developed a fundamental model to predict the optimal metal concentration. This model is also helpful in understanding some of the observed effects of metal modification.

One of the major applications of photocatalysis at the present time is NO_x abatement to help clean the ambient air and reduce health risks associated with air pollution. This particular application and the author’s contributions to it are described in detail in chapter 3. The author conducted intensive research in this area with the aim of improving the catalyst materials with respect to a wider spectral response as well as higher activity and selectivity. In particular in the latter aspect also the fundamental mechanisms governing the selectivity were studied in detail in order to allow a knowledge-based design of better, more selective catalysts. As it turned out that metal-grafted materials are ideal for this, these works are also closely linked with those described in chapter 2. Furthermore, the often overlooked effect of photocatalysis on ozone, which is inadvertently linked to NO_x *via* the Leighton equilibrium, was studied as well. Here, it was found that given appropriate catalysts, photocatalytic ozone decomposition may contribute greatly to the overall air cleaning effect of the technology. Finally, the overall effect of the technology on real-world scenarios is discussed, which is not only dependent on the kinetics of the photocatalytic reaction but also strongly influenced by the geometry and weather conditions of the site.

On the contrary, this is not an issue when reactions are performed in controlled environments, for instance to synthesize value-added products in a chemical reactor. Here, the reaction efficiency is a direct function of the reaction kinetics which consequently should be well understood to implement optimal processes. This is one of the main research areas of the author and the corresponding works are illustrated in chapter 4. One reaction which was intensely studied is the photocatalytic reduction of molecular oxygen to hydrogen peroxide leading to a full understanding of the effect of different reaction conditions. Also, the effect of introducing easily oxidizable, so-called sacrificial reagents into the system was studied in detail, taking the whole reaction pathway and intermediate oxidation products into account. The studies of the photocatalytic hydrogen peroxide generation have been particularly useful in the design of photoenzymatic processes, where a semiconductor photocatalyst is coupled with a peroxygenase enzyme to achieve highly selective oxyfunctionalization reactions. For these reactions, knowledge of the kinetics is particularly important as both sides of the reaction system, generation and consumption of peroxide, need to be precisely tuned to each other. To facilitate the kinetic studies, a kinetic model was developed which presents a compromise between complex numerical solution of the light distribution in the reaction medium and the simple but inaccurate assumption of uniform distribution. This model does consider the light distribution but in a generalized abstracted form so that it is easier and faster to apply to a given system. Subsequently, the model was applied to number of photocatalytic reactions which could be described with excellent accuracy. Moreover, the fundamental parameters obtained from fitting the model gave further insight into the reactions and allowed a directed optimization of the reaction conditions reaching in one case even a record-high apparent quantum yield of 142 %.

Finally, as illustrated above, industrial application of photocatalytic processes require specifically optimized photoreactors. The authors own work in this area is summarized in chapter 5, which encompasses general design considerations for suitable photoreactors and the corresponding light sources. Also, the energetics of photocatalytic reactions are discussed with a strong argument

for studying photocatalytic reactions at higher process temperatures to allow for technically useful heat generation. As a possible solution to circumvent the limitation of small light penetration depths demanding small reactor dimensions, the use of delocalized wirelessly-powered internal illumination is presented and discussed. Finally, the author gives a personal opinion of the future prospects of photocatalysis in the chemical industry.

2 Optimization of photocatalyst materials by modification with metals

One of the major challenges complicating widespread application of semiconductor photocatalysis is the often observed poor quantum efficiency of the overall process. In this case, the majority of the absorbed light energy is not converted into chemical energy but instead falls victim to recombination. This is an unproductive process that occurs when electron and hole meet each other again in the semiconductor before reacting with adsorbed molecules and annihilates the photo-generated charge carriers, dissipating their energy as heat or re-emission of a photon.^[34]

To prevent recombination, the charge carriers have to be spatially separated from each other and the time-span between their generation and their reaction with adsorbed molecules must be kept as short as possible, to give them as little time and opportunity as possible to recombine. The latter can easily be arranged by reducing the size of the photocatalyst particles down to dimensions much smaller than the average diffusion length of the charge carriers. Better charge separation, however, is much harder to achieve. Traditional methods known from photovoltaics for instance rely on creating an intrinsic electric field inside the semiconductor to drive the electrons to one and the holes towards the opposite direction. This can be realized by electrically polarizing the semiconductor, by constructing a p-n-junction or by utilizing the space-charge-layer formed at the interface with the electrolyte. However, all of these mechanisms are not readily applicable when dealing with individual semiconductor particles with dimensions of only a couple nanometers. An alternative route is to modify the photocatalyst material with metals.^[P1]

This chapter describes the effect of metal addition to semiconductor photocatalyst materials with the aim of improving their activity through better charge separation and/or surface-bound catalytic properties. The author's own work in this area, focused in particular on understanding the effect of metal addition and predicting its optimal concentration, is published in the references [P1-P2](#).

2.1 Fundamental aspects of metal-ion doping and prediction of the optimal doping ratio

Doping the photocatalyst with metal ions has successfully been explored as a means to reduce recombination rates. Metal dopants in the semiconductor are thought to be able to capture the roaming charges inside the semiconductor, trapping them.^[35] These trapped charges reduce the amount of free charge carriers and thus their recombination rate. In 1994, Choi, Termin and Hoffmann published an extensive study on colloidal TiO₂ nanoparticles doped with a variety of transition metal ions.^[35] They found that almost irrespective of the metal used, the addition of 0.5 at.% of metal ions dramatically improved the photocatalytic activity. With a few exceptions, the procedure improved the material's quantum yield for both reduction and oxidation reactions. They attributed the observed improved activity to better charge separation. Since the doped metal ions induce additional localized states within the band gap they can act as electron or hole traps. This reduces the amount of free charge carriers and thereby the recombination rate. The longer charge carrier lifetime due to reduced recombination could be experimentally verified

using laser flash photolysis with transient absorption spectroscopy and correlated well with the increased photocatalytic activity.^[35]

In the wake of this study, there have been numerous publications on metal-doped semiconductors for photocatalytic applications utilizing the same principle. The common consensus amongst all of these studies is that metal-doping can enhance the intrinsic photocatalytic activity if applied in the correct dosage. Usually, an optimal doping ratio is observed, above which the activity decreases again. The decrease at higher doping ratios can be attributed to the appearance of recombination centers once the average distance between dopants becomes very small.^[35,36] Unfortunately, despite the high number of publications on the topic there is a profound lack of systematic studies so there is little insight into how the materials really work and what the optimum parameters for a given system are. In practically all cases, only a few different dopant concentrations were studied. Also, in many studies, fundamental data such as the particulate size are not stated so they cannot be properly evaluated. Moreover, virtually every study used their own non-standardized activity test, making a proper comparison almost impossible. Even if the same host material and dopant is employed, the observed optimal doping ratios vary wildly between the different studies. Many researchers report a rather high optimal doping ratio of around 0.5 at.% while others find that their optimum is orders of magnitude lower in the range of 0.001 to 0.1 at.%.^[35-39] Analysis of this controversy suggested that the optimal doping ratio might be dependent on the particulate size.^[40]

Several years ago we proposed a model that attempts to explain and predict this size dependency of the optimal doping ratio.^[41] The model is based on the simple assumption that any particle that lacks at least one dopant atom cannot participate from any positive effect the doping might cause.^[41] Under this assumption, for any given particle size the minimum doping level necessary to guarantee at least one dopant per particle can be calculated under the conditions of homogeneous distribution of the dopants and spherical particle shape.^[41] Due to the drastically reduced number of atoms per particle, the minimum doping level is exponentially higher for smaller sized particles.

When analyzing a set of 14 different data set from various literature sources, the respective calculated minimum doping level corresponds very well with the experimentally observed optimal doping ratios, *i.e.*, it seems best to add just enough dopants to guarantee at least one dopant per particle, but no more.^[35-38,40-47] However, upon further analysis it was found that the optimal number of dopants per particle increased linearly with the particle size, larger photocatalysts seem to favor more dopants per particle. Even though the precision of this first model was limited due to the small number of used data points it allowed a good first indication of the optimal doping ratio for a given material, significantly reducing the amount of experiments required for optimization.^[41]

2.2 Refined model of the optimal doping ratio: surface grafting versus doping

As described above, the optimal number of doped atoms appears to increase with the particle size, *i.e.*, the optimal doping ratio shows a second-order dependence on the particle size. This suggests a surface-based effect rather than a bulk one which was the basis for the original model, since the latter would incur a third-order dependency. Also, there is good reason to assume that surface metal dopants are more effective than bulk dopants as charge carrier traps since they can release their trapped charges directly onto adsorbed reactants. Charges trapped by bulk dopants, on the other hand, first have to be de-trapped and brought to the surface before they can react.^[P1] Surface-bound metal centers have also frequently been reported to enhance both

charge transfer and multi-electron reactions. In particular, the oxygen reduction reaction (ORR) which is very important in environmental applications is enhanced by many metal ions on the photocatalyst surface by allowing multi-electron transfer reactions with more favorable redox potentials.^[48–51]

For these reasons, the original model was re-evaluated under the assumption that only dopants located at the surface of the photocatalyst particles contribute to the activity enhancement. Using a simple core-shell model, the fraction of dopants located at the surface can be calculated by assuming uniform distribution and by approximating the surface layer thickness to be equal to the nearest neighbor distance.^[P1] Interestingly, in this calculation the optimal doping ratio of all data sets used in the original model falls between the narrow corridor of 1 to 10 surface dopants per particle with a weighted 3, now irrespective of the particle size. Coincidentally, this equals 95 % of all particles having at least one dopant at the surface, so basically just enough to guarantee good coverage.^[P1]

In order to substantiate this theory and also address the second problem of the original model, the limited database, the number of data points used was drastically increased on the one hand by including more studies^[52–58] and on the other hand by also evaluating the whole dataset in each report instead of just the value of the optimal doping ratio. The latter was accomplished by normalizing the datasets and fitting them to an empirical function.^[59]^[P1] Altogether, this extended database amounts to a total of 177 data points from 29 data sets taken from 17 independent sources.^[P1]

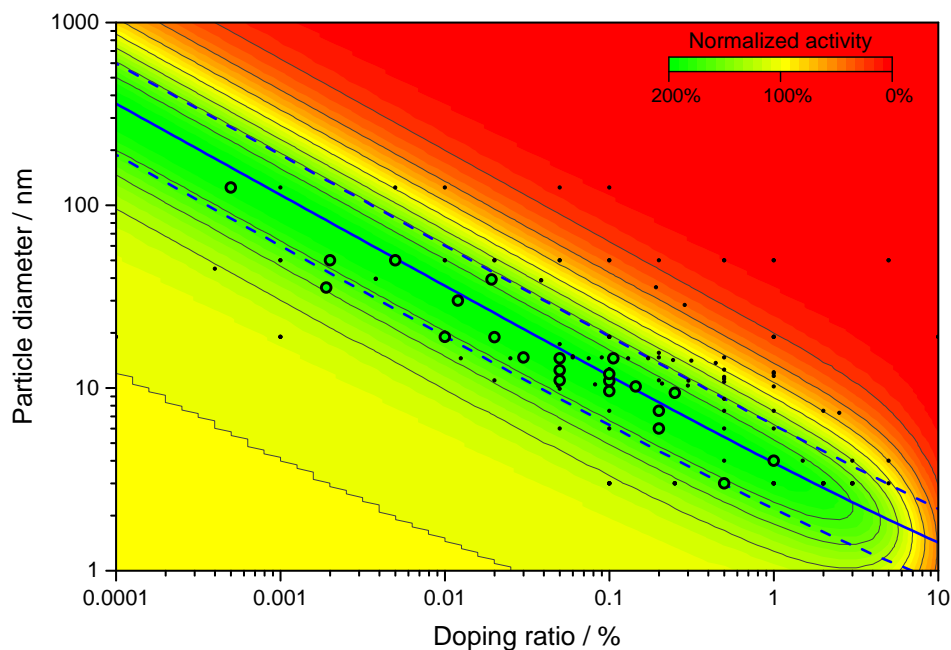


Figure 2.1: The relative normalized activity data as a function of doping ratio and particle size as calculated by the refined model. All data points are plotted as small black dots with their respective optimal doping ratio marked by a large black circle. The solid and slashed blue lines represents the calculated optimal doping ratio at 3.54 and the corridor where there are between 1 and 10 surface dopants present per particle, respectively.^[P1]

In the next step, a global optimization over all data sets was performed to calculate the optimum number of surface dopants per particle which considered not just the maxima in activity but also all the other data points given. The optimization yielded a best fit for 3.54 as the ideal number of surface dopants. With this parameter it is possible to calculate a three-dimensional matrix for the relative photocatalytic activity spanning the whole parameter-space of both,

doping ratio and particle size. The resulting plot along with the points used to calculate the parameters can be seen in Figure 2.1. The plot fits the used data sets very well and almost all experimentally determined optimal doping ratios fall within the corridor of 1 to 10 dopant atoms at the surface per particle, most of them near the calculated optimal line at 3.54. [P1]

Surprisingly, this much more complicated approach yielded only a marginally different result from the previous simple approach. However, it is substantiated by a much larger database and allows predicting the optimal doping ratio with increased certainty for a given material and particle size. Also, this refined fundamental model fits the observed behavior much better than in the original version and is in line with the emerging theory that metal grafting is superior to metal doping in terms of activity increase. [P1] Again, the calculated optimum of 3.54 dopant atoms present on the surface of each particle is again just about enough to guarantee every particle (>97%) has at least one. The doping ratio necessary to achieve this can be calculated with the new model, eqn. 2.1, using $n_{d,s,opt} = 3.54$, the molecular mass M of the material, the particle size d and the thickness of the surface layer δ . [P1]

$$r_{d,opt}(d) = \frac{n_{d,s,opt} \cdot M}{\pi \cdot N_A \cdot \rho \cdot (\delta d^2 - 2\delta^2 d + \frac{4}{3}\delta^3)} \quad (2.1)$$

The degree of correlation with the model is remarkable given the number of other parameters involved, *e.g.*, different materials, dopants, synthesis methods and activity tests. This suggests that indeed the doping ratio-size-activity relationship is predominantly governed by the number of surface dopants and all the other parameters only seem to play the minor role of fine-tuning the optimal doping ratio within the order of magnitude already set by the former effect. [P1]

2.3 Advantages of metal-grafted materials

As shown in the previous section, it appears as if doped metal ions situated on the surface of the particle are solely responsible for the positive effect on the photocatalytic activity achieved by doping. These serve not only to efficiently extract the charges from the photocatalyst but also serve as co-catalysts to enhance the charge transfer rate to the target substrates. Dopants located in the bulk, on the other hand, only serve as recombination centers once their concentration reaches a critical level and cluster formation starts to become an issue and should therefore be avoided. [36,41] [P1] Other authors have also observed the beneficial effect of surface versus bulk doping. [60–64] If that is indeed the case, is it possible to selectively dope the surface of the particle to achieve the same effect? That way, the detrimental impact of bulk dopants could be avoided and also much less mass of the doping element would be required.

A process resembling selective surface doping has been explored by Hashimoto *et al.* since 2008. [51] This procedure is described as “grafting” and involves the adsorption of metal-ions onto the surface of the semiconductor photocatalyst. Among other effects such as visible light sensitization, these metal-grafted materials exhibit enhanced intrinsic photocatalytic activity. The latter is attributed to better charge separation and improved oxygen reduction properties, both of which are observed for the corresponding metal-doped photocatalysts, as well. [P1]

This raises the question whether metal ion grafting actually produces the same result as surface doping, *i.e.*, whether the grafted metal ions are chemically identical to doped metal ions that happen to be located at the surface. In fact, Co(II) ions are reported to adsorb on rutile “at sites corresponding to the Ti-equivalent positions in an extension of the rutile structure” [65], *i.e.*, they are acting as if they were dopants in the host material, and there is good reason to assume a similar mechanism for other metals such as Fe(III) or Cu(II). [51]

At the moment there is not enough data available yet to offer a definite conclusion about this issue. Also, while some reports tentatively suggest an optimal metal-to-semiconductor concentration ratio for metal-grafted semiconductors there seems to be only little information about its position and whether or not there is a size-dependency as well. [48,49,63,66–68] Further studies will be necessary to elucidate whether this model is readily applicable to surface grafting and where the optimal loading is for those materials. Presumably, the absence of detrimental bulk dopants will in this case allow for more flexibility, potentially leading to higher numbers of grafted ions per particle at the optimum. An indication of this can be seen in our studies with iron-grafted TiO_2 for NO_x abatement, see section 3.3.

3 Air pollutant degradation using photocatalysis

The air we breathe is one of our most precious resources. However, even in modern industrialized countries, it is often contaminated with many different harmful substances such as ozone, volatile organic compounds (VOCs) and nitrogen oxides (NO_x) which present a hazard to our health and the environment. Nitrogen dioxide (NO₂) in particular has been the focus of new environmental legislation, such as the directive 2008/50/EC of the European Union, aimed at minimizing its emissions. However, the imposed limits are frequently exceeded in many European cities.^[69,70] Some sampling stations even register concentrations as high as 80 µg m⁻³ NO₂, twice the allowed value.^[71] This has also been made an issue of strong public interest since the revelation of defeat devices in diesel cars in 2017. The chosen actions to achieve the target values, namely low emission zones, forbidden areas for heavy vehicles or more strict emission values for vehicles have had only negligible effects on the concentration of NO₂ in recent years.^[69,72] Although extremely difficult to quantify, epidemiological studies estimate the number of premature deaths as a result of air pollution caused by land-based traffic in the 6 to 7 digit range per year.^[73] For instance, the 2017 Air Quality in Europe Report of the European Environmental Agency attributes an annual 78.000 to 229.000 premature deaths in the EU-28 as a result of elevated NO₂ levels.^[74]

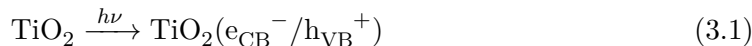
The majority of the NO_x emissions are generated through high temperature processes of anthropogenic nature, *i.e.* combustion engines, gas- or oil based heating systems and industrial furnaces.^[75] Many technologies have been developed to either reduce the formation of or treat the air pollutants directly at the emission source, this is typically achieved using a three-way catalyst in petrol-powered cars or using selective catalytic reduction (SCR) in diesel-powered vehicles. However, this direct reduction at the emission source appears more difficult than anticipated, in particular due to the dramatically dynamic load and environmental conditions.^[76] Additionally, there are many emission sources such as residential or commercial heating, gas-fired stoves or ships which have no or only limited exhaust treatment. To really achieve widespread clean air, every single one of these emission sources needs to feature an efficient treatment system. Since this is really difficult to accomplish, at least in sensible time-spans, alternative measures which enable to actively reduce the pollutant concentration in the ambient air, *i.e.* immission rather than emission reduction, are very appealing. One of the technologies which can achieve this is semiconductor photocatalysis.

This chapter is devoted to the use of semiconductor photocatalysis to combat NO_x-based air pollution. The author has focused his research in this area at optimizing the employed photocatalyst materials with respect to their spectral response, activity and selectivity. The following pages present a summary of the publications [P2-P11](#), which are described and put into context.

3.1 Mechanism of photocatalytic NO_x oxidation

The basic principle of photocatalysis has already been outlined in the introduction. After the photocatalyst (here exemplary TiO₂) is excited with photons whose energy exceeds the band gap, electron-hole pairs are created, eqn. 3.1. Once the charges diffuse to the catalyst surface

they can react with adsorbed molecules. Under environmental conditions, the usual electron acceptor is molecular oxygen and the electron donor is water. The products of oxygen reduction are superoxide radicals and, after subsequent protonation, hydroperoxyl radicals (eqns. 3.2-3.3). Water, on the other hand, is oxidized to the strongly oxidizing hydroxyl radicals (eqn. 3.4).



Interestingly, due to this mechanism, both the oxidation and the reduction reaction yield strongly oxidizing reactive oxygen species (ROS). No oxidant other than the ubiquitous molecular oxygen is required. These highly reactive species subsequently react with both NO and NO₂ and oxidize them to nitrate. NO can be oxidized to NO₂ either in a two-step process *via* nitrous acid (HONO) with hydroxyl radicals, eqns. 3.5-3.6, or with hydroperoxyl radicals which yields peroxyxynitrous acid (HOONO), eqn. 3.7. This intermediate is highly unstable and quickly decomposes to form a hydroxyl radical and NO₂ (eqn. 3.8) or isomerizes to nitric acid (eqn. 3.9).^[77] It has been suggested that the surface pH of the catalyst plays an important role in this reaction, as the deprotonated form, peroxyxynitrite (OONO⁻) is much more stable so a higher pH might lead to less NO₂ release through this pathway.^[78] As the NO oxidation rate steadily decreases with increasing humidity while the NO₂ oxidation rate has a maximum at about 10% humidity, it has been suggested that the main oxidation pathway for NO is through hydroperoxyl radicals (eqn. 3.7) rather than hydroxyl radicals (eqn. 3.5).^[79] NO₂ on the other hand is directly further oxidized with a hydroxyl radicals, forming nitrate or nitric acid, eqn. 3.10.^[80,81] **[P3]**



The mechanism of photocatalytic NOx oxidation is summarized in Figure 3.1. The nitrate formed by the NOx oxidation remains adsorbed on the photocatalyst as nitrate or can diffuse to deeper layers of the material or other nearby adsorbents in the matrix. The maximum attainable nitrate surface coverage is about 2 molecules/nm².^[82] This nitrate can later be readily desorbed either by artificial washing or by rainfall. This is not a problem in terms of nitrate pollution in the ground water, as the natural mineralization pathway for NOx would also eventually lead to nitrate, so no higher concentrations are formed.^[75] However, the natural mineralization pathway is much slower, leading to longer exposure times of the population and the environment to the toxic NOx gases and the formation of particulate matter, *e.g.* ammonium nitrate.^[75]

However, it should be noted that the nitrate is not necessarily a non-reactive end-product of the reaction since it has been suggested that both oxidative and reductive re-nitrication can take place. In these reactions, the nitrate is converted back into NO and NO₂.^[83] **[P4]** As both of these pathways are strongly dependent on the amount of adsorbed nitrate, a high nitrate surface coverage should be avoided in practice.

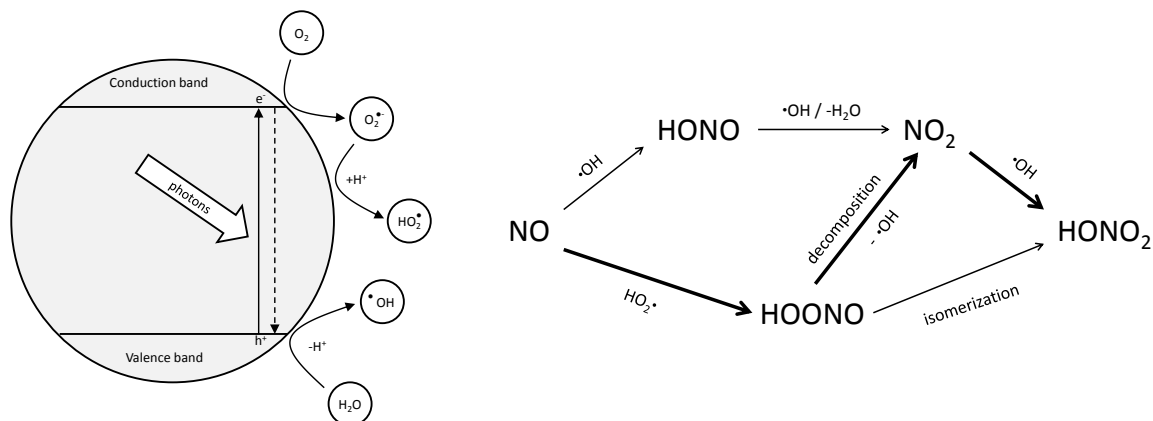


Figure 3.1: Left: The typical primary processes occurring at the semiconductor particles that lead to the generation of reactive oxygen species (ROS). Right: The major reaction pathways of NO/NO₂ to nitric acid (HONO₂) over illuminated titanium dioxide surfaces with the intermediate steps. The predominant pathway is highlighted with bold arrows.

The photocatalyst can either be incorporated into building materials such as concrete, roof tiles, paving stones or facade paints so that the corresponding building surfaces passively clean the ambient air using sunlight. Alternatively, dedicated air-cleaning devices using artificial lighting can be employed, for instance in ventilation systems.

3.2 Catalyst materials

The most widely used material for this application is titanium dioxide (TiO₂), mostly in its anatase modification or as a mixture of anatase and rutile. This material is preferred since it is industrially produced in large quantities, available at affordable prices, chemically inert, non-toxic and readily compatible with a variety of building material matrices. Other materials such as zinc oxide (ZnO) have also been explored but found inferior due to lower chemical compatibility and toxicity issues.^[36,39,84,85] With a bandgap of 3.0 to 3.2 eV, TiO₂ does not absorb visible light and if made as sufficiently small particles or films it is optically transparent, which is important for some applications. However, this also means that the material can only be excited using ultraviolet light.

The sunlight only contains a small fraction (<5%) of ultraviolet light, which is further diminished at morning or evening hours or in the winter months, particularly at higher latitudes.^[P5] To achieve a more robust system that works under all conditions, it is therefore desirable to use photocatalyst materials which can also utilize part of the visible light spectrum.

The most obvious option to achieve this would be to use a photocatalyst material which can intrinsically absorb visible light. Here, however, the challenge is that many other suitable oxidic materials such as hematite (Fe₂O₃) or tungsten oxide (WO₃) are not reducing enough, *i.e.* have a too low conduction band potential, to reduce molecular oxygen *via* the one-electron reaction. Nonetheless, if combined with an oxygen reduction co-catalysts these materials can show some activity.^[86] Another option is graphitic carbon nitride (C₃N₄), which can absorb visible light up to approximately 460 nm and is even more reducing than TiO₂.^[87–91] However, little is known about the long-time stability and performance of these materials as well as potential negative interactions with the building material matrices. Therefore, research efforts have mostly been focused on modifying the approved above-mentioned materials TiO₂ and ZnO through doping to achieve visible light sensitivity.^[39,84,92,93]

One of the most promising approaches in this area is nitrogen doping.^[94–97] This is achieved by mixing the titanium dioxide precursor with ammonium compounds prior to calcination. Some of the nitrogen is then incorporated into the titanium dioxide lattice.^[98–100] It has been shown through spectroscopy, that nitrogen does not directly replace oxygen in the lattice but rather occupies interstitial positions, where it is closely associated with a lattice oxygen, effectively forming a $[\text{N}_i\text{O}]^{3-}$ adduct located on a lattice oxygen position.^[101] ^[P6] Since this has three negative charges versus two of the oxygen, this constitutes p-type doping, with additional undesired side-effects such as reduced donor density.^[P7] The 2p orbitals of the nitrogen dopants create additional acceptor levels which are located slightly above the valence band of the material.^[97] ^[P7] Consequently, the transition from the acceptor levels to the conduction band is smaller than the band gap and allows for visible light absorption, usually in the region of 400 to 500 nm.^[P7]

The amount of nitrogen that can be incorporated by these low-temperature solution-based methods is limited. However, if an additional n-dopant is employed to compensate for the excess charge of the nitrogen, much higher levels of doping can be achieved. Using this strategy and partially substituting Ti(IV) in the lattice by Nb(V) or W(VI), we were successful in producing materials which had a much higher degree of nitrogen-doping and visible light absorption than without compensating dopants (Figure 3.2a).^[P7,P8] Furthermore, we could show that for the W/N-system the amount of nitrogen doping can be precisely controlled by the amount of added tungsten (Figure 3.2b).^[P7] Theoretical calculations predict that in these systems, the nitrogen dopants are preferentially located in close vicinity to the cation dopant.^[102] We could experimentally validate this *via* EPR spectroscopy, showing that the nitrogen dopants exhibit a close-range electronic coupling to the tungsten dopants.^[P6]

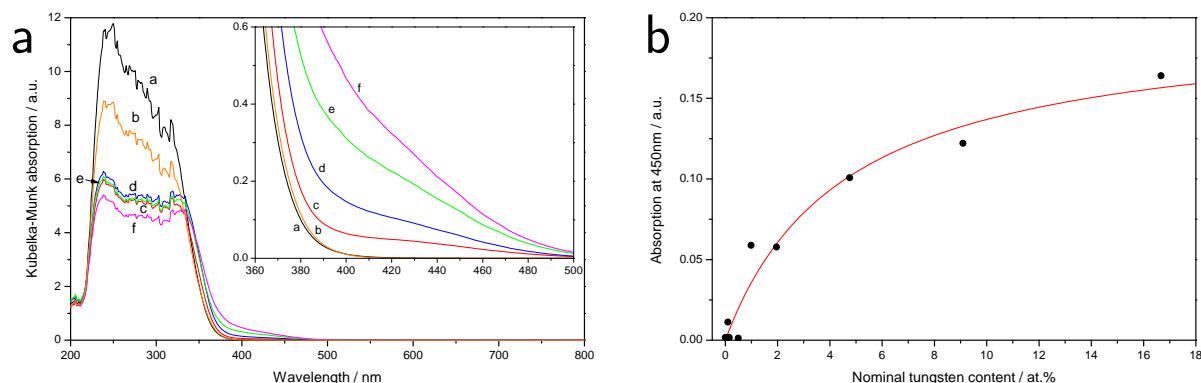


Figure 3.2: Left: UV-vis diffuse reflectance spectra of different W/N-codoped TiO_2 samples. The inset shows a magnified version of the area from 360 to 500 nm. Displayed are an undoped control (a), a purely W- (b) or N-doped control (c) and W/N-codoped samples with increasing W-content (d-f). Right: Amount of doped nitrogen, estimated by the absorption at 450 nm, in relation to the nominal tungsten content.^[P7]

Quite interestingly, it could be shown that these materials also exhibit the ability to store the photo-generated electrons for prolonged periods and thereby exhibit photocatalytic activity “in the dark”. This was attributed to trapping of the conduction band electrons as W(V) which appears to be quite stable and only slowly reacts with molecular oxygen to discharge the stored electrons.^[P9]

As expected, these materials were also photocatalytically active under visible light illumination.^[P6] Unfortunately, careful evaluation revealed that the visible light activity is accompanied by a decrease of the intrinsic activity under ultraviolet light illumination.^[P3] The latter was attributed to the slightly lowered conduction band edge of the nitrogen doped materials which makes the already challenging reductive activation of molecular oxygen even more difficult.^[P7] This means that under daylight conditions, the net positive effect of these materials is only small

as the larger number of usable photons is mostly compensated by the reduced intrinsic activity. However, for applications which are purely reliant on the use of visible light such as indoor wall paints these materials are still an interesting option.

We also discovered that these materials show an increased selectivity towards nitrate in comparison to undoped TiO_2 (*vide infra*). While the pristine material only shows a selectivity of less than 30%, this is increased to more than 90%.^[P3] However, control experiments showed that this effect is not associated with the nitrogen doping and is purely the result of tungsten doping.^[P3] Intrigued by this effect we wanted to find out what the underlying mechanisms are that govern the selectivity and if this knowledge could be used to custom-tailor more selective catalysts.

3.3 Optimization of the selectivity and activity using metal co-catalysts

As mentioned in the description of the reaction mechanism (Figure 3.1), during the oxidation of nitrogen monoxide to nitrate it passes through two intermediate species, namely nitrous acid and nitrogen dioxide. These two compounds are both much more harmful than nitrogen monoxide itself.^[103–105] The generation and release of these toxic intermediates would be the exact opposite of what the technology strives to achieve and must therefore be absolutely minimized.^[P3] This effect can be expressed as the selectivity to nitrate (S , eqn. 3.11), where a high value is desirable as it corresponds to a low fraction of by-products.

$$S = \frac{\Delta\text{NO}_x}{\Delta\text{NO}} \quad (3.11)$$

Unfortunately, most of the currently employed photocatalyst materials show rather low selectivities of well below 50%, indicating that NO_2 rather than nitrate is actually the main product.^[P3] This is illustrated exemplary for the popular material Aeroxide[®] P25 (Evonik) measured under standardized ISO 22197-1 conditions (Figure 3.3a).^[106] ^[P4] A detailed investigation revealed that the low selectivity appears to be an intrinsic property of the employed base material and that anatase is more selective than rutile (Figure 3.3b).^[P3]

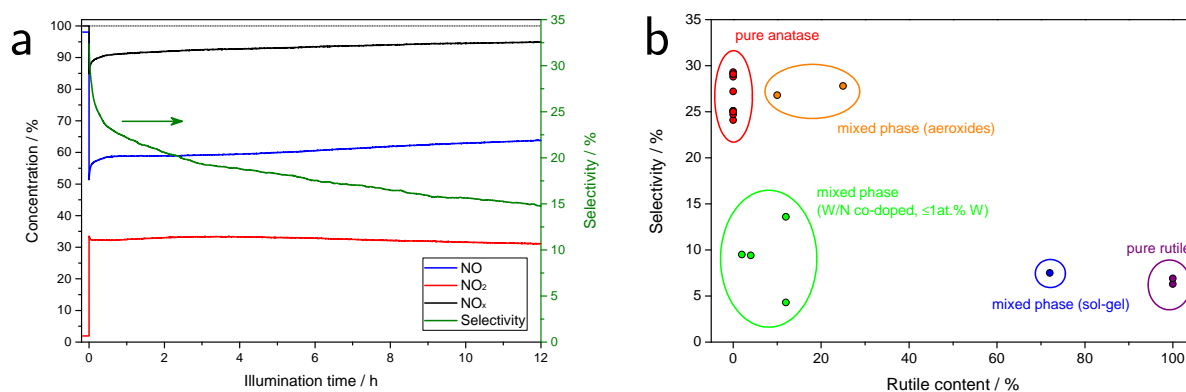


Figure 3.3: Left: A representative experiment for the photocatalytic oxidation of nitric oxide (NO) according to ISO 22197-1 using Aeroxide[®] P25 powder. Plotted are the relative concentrations of NO (blue), NO_2 (red) and NO_x (black) on the left axis as well as the selectivity towards the desired product nitrate (green) on the right axis.^[P4] Right: The selectivity of the photocatalytic reaction with respect to nitrate formation versus the rutile content in the phase composition.^[P3]

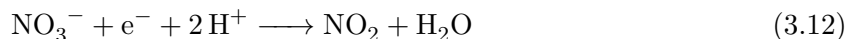
The example shown in Figure 3.3a also illustrates that the selectivity decreased significantly

with prolonged reaction times. The adsorption capacity for NO₂ on TiO₂ is much higher than that for NO and should therefore buffer the NO₂ formation to some extent.^[107] However, significant NO₂ evolution is observed immediately upon illumination. This suggests that there are two different aspects to consider. On the one hand there is the intrinsic selectivity of a material which is observed at the very beginning of an experiment with a clean surface. On the other hand, the selectivity decline during the reaction needs to be considered.

The most obvious reason for the first aspect is that the oxidation rate of NO₂ to nitrate is much slower than the oxidation of NO to NO₂ and the latter therefore accumulates during the reaction like in classical follow-up reaction kinetics. For instance, over pristine titanium dioxide, the ratio of the oxidation rates is as high as 10 in favor of NO.^[P2,P4] A more selective catalyst consequently must be much more active towards NO₂. Another reason lies in the reaction mechanism itself. Most of the NO is oxidized with hydroperoxyl radicals to peroxyxynitrite which spontaneously decomposes to form NO₂. If the life-time of the peroxyxynitrite is increased, this reaction could be slowed down in favor of the direct isomerization to nitrate. This could for instance be achieved by deprotonation on alkaline surfaces, since the anion is much more stable.^[78] This could also explain why more alkaline materials or building matrices such as concrete typically exhibit higher selectivity.^[78] Another approach would be to use a material which actively catalyses the isomerisation to nitrate.

However, if these were the only mechanisms at work, the selectivity should be constant in prolonged experiments. Since this is not the case, there rather seems to be an additional mechanism in place that leads to a significant decrease in selectivity over time. As essentially, the only thing changing is the concentration of accumulated nitrate on the surface, this is likely the cause for the observed phenomenon. This nitrate accumulation seems to poison the catalyst in a way that not only reduces its activity due to blocked surface sites but also reduces its selectivity.

The nitrate formed during photocatalytic oxidation is usually considered to be the inert end-product that stays on the photocatalyst surface until it is eventually washed off by rain. However, there are some experiments which show that a nitrate-rich photocatalyst surface can release significant amounts of NO₂ upon illumination, even in a NO_x free atmosphere.^[83] Presumably, this is caused by a photocatalytic reaction with adsorbed nitrate to nitrogen dioxide, which is subsequently desorbed and released. Previously, this has been attributed to photocatalytic oxidation of nitrate to NO₃ with subsequent photolysis, leading to NO, NO₂ and O₃.^[83,108] However, the reduction of nitrate is also possible and will directly yield NO₂, eqn. 3.12.



The adsorbed nitrate on the titanium dioxide will be in constant competition with molecular oxygen for the electrons. This fits well with the observation that the selectivity decrease is less pronounced at higher oxygen partial pressure.^[P3] Unfortunately, oxygen reduction on pristine titanium dioxide proceeds slowly and will often present the rate-determining step of the overall reaction.^[109] However, if an alternative electron acceptor is present, titanium dioxide will readily reduce it instead. Judging by the reduction potential, nitrate is a much better electron acceptor than molecular oxygen.^[110,111] Consequently, the reduction of nitrate versus molecular oxygen is thermodynamically favored and even very small amounts of nitrate can already significantly affect the reduction behavior. This means that even though this is predominantly a long-term effect, it might also already affect the observed selectivity at the very beginning of the reaction, making a clear differentiation with the above-mentioned other mechanisms difficult.^[P4]

Based on this theory that the back-reduction of already formed nitrate is the sole reason for decreasing selectivity with longer reaction times, we developed a model to describe the relationship between observed selectivity and nitrate surface coverage (θ), eqn. 3.13. In this equation, S_0

represents the initial or intrinsic selectivity of the material when no nitrate is yet present, k_o is a dimensionless figure for the relative oxygen reduction rate and α is a dimensionless attenuation factor. A detailed derivation of the formula can be found in the respective publication. [P4]

$$S(\theta) = S_0 - \theta \cdot \frac{(2 + S_0)(4 - 3(1 - e^{-\alpha\theta}))}{4(\theta + k_o(1 - \theta)) - 3\theta(1 - e^{-\alpha\theta})} \quad (3.13)$$

This equation yields excellent fit to the observed behavior for pristine TiO_2 materials as well as modified ones (*vide infra*), supporting the theory that back-reduction of nitrate is indeed the cause of the lowered selectivity. [P2,P4] This also explains the different selectivity of the three common titanium dioxide modifications, anatase, rutile and brookite. We observed that brookite (39 %) is the most selective of the three, closely followed by anatase (25 to 29 %), while pure rutile is very unselective (6 to 7 %). [P3] This can be readily explained by their different conduction bands, which are increasingly unsuitable for oxygen reduction. [112,113] [P7]

This pathway for NO_2 formation could be suppressed by making the oxygen reduction more favorable, for instance by employing co-catalysts for the oxygen reduction reaction (ORR). Well known ORR-catalysts are for instance noble metals such as platinum or palladium. [114–116] Consequently, titanium dioxide materials decorated with small amounts of the noble metals show an increased selectivity. [115,117–119] We also achieved similar results when adding 0.1 at.% of ruthenium to ZnO whereupon the selectivity was increased from 55 % to 87 %. [84] However, due to their limited production and unfavorable economics, using platinum-group metals even in sub-percent concentrations would be challenging for large volume applications in building materials such as concrete. [120] The observation that the above-mentioned W-doped and W/N-codoped titanium dioxide are more selective can also be readily explained by this mechanism as these materials also have an improved oxygen reduction behavior. [P10]

Unfortunately, all of these examples for more selective DeNOx photocatalysts have either utilized very expensive metal co-catalysts (Pt, Pd, Ru) or the selectivity increase was accompanied by a reduction in absolute activity (W-doped TiO_2). However, improved ORR can also be achieved by far easier means. It is well known that grafting a photocatalyst with certain transition metal ions such as Cu(II) or Fe(III) significantly increases their oxygen reduction capabilities. [63,121,122] The grafting can easily be achieved with wet impregnation techniques and only uses very small amounts of abundant and affordable elements.

We consequently explored this type of material for photocatalytic NOx abatement. To our satisfaction, it turned out that even grafting very small amounts (<0.1 %) of Fe(III) ions onto different commercial TiO_2 powders dramatically increased the selectivity up to more than 90 %. In this case the intrinsic activity of the materials was not compromised. On the contrary, the activity was even higher than for the pristine material. Overall, the amount of total NOx removed in a standard ISO 22197-1 test was increased from 10 % up to 48 %, an increase by a factor of almost 5. [P2]

Impressed by this much better than expected performance, we analyzed these materials in more detail. Figure 3.4a shows the observed selectivity of the TiO_2 grafted with different concentrations of iron in dependence of their nitrate surface coverage. It is apparent that both the initial selectivity and also the long-term performance is dramatically improved in comparison to the pristine material. [P2] The profiles also fit very well to our proposed model which substantiates the underlying theory of reductive re-nitrication. Fitting the model to the data also allows to extract the intrinsic selectivity and relative oxygen-to-nitrate reduction rate ratios, which are shown in Figure 3.4b.

The intrinsic selectivity already sharply jumps up at a very small iron loading of only a few ppm which is extremely challenging to detect with conventional means but could be verified

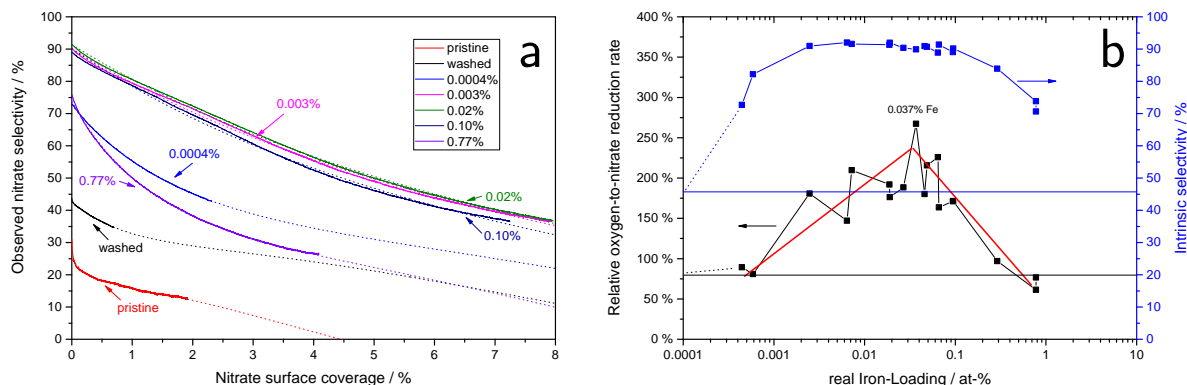


Figure 3.4: Left: The behavior of the observed nitrate selectivity with increasing nitrate surface coverage for a selection of iron-grafted TiO_2 samples. The numbers in the figure indicate the iron content of the respective samples. Also displayed are the best fits to our proposed model (eqn. 3.13) as dotted lines. [P2] Right: The relative oxygen reduction rate (black circles, left axis) and initial selectivity (blue filled circles, right axis) of the samples with varying iron-grafting ratio as extracted from the fits on the left-hand side. The horizontal lines represent the respective values of the ungrafted reference samples. [P2]

using EPR spectroscopy. [P2] After that the selectivity reaches a broad plateau over several orders of magnitude of iron concentration up to about 0.1 at.%, after which it drops again. Interestingly, the onset of the ideal performance is between 0.0006 to 0.003 at.% which corresponds to 2 to 10 atoms per particle, matching exactly the predicted optimal value according to our model (section 2.2). [P1] This is a very promising indication that our model to predict the optimal metal content might indeed be applicable to metal-grafted materials, as well. The analysis of the oxygen reduction performance allows to further differentiate these samples and pins down the ideal iron concentration at 0.037 at.%, which corresponds to 148 atoms per particle. This indicates that in the absence of immediate negative effects (bulk defects) the optimal grafting ratio might be higher than the optimal doping ratio. The iron ions grafted onto the TiO_2 surface are relatively stable and only minimal amounts are lost upon washing. Nonetheless it might be beneficial to employ a slightly higher than the optimal amount of iron to make the materials more robust against loss of the adsorbed ions. [P2]

This readily explains why the materials are so much better in their long-term performance than the reference materials as the tolerance towards nitrate build-up is much higher. However, it cannot explain the extremely high intrinsic selectivity. Therefore, we studied the reactivity in more detail and found out that their activity towards NO_2 oxidation is also greatly improved. Kinetic analysis revealed that the first-order reaction rate constant for NO_2 oxidation is increased by a factor of 9 upon iron-grafting, almost putting it on par with that of NO oxidation. We attribute this to strongly reactive ferryl ions (FeO^{2+}) being formed on the photocatalyst surface, either by photocatalytic oxidation of Fe^{3+} or mediated through other oxidative species (Figure 3.5a). These ferryl ions react basically diffusion controlled and indiscriminately with both NO and NO_2 , leading to oxidation rates of similar magnitude. [123,124] [P2]

However, even though the NO_2 oxidation rate is greatly increased, this alone fails to explain that the selectivity exceeds 90 % since usually kinetics of similar magnitude in consecutive reactions still lead to significant build-up of the intermediate. Therefore, we proposed an additional mechanism which directly addresses the third pathway for NO_2 formation, the decomposition of peroxyntrous acid. It is well known that some iron complexes and metallo-enzymes strongly coordinate peroxyntrite and can catalyse its isomerisation to nitrate. [123,125,126] We proposed that iron ions grafted on the TiO_2 behave similarly and catalyse the peroxyntrite isomerisation (Figure 3.5b). [P2]

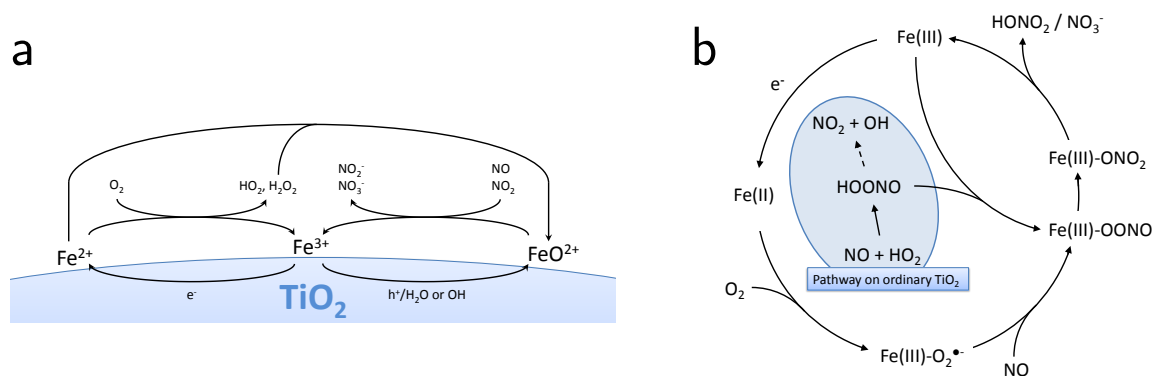


Figure 3.5: Left: The proposed reaction mechanisms that lead to the formation of the highly oxidizing ferryl ions (FeO²⁺).^[P2] Right: The proposed reaction mechanisms for peroxyxynitrite/peroxyxynitrous acid isomerisation on the grafted Fe(III) that would prevent NO₂ release through peroxyxynitrous acid decomposition.^[P2]

Since this material addresses all three proposed mechanisms of NO₂ formation simultaneously and effectively, is long-term stable as well as easy and inexpensive to manufacture it can be seen as an ideal solution to the selectivity problem. Interestingly, we also observed that these iron-grafted materials are excellent catalysts for photocatalytic ozone abatement.

3.4 Photocatalytic ozone decomposition

Another harmful air pollutant is ground-level ozone (O₃). While this has in recent years not been in the focus of public interest, in Europe many measurement stations frequently exceed the limit values, particularly in the southern countries.^[74] In urban areas, ozone itself often does not present a significant problem owing to its reactivity with the high concentrations of NO_x present. While there often is an ozone background of several tens of ppb, it is typically not observed in that magnitude and mostly present in the form of NO₂ which is formed by reaction of ozone and NO, eqn. 3.14.^[69] However, as described by the Leighton equilibrium, some of that NO₂ photolyses back to NO and O₃ during daytime, eqns. 3.15 and 3.16.^[127]



Due to these reactions, NO₂ and O₃ are always dependent on each other. So each molecule of ozone that can be decomposed effectively equals one NO₂ molecule that is not formed out of NO in the first place. Therefore, ozone abatement can be considered as an indirect but equally effective way to reduce ambient NO₂ levels. Also, in more rural areas with very low NO_x levels, ozone can present a significant problem as it is not immediately quenched by NO and can therefore reach dangerous concentrations. The air quality in those areas would also greatly benefit from a reduced background ozone level.

It is well known that ozone can be photocatalytically degraded on illuminated titanium dioxide surfaces.^[128] As evidenced by EPR spectroscopy, the reaction proceeds both *via* reductive activation, forming an ozone anion radical (eqn. 3.17), and also oxidatively *via* photo-generated hydroxyl radicals, forming a tetraoxygen anion radical (eqn. 3.18).^[128] Both of these short-lived intermediates readily decompose to form O₂ and O₂•⁻ (eqns. 3.19-3.21). The latter is also

helpful in the general context of air pollution control as it can directly contribute to the overall photocatalytic oxidation efficacy.



The study of photocatalytic ozone abatement for the purpose of environmental air pollution control has been largely neglected in favor of direct NO_x abatement. Only few studies exist which report on the photocatalytic ozone abatement properties of titanium dioxide.^[127–130] This is partly due to the poor efficiency for ozone decomposition of pristine titanium dioxide. However, we could show that the ozone decomposition efficiency can be dramatically improved by grafting the photocatalyst with small concentrations of transitions metal ions.^[P11]

By grafting different commercially available titanium dioxide materials with small amounts of copper, manganese or iron ions, the performance towards ozone decomposition was greatly increased by up to a factor of 4. Even though all of the metals studied improved the performance, copper and iron proved to be the most effective at low loading, while higher concentrations were required of manganese. However, the materials modified with the latter were also quite effective in the absence of light, presumably due to the intrinsic activity of manganese oxides towards ozone.^[131–133] Interestingly, the procedure worked almost equally well on all of the different commercial titanium dioxide powders tested suggesting universal applicability.^[P11]

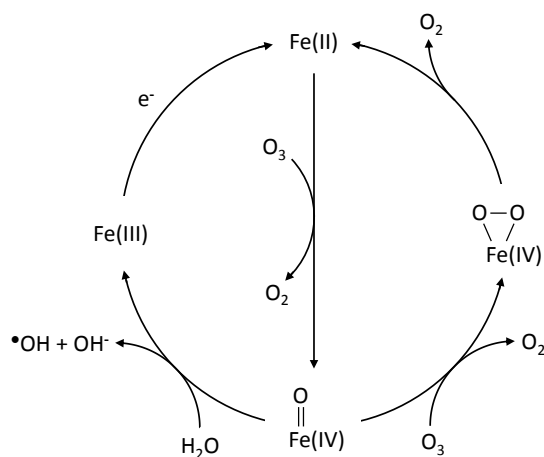


Figure 3.6: The proposed mechanism of ozone degradation over Fe-grafted TiO₂.^[P11]

As illustrated in Figure 3.6 for the case of Fe(II)-grafting, we suggested a mechanism similar to the well-studied ozone decomposition over manganese oxides.^[131–133] In the first step, the Fe(III) is photocatalytically reduced to Fe(II), which has a much higher reactivity with ozone and can form ferryl ions (Fe(IV)=O) as a result of the reaction.^[134,135] The latter is able to react with another ozone molecule, leading to its eventual disproportionation and regenerating the catalytically active Fe(II).^[133] The catalytic cycle may also be initiated by direct or indirect oxidation of Fe(III) to ferryl ions and is only terminated once the relatively inactive Fe(III) is formed again by secondary reactions.^[P11]

Overall, the photocatalytic ozone decomposition presents an interesting means to improve the overall air pollution efficacy that can be achieved with relatively little effort and is also free from by-products as only oxygen is formed.

3.5 Efficacy and limitations of the technology

The technology has mostly been applied to construction materials such as concrete, roof tiles, window panes or paving stones, where a small fraction of photocatalyst is coated onto the surface or mixed into the bulk. These materials should then help to mitigate air pollution once they are installed at a suitable site. The actual effect in real-world scenarios is extremely difficult to predict and measure as it is not just dependent on the nature and amount of photocatalytically active materials but also on the geometry of the site, fluctuating weather and sunlight conditions as well as the background pollution and emission sources. Nonetheless, there have been several attempts to simulate the effect of photocatalytic NO_x abatement in real-world scenarios using microclimatic modeling. These suggest an overall effect of 5 to 10 % reduction and indicate that the efficacy is strongly dependent on the wind direction and speed as the local abatement effect is strongly superimposed by transport from the surrounding area.^[136]

To date, several field-tests have also been conducted in order to demonstrate the efficacy of the technology in real-world scenarios.^[137] These include artificial street canyons and tunnels, where extremely high reduction in NO_x of 37 to 82 % and 23 % in comparison with a photocatalyst-free reference site were reported, respectively.^[138–140] However, for both cases later studies were not able to reproduce this and only observed minimal changes in the NO_x concentrations, highlighting that achieving reproducible results in field-tests is almost impossible due to the high number of uncontrollable variables.^[141,142] Other studies performed in Hengelo, Copenhagen and Hong Kong were able to provide evidence that the NO levels are reduced but the NO₂ levels are almost unaffected.^[19,143,144]

Ultimately, the real world performance is strongly dependent on the specific application site and the nature of the used photocatalyst material. However, no matter the activity of the material, an upper limit will always be unavoidable due to limitations in the mass transport of the pollutants to the active surface, which can only readily be increased by functionalizing a larger fraction of the available surface. Under most conditions, the photocatalytically active surface will practically oxidize all NO molecules that reach its surface, leaving not much room for further improvement. However, the reactivity towards other targets such as NO₂ and O₃ is typically much lower in unoptimized materials. However, in light of the mass-transfer limitation, it is even more important that every pollutant molecule (NO, HONO, NO₂ and O₃) hitting the surface is completely converted. This highlights one of the major shortcomings of the studies so far, as non-selective ordinary TiO₂ was used which is not very active towards NO₂ and ozone. Consequently, most of the studies observe a reduction in NO and total NO_x but not in the relevant NO₂ levels. By using new materials that are much more active towards the latter and are also selective in the NO oxidation reaction such as the iron-grafted materials described herein, the overall observed efficacy in immision reduction could still be significantly improved.

Also, in applications which are not reliant on weather-controlled mass-transfer, such as dedicated air-cleaning devices with forced convection, much higher reaction-rates are possible. Therefore, a much higher degree of intensification and very high space-time-yields can be achieved in those devices, in particular due to the also possible high light intensity with artificial lamps. This will allow relatively small but effective devices that can for instance be incorporated into ventilation and air conditioning systems to provide clear air not just in particularly polluted spaces such as certain industrial and commercial sites but also in offices, houses or vehicles.

4 Kinetic modeling and optimization of photocatalytic processes

In addition to the removal of unwanted pollutants, photocatalysis may also be used in synthetic chemistry, to produce value-added products. However, a successful implementation of these reactions in industrially relevant processes requires them to be both efficient and productive, *i.e.*, have both high quantum yield and reaction rates at the same time. Also, the kinetics and the influence of all relevant reaction parameters need to be known precisely in order to properly set up and control the processes. Yet, relatively little is known about the behavior of photocatalytic reactions at the very high photon fluxes required to reach the productivity demands, *i.e.*, molar conversions in hours. Also, the influence of other reaction parameters is typically only studied one-dimensionally, *i.e.*, only varying one parameter at a time. However, precise kinetic modeling requires a holistic multi-dimensional approach that considers all relevant reaction parameters at the same time.

This chapter describes the author's research on kinetic modeling and optimization of photocatalytic processes which is centered around developing a holistic kinetic model for these reactions as well as the design of photoenzymatic reactions where a photocatalyst is coupled to an enzyme. The works presented herein have been published in the papers [P12-P20](#).

4.1 Kinetic analysis of the photocatalytic reduction of molecular oxygen to hydrogen peroxide

Hydrogen peroxide (H_2O_2) is a very important compound in semiconductor photocatalysis. Mainly being formed through reduction of molecular oxygen, it is one of the reactive oxygen species used in environmental applications to oxidize unwanted pollutants.^[145] Industrially, hydrogen peroxide is used in medicine, waste water treatment, as a ripening agent, in detergents and even as a liquid propellant.^[146–148] The compound is particularly interesting for oxidation reactions due to its exceptionally high content of active oxygen (47.1 wt.%) and its high oxidation potential over the whole pH range.^[146,149] Since oxygen and water are the only by-products of its reaction, it is also considered environmentally friendly. Therefore, it is mainly used in pulp and paper bleaching^[150,151] and also increasingly as a reactant in chemical syntheses.^[152–155] [P12–P14](#)

Today, hydrogen peroxide is predominantly produced *via* the anthraquinone process, which comprises of three separate reaction steps: hydrogenation, oxidation and hydration.^[149,156,157] The hydrogen gas required for the first step is usually derived from steam reforming which leads to a high overall carbon footprint. To overcome this issue, also the direct synthesis of H_2O_2 from molecular O_2 and H_2 over metallic catalysts, such as Pd and Au nanoparticles also been studied intensively.^[158] Moreover, the century-old electrosynthesis has also been rediscovered as a green method if renewable energy is used for H_2O_2 generation *via* oxygen reduction or water oxidation.^[149,159–163]

Additionally, the generation of hydrogen peroxide from molecular oxygen over irradiated semiconductors is well-known since Baur and Neuweiler first observed it over ZnO in 1927.^[164] As in this case, only water, oxygen and light are required, it can be considered as a green alternative

to the abovementioned variants. Since its original discovery, the photocatalytic formation was also reported on a number of other photocatalyst materials, both inorganic as well as carbon based materials which have also in some cases been specifically modified with metal co-catalysts to increase the efficiency.^[163,165–175]

The mechanism of hydrogen peroxide formation over illuminated semiconductors has been studied in detail by several authors.^[20,176–183] The reduction of molecular oxygen can proceed either *via* two consecutive one-electron transfers or one concerted two-electron transfer. In the absence of additional co-catalysts, one-electron reactions are much more probable and the reaction proceeds as illustrated in Figure 4.1a through two reversible single electron and proton transfer reactions *via* a superoxide radical cation, hydroperoxyl radical and hydrogen peroxide anion as intermediates.^[184] The peroxide formed may also be further reduced to hydroxyl radicals and finally water. It should be noted that in addition to the photocatalytic reactions that are illustrated here, particularly the radical intermediates may also undergo a number of non-photoinduced reactions such as the disproportionation of superoxide radicals.

In the absence of other reducing agents, water will act as the electron donor, usually being oxidized to molecular oxygen. However, this reaction may also yield hydrogen peroxide as an intermediate or product, this is particularly expected of materials with a strong tendency for hydroxyl radical adsorption such as BiVO_4 .^[182] If easily oxidizable, so-called “sacrificial” reagents such as alcohols are introduced into the system they can replace water as the electron donor and this strongly inhibits other oxidation processes due to their lower oxidation potentials and faster reaction kinetics. This is shown exemplary in Figure 4.1b for the photocatalytic oxidation of 2-propanol as sacrificial reagent for H_2O_2 generation.^[185]

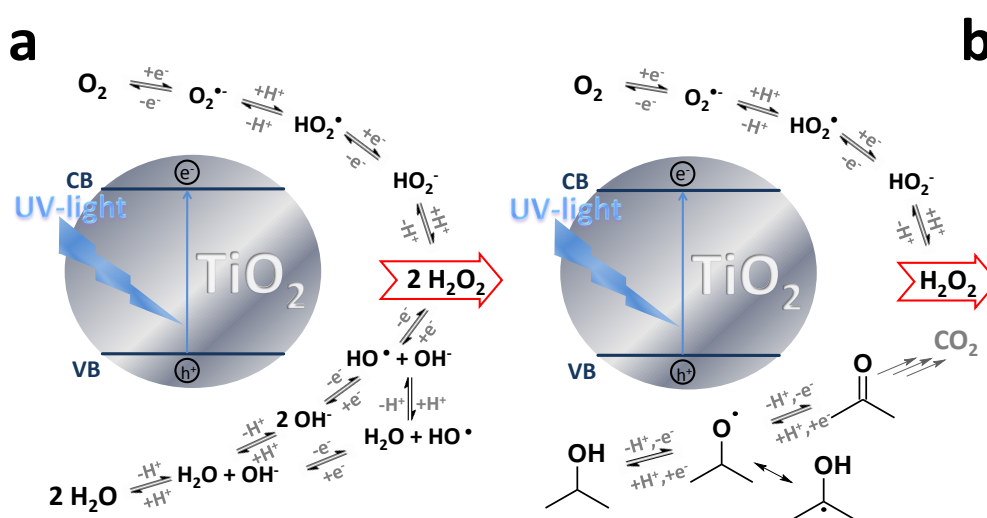


Figure 4.1: Schematic view of the possible reaction pathway of photocatalytic hydrogen peroxide generation *via* reduction of oxygen without (a) and with (b) 2-propanol as sacrificial electron donor in aqueous media. ^[P15]

In many of the potential applications for photocatalytic hydrogen peroxide generation, particularly those with coupled secondary processes (see section 4.5), precise knowledge of the reaction kinetics is very important to properly control and optimize the reactions. The kinetics of the photocatalytic H_2O_2 formation have already been studied in detail by Kormann, Bahnemann and Hoffmann in 1988.^[186] Briefly, the formation rate (r_F) is based on zero-order kinetics, while the degradation rate (r_D) is first-order with respect to the peroxide concentration, eqns. 4.1-4.2. Both of these have been reported to linearly depend on the absorbed photon flux (I_{abs}) and

individual quantum yields (Φ). In combination, they can be integrated to yield an explicit expression for the time-dependent H_2O_2 concentration, eqn. 4.3. Using this equation, both the formation and degradation rate constants can be extracted from concentration-time profiles using non-linear optimization. Over longer time-frames, an equilibrium is established, which, according to this simple model, is only dependent on the quantum yields for formation and degradation, eqn. 4.4.^[186] **[P15]**

$$r_F = \Phi_F \cdot I_{abs} = k_F \quad (4.1)$$

$$r_D = \Phi_D \cdot I_{abs} \cdot [\text{H}_2\text{O}_2] = k_D \cdot [\text{H}_2\text{O}_2] \quad (4.2)$$

$$[\text{H}_2\text{O}_2] = \frac{k_F}{k_D} (1 - e^{-k_D \cdot t}) + [\text{H}_2\text{O}_2]_0 \cdot e^{-k_D \cdot t} \quad (4.3)$$

$$[\text{H}_2\text{O}_2]_{eq} = \frac{k_F}{k_D} = \frac{\Phi_F}{\Phi_D} \quad (4.4)$$

However, when studying the behavior of the peroxide formation with different applied light intensities, we quickly noted that this is not the case and instead the equilibrium concentration also changes with the light intensity.^[P15] Kinetic analysis of the time-concentration profiles revealed that contrary to the model described above the degradation is only linearly dependent on the light intensity at low photon flux (Figure 4.2b).^[P15] At higher light intensity, the behavior becomes increasingly non-linear and finally levels off at a constant value. This is even more pronounced when an alcohol is present as a sacrificial electron donor since this suppresses the H_2O_2 degradation reaction (Figure 4.2a). In this case, the degradation rate is almost constant in the light intensity range studied.^[P15]

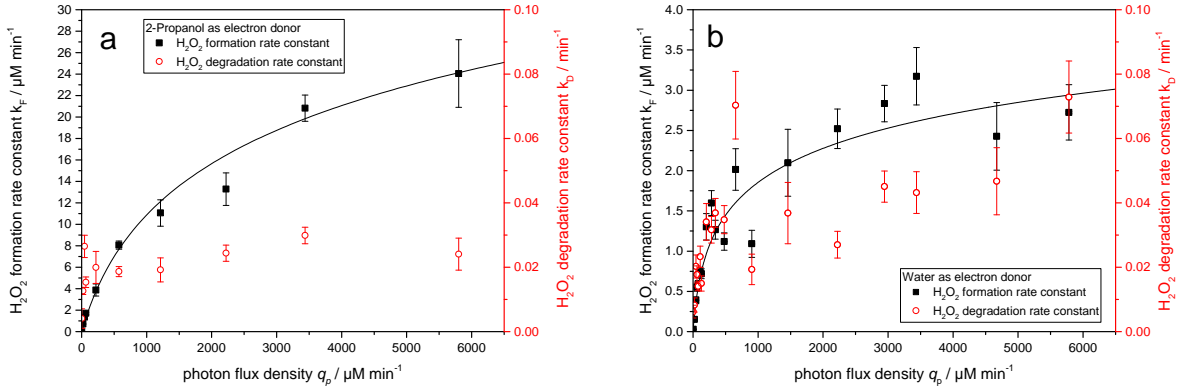


Figure 4.2: Dependence of the H_2O_2 formation (k_F , black boxes) and degradation (k_D , red circles) rate constants on the photon flux density a) (left) using 10 vol.% 2-propanol and b) (right) water as electron donor. Conditions: 0.1 mol L^{-1} phosphate, 2 g L^{-1} catalyst, 25°C , 365 nm light, 2 mL min^{-1} O_2 -bubbling, pH 7. Also shown is the calculated fit for the formation rate according to the developed model (section 4.3) as a solid black line.^[P15]

At the same time, the formation rate constant shows a similar behavior, albeit with a slower onset, *i.e.*, the non-linearity starts to show its effect at a higher light intensity. In combination, these two effects lead to the observation that the equilibrium concentration also increases with the light intensity and is not constant as suggested in the earlier model.^[P15]

When the catalyst concentration is varied, the formation rate first increases approximately linearly but then quickly plateaus in the area of 0.1 to 1.0 g L^{-1} , Figure 4.3a. Interestingly, the degradation rate is constant when an alcohol is present but increases linearly over the whole studied range without it. In consequence, the equilibrium concentration increases with catalyst

concentration when an alcohol is added but decreases with the catalyst concentration with water as electron donor. [P15]

The non-linear response of the formation rate on the light intensity is not surprising given that other authors have made similar observations for other photocatalytic reactions. [81,187,188] However, what was intriguing is that the change in the reaction order from linear to non-linear changed with different catalyst concentrations. This can be illustrated in a double logarithmic plot of the formation rate constant on the photon flux, Figure 4.3b. Here, it becomes obvious that the different catalyst concentrations have negligible impact at lower light intensity but significantly change the response at high light intensity. Also, vice versa, the saturation point in the catalyst concentration increases with the light intensity. This mutual inter-dependence of light intensity and catalyst concentration was reported by us for the first time and cannot be explained with the traditional models. A new model which accounts for this is discussed in detail in section 4.3. [P15]

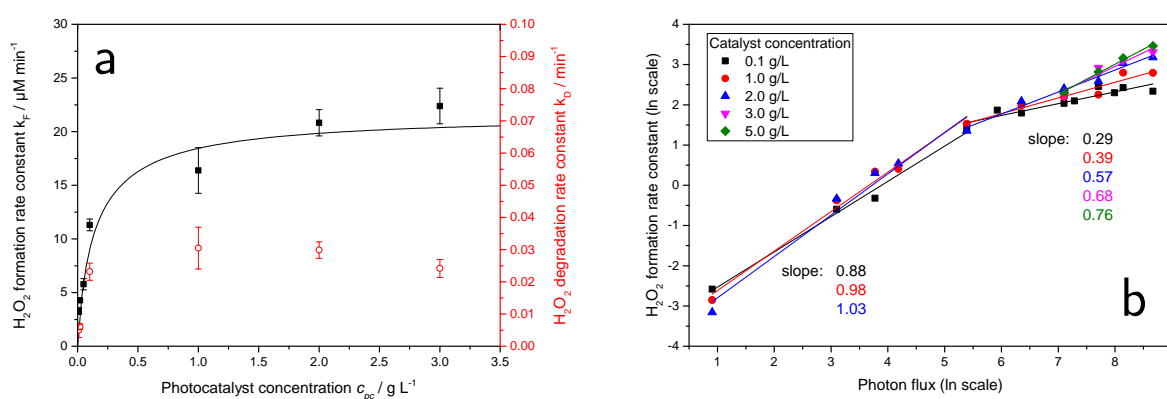


Figure 4.3: a) (left) Dependence of the H_2O_2 formation (k_F , black boxes) and degradation (k_D , red dots) rate constants on the catalyst concentration at a fixed photon flux of $3437 \mu\text{mol L}^{-1} \text{min}^{-1}$. Also shown is the calculated fit for the formation rate according to the developed model (section 4.3) as a solid black line. b) (right) The H_2O_2 formation rate constant in dependence of the photon flux for different catalyst concentrations on a double logarithmic scale. Conditions: 0.1 mol L^{-1} phosphate, 25°C , 365 nm light, 2 mL min^{-1} O_2 -bubbling, $\text{pH } 7$, $10 \text{ vol.}\%$ 2-propanol. [P15]

The addition of an alcohol such as 2-propanol increased the formation rate by approximately a factor of 7, the optimum alcohol concentration was determined at $10 \text{ vol.}\%$. [P15] The beneficial effect was attributed to the better oxidation kinetics of the alcohols in comparison to water, which not only have a more favorable redox potential but are also easier kinetically as less electrons are transferred. Also, the so-called “current doubling” effect improves the overall observed efficiency of the reactions. [189,190] The alcohols are first oxidized by the photocatalyst to their radicals in a one-electron transfer. These radicals are very reducing and may inject an additional electron into the semiconductor without the aid of an additional photon. [191] This effect effectively doubles the amount of electrons transferred. We also recognized that the effect of added alcohols may be even more complex as also the gas solubility is improved and the presence of intermediate oxidation products needs to be considered (see section 4.2). [P16]

Increasing the oxygen partial pressure also slightly increases the observed formation rates. [P16] As long as the availability of oxygen on the surface of TiO_2 is a limiting factor, the generation rate is dependent of the oxygen content. When the oxygen availability is not limiting anymore, a higher oxygen content does not further increase the generation rate. This saturation point appears to be reached at about 50% in this case. Compared to a study of photocatalytic H_2O_2 production over ZnO [186] where saturation was already reached at about 20% , one can conclude that the point of saturation is dependent on the magnitude of the generation rate, similar effects

have also been found for phenol degradation.^[192] If the reaction rate is lower, a lower gradient between liquid and gas phase oxygen is required to maintain saturation at the catalyst surface and therefore less oxygen content in the atmosphere is required.^[P16]

As additional parameters, also the temperature and the pH of the solution were studied. Regarding the former parameter, it was found that while with water as the electron donor, both the formation and the degradation rate are invariant of the temperature, they increase exponentially in the case of added 2-propanol. This indicates that water oxidation is rate-limited by a step that is not influenced by the temperature.^[P16]

Similarly, when studying the effect of the solution pH value, also quite a different behavior is observed with or without an alcohol being added. When an alcohol is present, presumably its oxidation is so fast that the reduction reaction becomes rate-limiting. So in this case, the effect on the oxygen reduction is most apparent and no systematic effect of the pH value was observed so this reaction seems to be relatively invariant of the pH value. On the contrary, in case of water oxidation, there is an exponential increase in the formation rate with higher pH, particularly above 7. Therefore, water oxidation appears to be very much favored in basic pH.^[P16]

Overall, it appears that both the formation and the degradation reaction rates have their own, quite different dependencies on pH, temperature, catalyst concentration and intensity and can therefore not be accurately described using the simple model described before if any of these parameters are varied.^[186] Also, there are significant changes in the behavior if other substances are added to the system such as alcohols which may act as sacrificial reagents. This motivated us to take an in-depth look at both the effect of sacrificial reagents and the kinetics of photocatalytic reactions and develop a new model which can accurately describe these observations, which are covered in the next two sections.

4.2 The effect of sacrificial electron donors on the kinetics of photocatalytic reactions

Sacrificial electron donors are often applied in photocatalysis to enhance the performance of reduction reactions in aqueous media as pure water oxidation is usually rather inefficient.^[190] Mostly, short-chain aliphatic alcohols, aldehydes or carboxylic acids are used for this purpose, which in addition to their superior oxidation kinetics can also donate additional electrons due to the current doubling effect described in the previous section.^[189,190] In many photocatalytic reduction reactions such as hydrogen production, carbon dioxide reduction or nitrogen fixation, the use of sacrificial electron donors is very popular. They are used not only to speed up the overall reaction but also to selectively study the reduction reaction without risking the oxidation half-reaction to become rate-limiting.^[193-196] However, only in few cases, the sacrificial reactant is completely consumed in the reaction and leaves no by-products which can undergo further reactions or modify either the solution or the catalyst in the process.^[190] On the contrary, even in the relatively simple case of methanol, the oxidation pathway proceeds through formaldehyde and formic acid, both of which may act as electron donors themselves, superimposing the effect of the original reagent. Moreover, the intermediates may accumulate, leading to unwanted side-reactions or pH changes as well as complicating the work-up and product isolation. This is typically ignored and may lead to false conclusions regarding the efficiency and suitability of individual compounds evaluated as electron donors.

The study of an oxidation reaction always requires a corresponding reduction reaction as well. Ideally, this reduction reaction should be well known and not need a co-catalyst so the catalyst is not artificially altered for the purpose of the study. Therefore we chose the photocatalytic reduction of molecular oxygen to hydrogen peroxide, since we already studied the effect of many

reaction parameters for that reaction as described in the previous section.

We chose the commonly employed alcohols methanol, ethanol, 2-propanol and *t*-butanol (2-methylpropan-2-ol) to study the effect of different electron donors. The corresponding aldehydes, ketones and carboxylic acid are studied indirectly as well as they appear as intermediates in the oxidation pathways anyway. Photocatalytic experiments were conducted with the respective alcohol in a starting concentration of 10 mM where the concentration of the alcohol as well as all intermediates were monitored over time. Afterwards, the concentration-time-profiles were fitted using a kinetic model based on a Langmuir-Hinshelwood approach and the oxidation pathways outlined below. As many of the intermediates appear in more than one pathway, the optimization was done globally, *i.e.*, only delivering one shared value for each kinetic constant determined from all the data sets. The resulting kinetic constants are reported in Table 4.1.

Table 4.1: Calculated zero- and first-order oxidation rate constants for various alcohols and their oxidation intermediates derived from the kinetic modeling, normalized to the methanol rate constant. For the intermediates, zero-order rate constants could not be accurately determined as their concentration was never high enough during the experiments. ^[P16]

Electron donor	k^0/k_{MeOH}^0	k^1/k_{MeOH}^1
Methanol	100 %	100 %
Formaldehyde	<i>n.d.</i>	1170 %
Formate	<i>n.d.</i>	462 %
Ethanol	214 %	118 %
Acetaldehyde	<i>n.d.</i>	121 %
Acetate	<i>n.d.</i>	47 %
2-Propanol	182 %	25 %
Acetone	<i>n.d.</i>	9 %
<i>t</i> -Butanol	303 %	3 %
2-Methylpropan-1,2-diol	<i>n.d.</i>	18 %
2-Hydroxy-2-methylpropanal	<i>n.d.</i>	13 %
2-Hydroxy-2-methylpropionic acid	<i>n.d.</i>	5 %

The oxidation pathways of methanol and ethanol are quite well described in the literature and illustrated in Figure 4.4. ^[11,197–201] In the first step, the alcohol is oxidized in a one-electron transfer followed by deprotonation (effectively an α -H abstraction), leading to the corresponding carbon-centered alcohol radicals. These are so strongly reducing that they practically immediately inject an additional electron into the photocatalyst, oxidizing themselves to the aldehyde in the process. ^[189–191]

The same procedure is repeated for the aldehyde which again after two consecutive one-electron transfers and additionally in this case, hydration, results in the formation of the corresponding carboxylic acid. It appears that with the exception of the extremely fast reacting formaldehyde, the oxidation rates of the alcohol and the corresponding aldehyde are of similar magnitude. ^[P16] Further oxidation will yield the corresponding carboxylate radical. ^[176,191,202] In the case of formic acid, this radical readily decomposes to carbon dioxide while donating its final electron. Longer chain carboxylates such as acetate release carbon dioxide from their carboxylate radicals. ^[201] However, the hydrocarbon radical formed this way immediately reacts with oxygen and after rearrangement is oxidized directly to the shorter chain aldehyde, formaldehyde in the case of acetate. The corresponding shorter chain alcohol was not detected in any of the studied cases. ^[P16]

While the oxidation of formic acid showed one of the highest kinetic constants of all compounds tested and was faster than that of methanol, in all other cases the carboxylic acids reacted

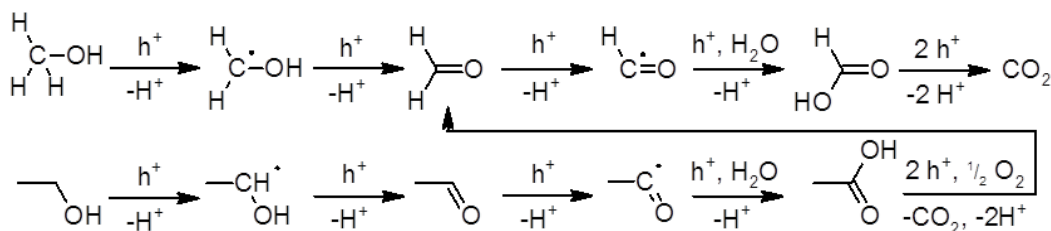


Figure 4.4: The complete photocatalytic oxidation pathways of methanol and ethanol. [P16]

significantly slower than their alcohol and aldehyde counterparts. We attributed this to the lack of α -H-atoms in these intermediates which requires breaking a C-C bond instead. These reactions appear to be generally slower and often present the rate limiting step. [P16] A similar behavior was observed with 2-propanol, which as a secondary alcohol is oxidized to its ketone, acetone. The further oxidation, which again requires breaking a C-C bond to form formaldehyde and acetaldehyde, was also found to be relatively slow and rate limiting. [203,204] [P16]

In some cases, the complete oxidation can be quite complex with several concurrent pathways. This is illustrated in Figure 4.5 for the case of *t*-butanol, which is also often employed as electron donor. Typically, this is not studied as a complete oxidation reaction and the tertiary alcohol is just assumed to donate one electron and then form a stable radical product. [205–207] However, our detailed kinetic analysis shows that this is far from the truth and indeed complete oxidation takes place, liberating quite a substantial amount of reduction equivalents from intermediate oxidation reactions (*vide infra*). Again here, carboxylic acids and ketones present the most stable intermediates due to their slow oxidation kinetics. [P16]

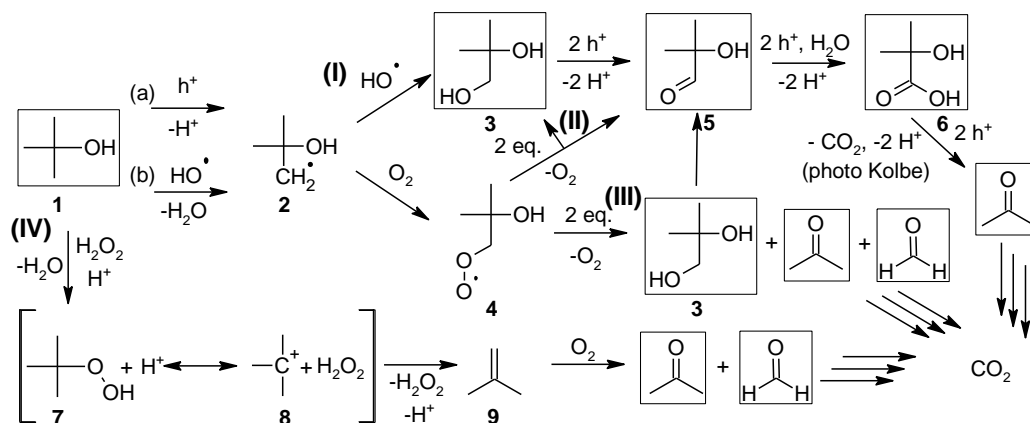


Figure 4.5: The complete photocatalytic oxidation pathway of *t*-butanol. [P16]

Interestingly, the kinetic analysis revealed that at these concentrations of sacrificial electron donors, the amount of total reduction equivalents generated is much higher than just from the alcohol oxidation (Table 4.2). Overall, the alcohol oxidation contributed only 30 to 80% when analyzing the first two hours of reaction. It was found that only a quarter to a third of the theoretically generated reduction equivalents actually find their way into the reduction product. This indicates that a significant amount of unproductive non-photocatalytic side-reactions takes place which scavenge reduction equivalents, *e.g.*, direct reaction of intermediates with molecular oxygen. The total number of theoretically generated reduction equivalents is surprisingly similar

for all cases, except for *t*-butanol which apparently generates about 70 to 80 % more. However, in this case, the corresponding reduction reaction was found to be less efficient, indicating an even higher fraction of side-reactions. [P16]

Table 4.2: Overview of the effect of the different alcohols on the theoretically generated reduction equivalents (RE), the fraction of them originating from the original alcohol oxidation and the fraction found in reduction product (H_2O_2). The calculations are based on analysis of the kinetics in first two hours of the reaction. [P16]

Electron donor	Theoretical RE	RE from the alcohol	RE found in the product
Methanol	$41.6 \mu\text{M min}^{-1}$	50 %	28.9 %
Ethanol	$40.1 \mu\text{M min}^{-1}$	80 %	27.7 %
2-Propanol	$43.8 \mu\text{M min}^{-1}$	76 %	24.0 %
<i>t</i> -Butanol	$72.4 \mu\text{M min}^{-1}$	30 %	6.4 %

Overall, this indicates that the oxidation rate of a sacrificial electron donor cannot be inferred by just looking at the rate of the corresponding reduction reaction and the latter may in fact also change during the course of the reaction as more intermediates are formed and take part in the reaction. To minimize interference from intermediates a compound should be used which is either only oxidized once to a relatively stable intermediate such as 2-propanol, or is oxidized completely very fast without accumulating intermediates such as methanol.

4.3 A holistic approach for kinetic modeling of photocatalytic reactions

Understanding and modeling the kinetics is an essential part of optimization and implementation of chemical reactions. In the case of photocatalytic reactions this is mostly done one-dimensionally, *i.e.*, only considering the effect of one parameter at the same time. For instance, many authors model the substrate concentration dependence using relatively simple approaches based on Langmuir-Hinshelwood type kinetics. [28,208] When the light intensity dependence is studied, the common observation is that while linear for low light intensities, at some point the response of the reaction rate to the light intensity becomes non-linear and yields increasingly diminishing returns. [81,187,188] However, the use of an average light intensity as done in those cases is only a valid approach if the reaction rate scales linearly with the light intensity at every point in the reaction vessel which is often not the case. Accurately considering the distribution of the light intensity and absorption inside the reactor and calculating local reaction rates to integrate into a global average is only done in select few and very specific cases. [28,30,209–211] Unfortunately, even though there have already been several attempts at simplifying this task, [31,212–216] the majority of reports still use the abovementioned linear light dependency models.

Moreover, as shown recently by us, [P15] most of the reaction parameters show mutual interdependence on each other and therefore cannot be properly studied in one-dimensional approaches where just one parameter is varied. Instead, this calls for a holistic approach that takes the light intensity and distribution, catalyst and substrate concentration as well as the temperature into account at the same time.

Such a model is described in this section. It is essentially based on three elementary reaction steps (*R1-3*), which are illustrated in Figure 4.6. While in the overall reaction, always a reduction and oxidation have to take place, for the sake of simplicity only one of those half-reactions is considered, whichever one is slower and rate-determining. This is done under the assumption that the corresponding other half-reaction is much faster and has no effect on the overall observed reaction rate.

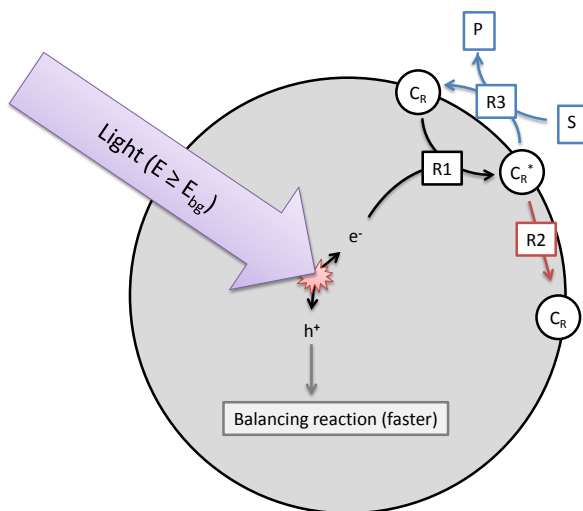


Figure 4.6: Illustration of the three elementary reactions which are the basis of the kinetic model. Shown are the generation of reactive surface sites ($R1$), the recombination ($R2$) and the charge transfer to the target substrate ($R3$). [P19]

The first reaction step ($R1$) is the generation of reactive surface sites (c_R^*) by trapping of photo-generated charge carrier at surface sites (c_R). These reactive surface sites can relax back to the ground state by recombining with their respective charge-carrier counterpart ($R2$) or be transferred to the target substrate to yield the desired product ($R3$). [P19]

Under the assumption that these processes are much faster than macroscopic mixing and changes in the substrate concentration, a pseudo-steady-state approach yields an explicit equation for the concentration of reactive surface sites and the substrate reaction rate (r), eq. 4.5, dependent on the intrinsic quantum yield (ϕ), catalyst concentration (c_0), local volumetric rate of photon absorption (LVRPA, L_p^a), recombination rate constant (k_r) and charge-transfer rate constant (k_1^*). [P19]

$$r = \frac{\phi \cdot L_p^a \cdot k_1^* \cdot \theta \cdot c_0}{\phi \cdot L_p^a + k_r + k_1^* \cdot \theta \cdot c_0} \quad (4.5)$$

This general rate law has the two limiting cases, that the light intensity is either very high or very low in relation to the reaction's kinetic limit. These limiting cases are also illustrated in Figure 4.7. At low light intensity, the reaction is purely governed by the flux of absorbed photons. In this regime, the observed overall photonic efficiency is constant. Parameters affecting the rate of electron transfer from the photocatalyst to the substrate have only negligible effect here. If on the contrary, the local light intensity is very high, the reaction is completely limited by the intrinsic kinetics of the reaction. In this case, the photocatalyst effectively behaves like an ordinary (thermal) catalyst, since all of the reactive sites are permanently active due to the high photon flux. Most cases will not fall into either category but somewhere in between, where the reaction rate shows a saturation-type behavior with respect to the light intensity. [P19]

Interestingly, both the limit of linearity and also the point of saturation are dependent on the catalyst concentration. The higher the catalyst concentrations is, the longer the linear regime and the more light is needed to be fully saturated with photons. This inter-dependency of catalyst concentration and light intensity was recently reported by us for the case of photocatalytic

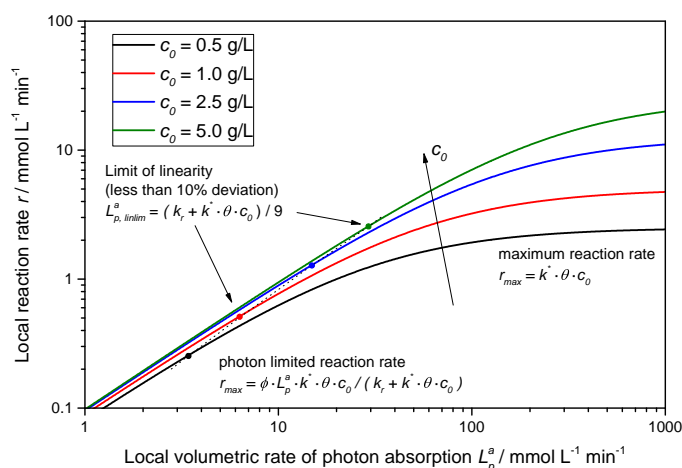


Figure 4.7: Exemplary dependency of the local reaction rate (eq. 4.5) on the light intensity for different catalyst concentrations in a double logarithmic plot. Parameters used: $\phi = 0.1$, $k_r = 500 \mu\text{mol L}^{-1} \text{min}^{-1}$, $k_1^* = 5000 \mu\text{mol g}^{-1} \text{min}^{-1}$, $\theta = 1$. [P19]

hydrogen peroxide formation by reduction of molecular oxygen (see section 4.1). [P15] Since typically, the two parameters are not studied in depth at the same time, this effect had been largely invisible up until then. The conclusion here is that it is possible to at least partly counteract efficiency losses at higher light intensity by employing a higher catalyst concentration. However, since there are obvious limits to this in terms of dispersibility of the photocatalyst in the reaction medium, other measures should also be taken at very high light intensity (*vide infra*).

Close inspection of the rate law reveals that it can be re-written into a pseudo-Langmuir-Hinshelwood form. However, in this case the obtained parameters do not resemble their classical physical meaning and are, in fact, influenced by a number of other parameters such as the light intensity. [P19] This was also confirmed experimentally by other authors. [28,208,217,218] Consequently, if the substrate concentration is the only parameter varied, Langmuir-Hinshelwood kinetics may be employed to fit and extrapolate the data, but it will not give usable information about the underlying physical processes.

The rate law presented above describes only a local reaction rate, dependent on the local light intensity. Therefore, it can only be used to analyze observed global reaction rates if it is linear with respect to the light intensity at every point of the reaction. However, particularly for reactions with bad kinetics this will often not be the case even for moderate light intensities. In these cases, the reaction rate has to be integrated over the whole reaction medium, taking the local light intensity distribution into account. [P19]

While this is often a very challenging and time-consuming task, it may be vastly simplified if several conditions are met. If the light is only attenuated alongside one direction in the reactor and scattering effects are ignored, the light absorption behavior may simply be approximated using the Lambert-Beer law. [31] In this case, the rather simple explicit equation valid for most cases is obtained for the global average reaction rate ($\langle r \rangle$), eqn. 4.6. Its rate is now dependent on the optical density (α) and the volumetric photon flux density (q_p , ideally determined using chemical actinometry). [P19]

$$\langle r \rangle = \frac{k_1^* \cdot \theta}{\alpha} \cdot \ln \left(\frac{\phi \cdot q_p \cdot \alpha \cdot c_0}{k_1^* \cdot \theta \cdot c_0 + k_r} + 1 \right) \quad (4.6)$$

An exemplary plot of this equation is shown in Figure 4.8a. Here, three regimes are apparent: At low light intensity, the reaction scales linearly with the light intensity across the whole reaction medium (**A**). At some point, non-linearities start to appear in some parts of the reactor (the “bright” zone) and the average reaction rate starts to show diminishing returns (**B**). This corresponds to the non-linear response that was often reported for photocatalytic reactions at higher light intensities. If extremely high light intensities are used, the reaction will be limited at every point in the reactor (**C**). Here, the photocatalyst behaves like an ordinary thermally activated catalyst. This state, however, is virtually impossible to achieve with conventional light sources unless very small reactors with dilute photocatalysts are used. [P19]

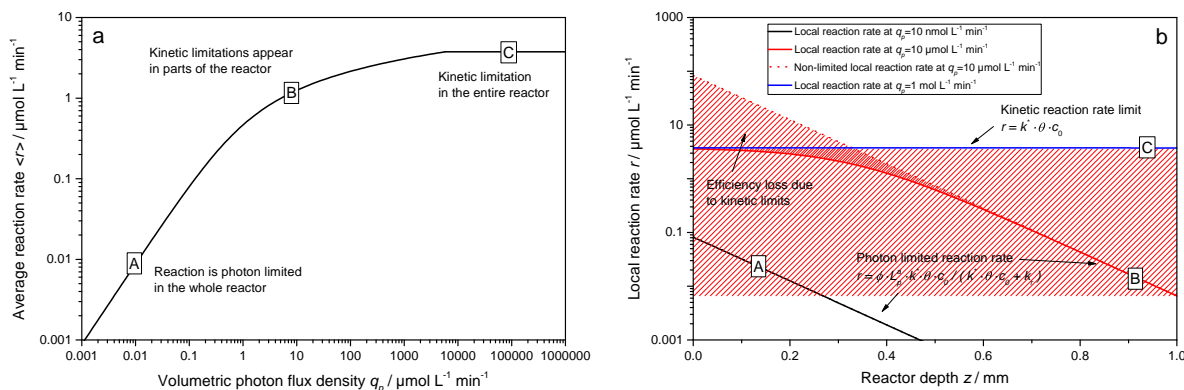


Figure 4.8: Left (a): Exemplary course of the average reaction rate in dependence of the photon flux according to the new model. Right (b): Locally resolved reaction rate as a function of reactor depth for the three cases marked A-C in a. Parameters used: $\phi = 1$, $c_0 = 2.5 \text{ g L}^{-1}$, $k_r = 500 \mu\text{mol L}^{-1} \text{min}^{-1}$, $k_1^* = 1500 \mu\text{mol g}^{-1} \text{min}^{-1}$, $\theta = 1$, $\epsilon = 16.4 \text{ L g}^{-1} \text{cm}^{-1}$, $d = 0.1 \text{ cm}$. [P19]

Figure 4.8 also nicely illustrates the fundamental dilemma of intensifying photocatalytic reactions. In order to avoid kinetic limitations, the light intensity needs to be so low that even at the beginning of the reactor no limitations manifest. This in turn means that in the rest of the reactor, the reaction only proceeds with orders of magnitude lower rates. One way to circumvent that is by using very dilute solutions or small dimensions that the light falloff through the reactor is only small (*e.g.* $< 50\%$). In that case, the reaction rate would not vary so much in the reactor and the average reaction rate is almost equal to the maximum local reaction rate, vastly increasing catalyst efficiency. However, this would also mean that a significant portion of the light is transmitted though the reactor and not used, dramatically reducing the overall photonic efficiency. Another possible solution is to use delocalized internal illumination so that the light distribution in the medium is more homogeneous (see section 5.4). [P19,P23]

Another important reaction parameter is the temperature. While this is one of the most important parameters in thermally activated catalysis and typically described *via* the Arrhenius law, this parameter is only studied in few photocatalytic systems. The rationale behind this seems to be that the reaction is initiated by the massive energy provided by the photons, so room temperature is sufficient to drive the reactions. [14,219–221] Yet, there are many publications which clearly show a temperature dependence of the photocatalytic reactions and use the Arrhenius law to calculate apparent activation energies (E_A^*) of 5 to 28 kJ mol^{-1} . [222–226]

The Arrhenius law can easily be integrated into the present kinetic model by modulating the kinetic constant accordingly. [P19] As shown exemplary in Figure 4.9, the temperature effects are strongly masked at lower light intensities, as improving the kinetics in that regime has negligible impact on the overall reaction, which is limited by the available photons here. However, at high light intensities, the temperature effect becomes much more prominent as it presents a way to

overcome kinetic limitation there and to extend the linear regime. Consequently, using higher temperatures is a promising approach to combine high productivity and high quantum yield. [P19]

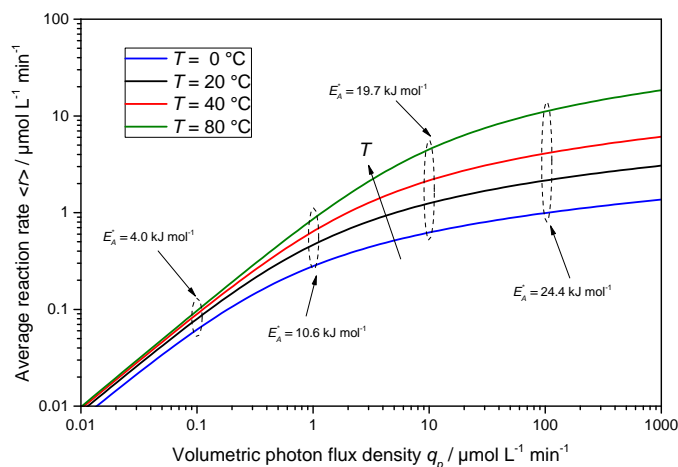


Figure 4.9: The change in average reaction rate is a function of light intensity for different temperatures calculated according to the new model. Also shown are the apparent activation energies E_a^* obtained from Arrhenius plots at a given light intensity. Parameters used: $\phi = 1$, $c_0 = 2.5 \text{ g L}^{-1}$, $k_r = 500 \mu\text{mol L}^{-1} \text{min}^{-1}$, $A = 3.325 \times 10^8 \mu\text{mol g}^{-1} \text{min}^{-1}$, $E_A = 30 \text{ kJ mol}^{-1}$, $\theta = 1$, $\epsilon = 16.4 \text{ L g}^{-1} \text{cm}^{-1}$, $d = 0.1 \text{ cm}$. [P19]

At this stage, the kinetic model is able to holistically model the reaction rate of a photocatalytic reaction in dependence of light intensity, catalyst and substrate concentration, temperature and reactor geometry using a simple explicit rate law. If course there are also some limitations in the applicability due to the assumptions made such as the negligence of scattering and the requirement of collimated uni-directional illumination. However, as shown in the following chapter, the model is able to quite accurately model the behavior of a number of experimentally studied reactions and thereby allows performance prediction and optimization of process conditions. [P19]

Noteworthy, if only the photon flux is varied in the set of experiments, the reaction rate can be abstracted to a very simple form which only has two parameters, eqn. 4.7. [227] However, in this case only the empirical parameters β and γ are used and it is not possible to obtain the direct physical information contained in the more detailed parameters.

$$\langle r \rangle = \beta \cdot \ln(\gamma \cdot q_p + 1) \quad (4.7)$$

It is instead recommended that not only light intensity but also at least one other parameter, *e.g.*, catalyst concentration or temperature, is studied at the same time to better resolve the properties of the catalyst. Since the intrinsic quantum yield is an optical property of the material while charge transfer kinetics and recombination rate are catalytic properties, this model allows to deconvolute the observed performance of the material into optical and catalytic effects.

According to the model, the optical properties of a photocatalyst primarily determine the performance at low light intensity, while the catalytic properties are important for the performance under high light intensity, this is illustrated in Figure 4.10. Consequently, if two catalysts are compared to each other, they may exhibit a different rank order if measured at different light intensities, even if all other parameters are kept constant. Since the inflection point between linear and non-linear regime is also dependent on the optical density this could even lead to different results depending on just the geometry of the employed reaction setup. This might explain a lot of ambiguity in the literature concerning catalyst optimization where often different “best catalysts” are reported for the same reaction.

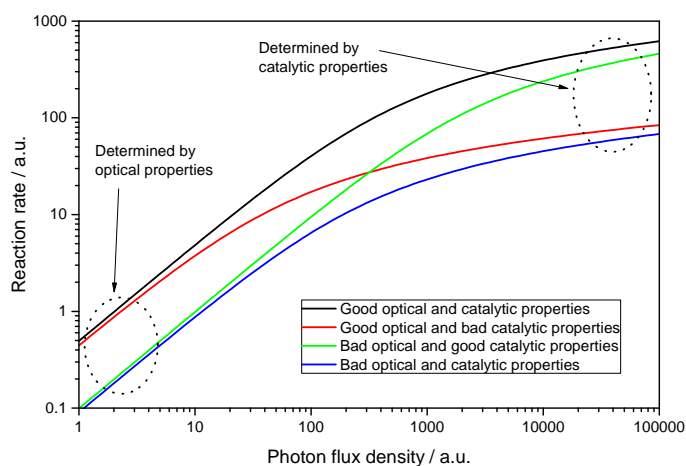


Figure 4.10: Schematic illustration of the reaction rate response to the light intensity for catalysts with good or bad optical and catalytic properties according to the model.

Furthermore, this methodology of separating optical from catalytic effects may help to more accurately determine structure-activity relationships of photocatalyst materials in future in order to pave the way for a knowledge-based catalyst design.

4.4 Applications of the new kinetic model

As a first step, the data obtained while studying the photocatalytic reduction of molecular oxygen to hydrogen peroxide (see section 4.1) was used to validate the model. As shown in Figure 4.11, the inter-dependence of both light intensity and catalyst concentration was quite successfully explained with this approach. Also, the dependence on substrate (molecular oxygen) concentration and temperature could be modeled rather well. The former was accomplished using a standard Langmuir isotherm and the latter by integrating an Arrhenius term into the kinetic constant, as described in section 4.3. [P15]

Overall, the results suggest that efficiency losses are mainly a result of the photocatalyst's poor electron-transfer kinetics to molecular oxygen. Consequently, by increasing the oxygen partial pressure, catalyst concentration and the temperature, the reaction rates and efficiency could be significantly increased, particularly at high photon flux. The best obtained values of up to 19.8% apparent quantum yield also presented a new benchmark for this reaction using non-modified TiO_2 . [P15] Contrary to many other studies, this efficiency increase was achieved not by altering the catalyst but solely by the model-based optimization of the reaction conditions.

As a next example, the photocatalytic reduction of nitrobenzene in ethanol was analyzed in detail with the model. [P20] In this reaction, nitrobenzene is reduced in six consecutive steps to aniline, while at the same time ethanol is oxidized to acetaldehyde. [228–230] These two products may even undergo further condensation to form quinoline compounds. [231–233]

The results indicated that the employed photocatalyst (Aeroxide P25) is a very good light absorber and could theoretically reach an apparent quantum yield of up to 184% in the absence of any other limitations. In this reaction, more than unity efficiency (up to 200%) are theoretically possible due to the current doubling effect. Remarkably, by using the model to further optimize the reaction conditions, up to 142% apparent quantum yield were experimentally confirmed. This presents the highest value reported to date for an organic synthesis reaction performed

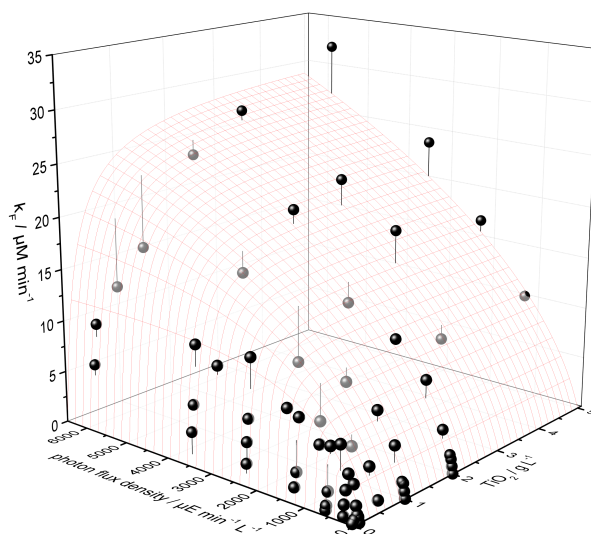


Figure 4.11: Interdependence of the measured H_2O_2 formation rate constant k_F on the catalyst concentration and the photon flux density shown as black and dark gray dots. Also shown is the calculated best fit to the proposed model as a surface plot; the vertical lines attached to the data points show their respective difference to the calculation. Data points that are black mean they are on or above the surface plot, and dark gray data points signify they are below the surface. [P15]

with heterogeneous photocatalysis and proves that these reactions may indeed be very efficient if properly optimized. [P20] Even at very high productivity of up to $7 \text{ g L}^{-1} \text{ h}^{-1}$ the efficiency was still very high (124 %) demonstrating the feasibility of using heterogeneous photocatalysis in large-scale synthesis reactions with acceptable space-time yield. [P20]

The photocatalytic oxidation of hydrogen chloride to chlorine (the photocatalytic equivalent of the Deacon process) was also analyzed using the model. [234] [P17] Since this is a gas-phase reaction studied using an immobilized photocatalyst film, direct application of the new kinetic model proved a bit complicated. However, by treating only the volume of the $36 \mu\text{m}$ thick porous photocatalyst film as the whole reaction volume, assuming no reaction happens in the gas-phase away from the photocatalyst, the model could be easily adapted to the present case. [P17] In this particular case, the model-based analysis revealed that the two reactants, hydrogen chloride and molecular oxygen, likely adsorb on separate sites. This was a conclusion based on the fact that a competitive adsorption isotherm approach did not yield a satisfactory fit to the model while two independent adsorption isotherms could explain the experimental results perfectly. [P17]

Overall, the model reproduced the measured data points and was able to simulate the effect of the reactant concentrations, light intensity and temperature. As shown in Figure 4.13, the degree of accuracy is quite remarkable for the latter two cases. Noteworthy, the non-linearity in the light intensity dependence suggests a strong kinetic limitation of the reaction which is also substantiated by the fact that the temperature-dependence is almost ideally exponential. However, in the latter case, there is a slight deviation from ideal Arrhenius behavior, and our model actually fits better here due to the fact that at higher temperature, the kinetic limitation begins to lose in dominance and other factors also play a role. [P17]

As mentioned above in this case, intrinsic kinetics of the catalyst seem to be the limiting factor that prevent higher efficiency and turnover rates. Higher temperatures could help to overcome this but would shift the equilibrium of the reaction away from the product side and thereby

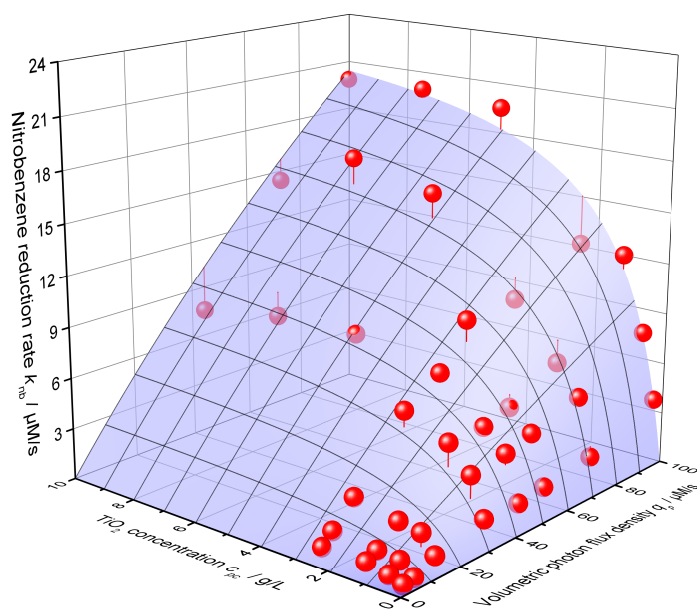


Figure 4.12: 3D-Plot of the nitrobenzene reduction rate as a function of both the volumetric photon flux density and the photocatalyst concentrations. The blue surface shows the best calculated fit according to the new kinetic model. Deviations from the calculation are illustrated by vertical lines attached to the data points. [P20]

limit the maximum attainable conversion. Alternatively, employing a better catalyst, *e.g.*, by employing co-catalyst materials, could solve this problem. Figure 4.14 illustrates that a better catalyst with a higher kinetic constant could extend the linear regime and increase the overall observed reaction rate significantly, particularly at higher photon flux. [P17]

Notably, other authors have also taken up the model to evaluate their own data. For instance, recently the photocatalytic degradation of dichloroacetic acid in a black-body reactor was successfully modeled using this approach. [227] Even though in this case the simplification of the linear light path does not hold true because a point light source was applied, the calculation still yielded a good fit. This is likely due to the fact that if the change in diameter between the inner shell housing the light source and the whole reactor is not very high, also the radial light attenuation can be neglected.

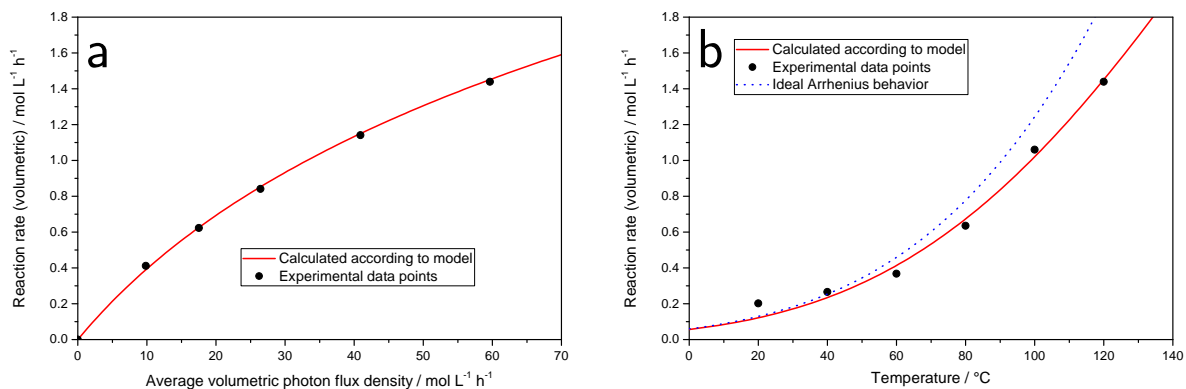


Figure 4.13: Reaction rate of the photocatalytic oxidation hydrogen chloride to molecular chlorine in dependence of a) the light intensity and b) the temperature. [P17]

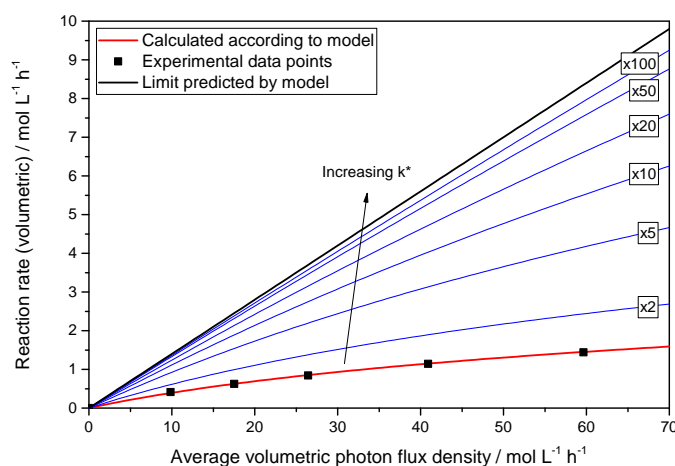


Figure 4.14: Simulation of the theoretical reaction rate of the photocatalytic oxidation hydrogen chloride to molecular chlorine in dependence of the light intensity with hypothetically higher kinetic constants. [P17]

4.5 Modeling and optimization of photoenzymatic cascade reactions

One very interesting application of semiconductor photocatalysis is to couple them with enzymes in what we call photoenzymatic cascade reactions. Here the idea is to combine the exceptional catalytic selectivity of enzymes with the photocatalysts' ability to create high-energy reagents. [235] Of particular interest in this topic are hydrogen peroxide dependent enzymes such as peroxidase and peroxygenase enzymes, which selectively catalyze oxygen-transfer reactions using hydrogen peroxide as stoichiometric reagent. Figure 4.15 illustrates a selection of reactions which have been reported with these enzyme classes. [P18]

These catalysts owe their exceptional reactivity to highly reactive heme groups in the active site. In the resting state, this contains an Fe(III)-ion which after activation by reaction with hydrogen peroxide becomes a highly reactive Fe(IV) radical cation, which is also called Compound I. This may undergo two subsequent reactions with the substrate *via* the so-called Compound II intermediate to ultimately transfer an oxygen atom and regenerating itself to the resting state. [236–239] [P18]

However, the challenge in using these enzymes lies in the fact that while they require stoichiometric quantities of peroxide to function, they are often unstable even under millimolar concentrations of it. The reason for this can be found in other possible reactions with peroxides as shown in Figure 4.16. If Compound I reacts with an additional molecule of hydrogen peroxide this results in the effective disproportionation of two peroxide molecules to water and dioxygen, which constitutes the well-known catalase reaction. If in this pathway the intermediately formed Compound II reacts with yet another hydrogen peroxide molecule, hydroxyl radicals may be formed as a result of a Haber-Weiss reaction. This is also known as “catalase malfunction” and effectively inactivates the enzyme by irreversibly destroying the heme compound. Since three molecules of peroxide are required for this to happen, its rate scales exponentially with the peroxide concentration, giving rise to the high sensitivity of enzymes to even moderate peroxide concentrations. [240] [P18]

For a productive process it is therefore critical that the peroxide is continuously supplied in low concentrations. Amongst other methods evaluated for this purpose such as enzymatic, catalytic or electrochemical in-situ hydrogen peroxide generation, [241–252] one very advantageous way of doing that is by using semiconductor photocatalysis. [253] [P12,P13]

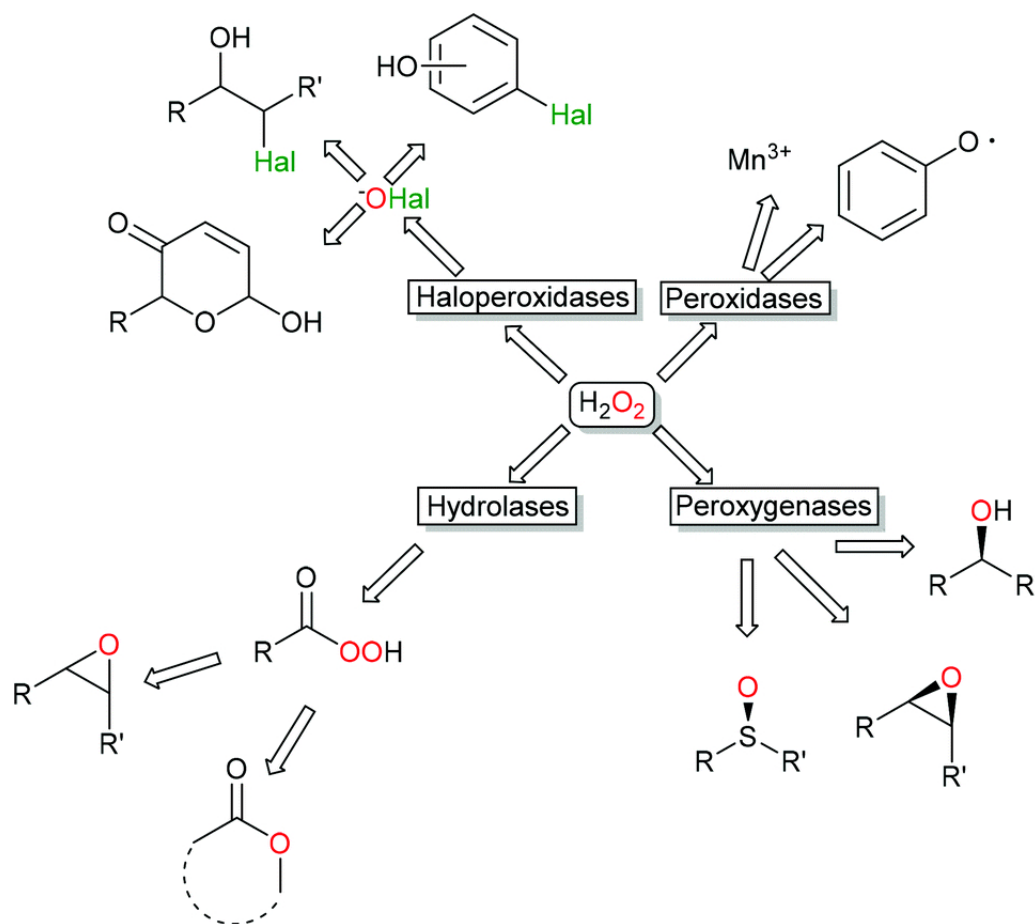


Figure 4.15: An overview of different reported reactions involving enzymes and hydrogen peroxide. [P18]

As discussed in detail in section 4.1, semiconductors such as TiO_2 can reduce molecular oxygen to hydrogen peroxide. Since they also degrade it at higher concentration, there is an intrinsic limit in the maximum H_2O_2 concentration reached in this system. Since this limit is typically well below the critical millimolar range, this can be considered as quite a powerful safety mechanism that effectively prevents peroxide runaway. Regardless, the generation of surplus hydrogen peroxide should still be avoided to achieve an overall efficient system. Therefore, the peroxide generation rate needs to be precisely tuned its consumption by the enzyme, which is now possible thanks to the detailed kinetic studies described in the previous sections.

However, these photocatalysts are also able to form a number of very reactive oxidizing radicals, namely superoxide and hydroxyl radicals, which may interfere with the enzyme and deactivate it. [P14] Particularly the latter are known to react with the heme group and lead to its irreversible degradation. [240] Consequently, it was observed that the enzyme deactivation rate in the photoenzymatic system (studied using the model reaction of ethyl benzene hydroxylation by AaeUPO coupled with TiO_2) increases linearly with the light intensity, in line with both the superoxide and hydroxyl radical formation rates. However, since hydroxyl radicals are mainly formed during water oxidation, they may be effectively suppressed if an alternative electron donor such as an alcohol is used. It was found that the addition of only 5 vol.% methanol decreased the hydroxyl radical formation rate by more than three orders of magnitude (Table 4.3). At the same time, the enzyme deactivation rate was reduced by 83%. Since the superoxide formation was in this case not reduced by instead significantly increased, it was concluded that hydroxyl

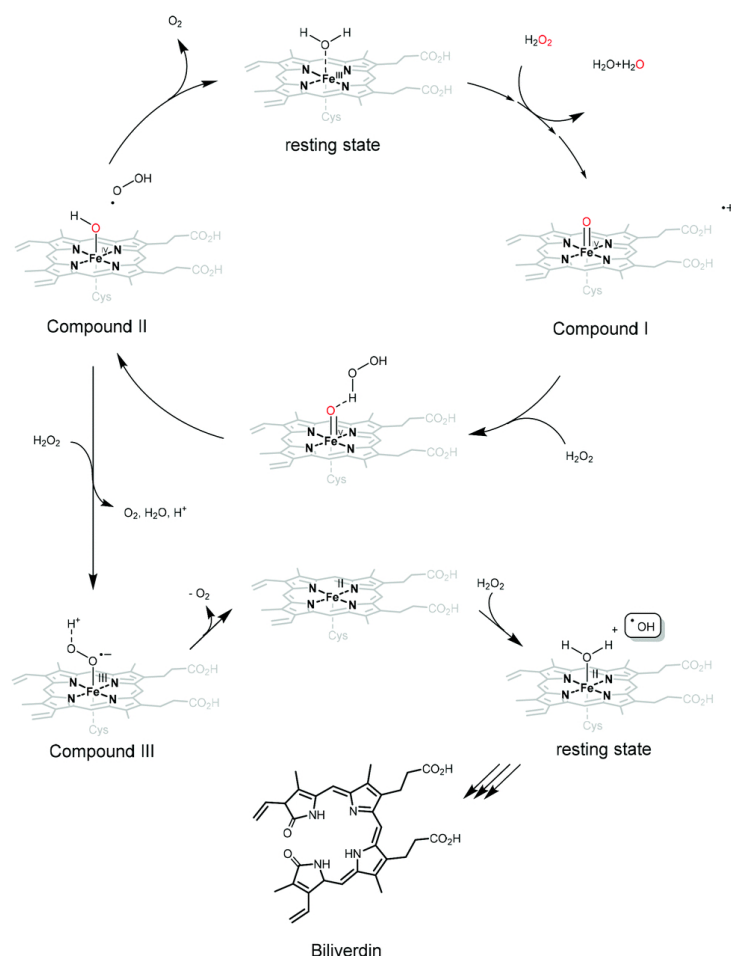


Figure 4.16: The proposed pathway of H_2O_2 -mediated inactivation in peroxygenase enzymes *via* malfunction within the catalase catalytic cycle. [P18]

radicals are indeed the main compound that leads to inactivation. [P14]

Table 4.3: Effect of different electron donors on the and ROS generation during the photoenzymatic hydroxylation of ethyl benzene with TiO_2 and AaeUPO. [P14]

Electron donor	Formation of $\cdot\text{OH}$	Formation of $\text{O}_2^{\cdot-}$	Formation of H_2O_2	Enzyme deact.	TON
Water	$732\,000\text{ nM h}^{-1}$	$280\text{ }\mu\text{M h}^{-1}$	$200\text{ }\mu\text{M h}^{-1}$	52 nM h^{-1}	4000
Methanol	240 nM h^{-1}	$1140\text{ }\mu\text{M h}^{-1}$	$460\text{ }\mu\text{M h}^{-1}$	9 nM h^{-1}	40 000
2-propanol	220 nM h^{-1}	<i>n. d.</i>	$330\text{ }\mu\text{M h}^{-1}$	12 nM h^{-1}	30 000
<i>t</i> -butanol	530 nM h^{-1}	<i>n. d.</i>	$460\text{ }\mu\text{M h}^{-1}$	17 nM h^{-1}	31 000

The addition of an alcohol has the additional advantage of increasing the reduction rate of oxygen as well as the solubility of both oxygen and the hydrophobic substrate. Even though similar effects could be achieved with other alcohols, methanol has the advantage of only small amounts of intermediates accumulating during the reaction (see section 4.2) and was therefore preferred.

The ultimate goal of this work will encompass a complete kinetic model of the entire photoenzymatic process, consisting of the photocatalytic hydrogen peroxide generation, the different enzymatic reactions as well as the enzyme deactivation. This model could then be used to completely simulate the process and predict optimum reaction conditions, which due to the

complexity of the system, is extremely difficult to do analytically. We have not yet succeeded completely with this part as a detailed kinetic analysis for the employed enzyme, taking catalase activity, side-reactions and inactivation into account, was not yet available. However, we were still able to optimize the photocatalytic hydrogen peroxide formation for a given enzymatic system. This resulted in either the highest turnover number (220 000), apparent quantum yield (13.6 %) or space-time yield ($2.6 \text{ g L}^{-1} \text{ d}^{-1}$) for a photo-driven AaeUPO-catalyzed reaction reported to far. [\[P14\]](#)

5 Reactor concepts for efficient photocatalytic processes

As photocatalytic reactions require photons basically as stoichiometric reagents, their efficient generation and transport into the reaction medium is an essential part of the design of photocatalytic processes. Particularly the development of suitable reactors presents a major challenge as they need to either incorporate the light sources or be transparent to allow illumination from outside. Additionally, the distribution of the light inside the reaction medium is very important to achieve efficient systems. Efficient photoreactor systems are not just relevant for photocatalytic processes but also for other light-driven processes such as pure photochemical conversions, reactions utilizing photoenzymes or the cultivation of phototrophic microorganisms.^[254] [P21,P22]

This chapter gives a general overview of different design aspects for photocatalytic processes and summarizes the work published by the author in this context in the papers **P21-P23**. Additionally, a personal perspective of the future prospects of photocatalysis in the chemical industry is given at the end of the thesis.

5.1 General considerations

As described in detail in section 4.3, efficient photocatalytic processes require a homogeneous as possible light distribution in the reactor. At the same time, high photocatalyst loadings are required to achieve a high catalyst surface area. However, the latter results in extremely low light penetration depths of typically a few millimeters at best.^[255,256] Consequently, there will be a dramatic falloff of light intensity over several orders of magnitude in medium- or large-scale reactors.

The desire to achieve high specific light intensities and also to minimize “dark spots” has sparked an explosive interest in reactor systems with at least one very small dimension such as photomicroreactors or falling film reactors.^[257–260] [P22] Particularly the former are very popular in combination with flow chemistry as they can be easily constructed by just coiling a transparent tube around the light source.^[261,262] While these reactor types achieve good illumination efficiency and a high surface-to-volume-ratio, they are often area intensive in scale-up and challenging to use with heterogeneous catalysts.^[263,264] The approach of scaling up by numbering-up of these small volume reactors also leads to significant challenges in process monitoring and control.^[265,266] Additionally, the requirement to invest into specific equipment such as photoreactors is often a substantial obstacle for industrial implementation of these processes.

An alternative approach to solve this dilemma is using internal illumination, *i.e.*, put the light sources inside the reaction medium. Different types of internal illumination such as immersion lamps^[267] or optical fibers^[268,269] have successfully been applied. Furthermore, wireless powering of light sources for photocatalytic degradation of organic pollutants has shown good efficiencies. Since the light sources themselves can easily be added to or separated from the reactor, it allows for more flexibility in selecting a suitable reactor. Even standard multi-purpose reactors can be used with these Wireless Light Emitters (WLEs) to power photocatalytic reactions, which could tremendously help wide-spread application. Since they move freely within the

reaction medium, they do not present significant obstacles for and can readily be used in stirred systems. The principle has for example been demonstrated with light emitters powered *via* the piezoelectric effect by ultrasonic waves^[270] or microwave-powered electrodeless discharge lamps.^[271,272] Compared to those methods, resonant inductive coupling (RIC) for powering of internal light sources, has great advantages for up-scaling photocatalytic processes.^[273] [P23] The possible energy transfer efficiency is already >75 % and the conductivity of water shows no negative impact on the energy transfer efficiency.^[274,275] Since there are already many well known applications for RIC such as charging of portable devices,^[276] endoscopic capsules^[277] or other sensors,^[278,279] synergistic effects in future development can be expected. LEDs powered by RIC were successfully introduced as a means to illuminate photobioreactors^[254,280] and for wastewater treatment.^[281] In both cases, a multitude of WLEs in a suspension was powered by one transmitting inductor while a single WLE consists at least of one LED, a receiving coil and a capacitance forming a resonant circuit. Our approach to utilize this technology for photocatalysis is described in section 5.4.

5.2 Suitable light sources

The most interesting light source to use is certainly the Sun, as it is available basically everywhere, free of charge and completely environmentally neutral. However, the polychromatic and fluctuating nature of the sunlight in combination with its relatively low intensity (about 1 kW m^{-2} at maximum) pose severe constraints for efficient utilization.

Fluctuations may be compensated by just modulating the production accordingly, this even enables a constant product quality, albeit at a lower average productivity.^[282] The polychromatic nature of the light means that there is always a compromise between the fraction of photons which can be used on the one side and the amount of energy that can be extracted from them on the other (*cf.* the Shockley-Queisser limit for photovoltaic cells).^[283] Even when Nature's idea of combining several photoabsorber materials is adopted in multi-junction or Z-scheme systems, the maximum attainable efficiency falls in the area of about 20 to 30 %.^[284-286] The low intensity may be counteracted by using solar concentrators, which however do not diminish the area demand of the site and also lead to significant side-effects such as intense heating.^[257,287-289]

Therefore, in any application where the desired reaction products are valuable enough to compensate for the energy cost, using artificial light sources is desirable since it enables more intensified, selective and controlled processes. This can still be done using solar energy, which is only first converted into electricity using solar cells and then converted again to the desired artificial light. Amongst the myriad of different technologies developed to create artificial light, in recent years light emitting diodes (LEDs) have solidified their status as the most efficient and versatile candidate.

The last decades have seen exponential increases in LED radiant flux and at the same time a dramatic reduction in costs which has even motivated the formulation of the so-called Haitz' law in analogy to Moore's law, Figure 5.1.^[291,292] Today, blue LEDs with efficiencies above 80 % exceeding 20 W cm^{-2} radiant flux density are already commercially available for very affordable prices (<1 €/W) with UVA variants expected to follow soon due to sharing the same technology basis.^[293] Theoretically, LED efficiency can even exceed unity by consuming ambient heat (Peltier effect), however, this will likely only be possible for (technically uninteresting) low power densities.^[294] Nonetheless, the efficiency of these devices is expected to closely approach unity in the near future, which will practically result in light energy cost matching the equivalent electricity cost.

At the same time, this enables radiant power densities in the range of kW L^{-1} , at which

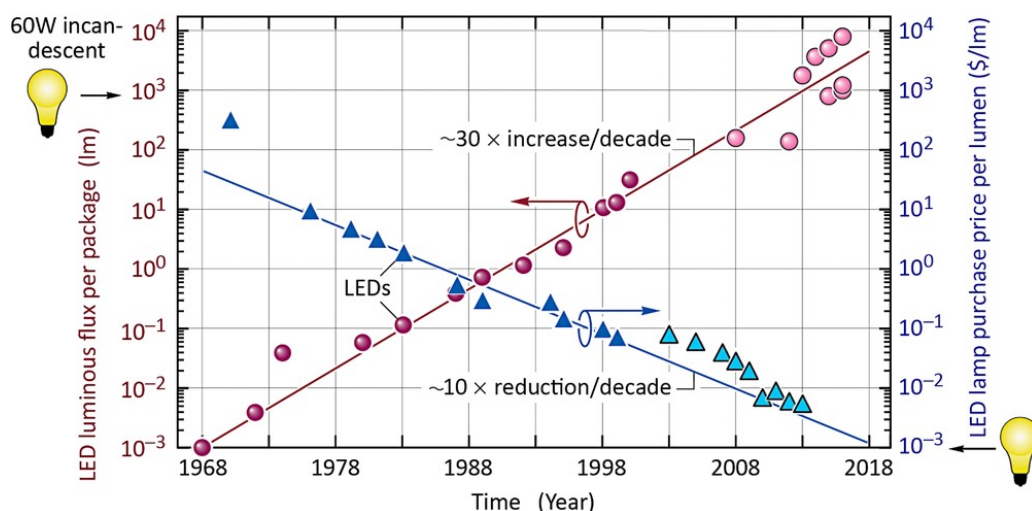


Figure 5.1: The trend in luminous flux and specific costs for LEDs in recent years. ^[290]

point further increases are unreasonable due to the constraints of thermal management. It is noteworthy that at perfect efficiency, this would allow very high reaction rates in the range of $\text{mol L}^{-1} \text{min}^{-1}$.

5.3 Energetic aspects and efficiency

Even though photocatalytic reactions are typically performed under mild conditions, *e.g.* ambient temperature, it always has to be kept in mind that these are high-energy processes due to the photon energy provided. Even when assuming perfect quantum efficiency, the facts that a UVA photon (385 nm) has an energy of 311 kJ mol^{-1} and often more than one photon is required per turnover means practically all of these reactions are highly exothermic. This is true not only for true photocatalytic reactions ($\Delta G < 0$) but also for most photosynthetic reactions ($\Delta G > 0$). For instance the reduction of nitrobenzene in ethanol to aniline and acetaldehyde features a nominal heat of reaction of -296 kJ mol^{-1} which due to the need of at least three UVA photons is further increased to at least $-1280 \text{ kJ mol}^{-1}$ if light energy is considered. ^[P20] The effective heat of reaction can be calculated according to eqn. 5.1 in dependence of the number of required photons per product (n), the photon's molar energy (E_{mol}) and the quantum efficiency (ϕ).

$$H_{r,\text{eff}} = H_r - \frac{n \cdot E_{mol}}{\phi} \quad (5.1)$$

This is plotted exemplary in Figure 5.2 for the mentioned case of nitrobenzene reduction. It is apparent that the heat production is exponentially amplified with lower quantum efficiency, reaching truly astronomical numbers.

This energetic catastrophe resulting from low quantum efficiency might be acceptable when using “free” sunlight, when producing high-value chemicals, *e.g.* pharmaceuticals, or when only very dilute concentrations of pollutants need to be removed, *e.g.* from waste-water. But for the production of commodity chemicals or lower-value intermediates using artificial lighting the associated waste of energy would render the process uneconomical and any “green” claims doubtful. Therefore, it is essential that the latter are operated at very high quantum yield to minimize unproductive thermal losses.

This also highlights that considerable effort needs to be invested into cooling these reactions if they are intensified. Alternatively, it could be considered to utilize the generated heat for

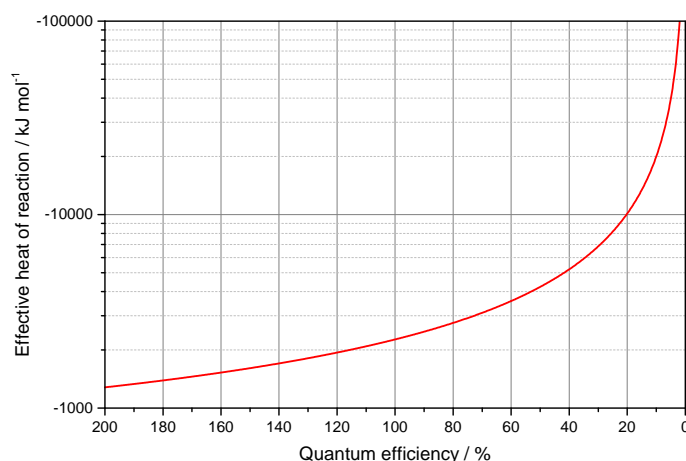


Figure 5.2: The effective heat of reaction of the photocatalytic reduction of nitrobenzene in ethanol in dependence of the quantum yield.

other processes, *e.g.* steam production or industrial drying processes, to increase the overall energy efficiency and economic feasibility of the photocatalytic process. In case of sunlight, this also enables the use of the residual spectrum not absorbed by the photocatalyst as heat. This approach has already been successfully implemented in simultaneous hydrogen production and water evaporation for desalination.^[295]

From an industrial perspective, it would be most useful to generate high pressure steam that can be used to power other chemical or industrial processes or even generate electricity. However, this would require operating the reaction at higher temperatures of ≥ 150 °C. Relatively little is known about the behavior of photocatalysts in that temperature regime as only few researchers ventured into this territory so far - however, with very promising results.^[296,297]

For instance, the photocatalytic oxidation rate of ethylene was found to more than double when the temperature was increased to about 160 °C.^[297] The same study predicts an upper limit of about 300 to 400 °C above which phonon-mediated recombination becomes a problem, which might be overcome by catalyst design though. We also recently discovered that mild temperature increases are beneficial for the photocatalytic reduction of nitrobenzene to aniline, the photocatalytic reduction of molecular oxygen to hydrogen peroxide and the photocatalytic oxidation of hydrogen chloride to chlorine.^[P15,P17,P20] Recently, it has also been reported that the photocatalytic water splitting reaction greatly benefits from elevated temperatures, reaching astonishing quantum yields of more than 80 % at 270 °C.^[296]

5.4 Internal illumination with wireless light emitters

As mentioned above, efficient photoreactors require the light distribution in the reactor to be as homogeneous as possible. The only realistic approach to achieve this in larger-scale reactors is the use of internal illumination techniques. Amongst others, using inductively coupled wireless light emitters (WLEs) is a promising way to accomplish this. The use of delocalized small light sources located inside the reaction medium also allows to directly coat the photocatalyst onto the emitters. This makes the separation and re-use of the photocatalyst much easier and effectively presents a completely integrated system that can be handled just like an ordinary supported catalyst, for instance in fixed-bed or fluidized-bed operation. Even standard stirred tank reactors are an option. This approach has the additional advantage that no light actually enters the

reaction medium anymore, enabling even reactions with light sensitive or strongly absorbing reagents. [P23]

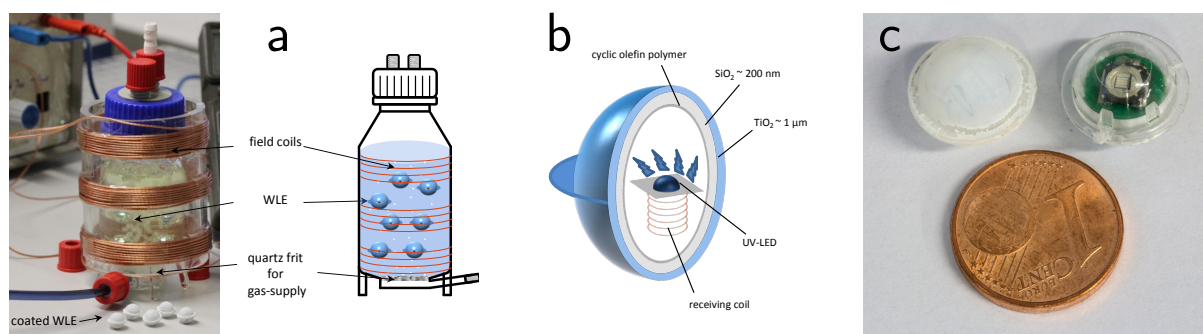


Figure 5.3: A photograph and scheme of the employed setup for the reactions with WLE (a), the composition of each individual WLE (b) and a photograph of an uncoated and a coated WLE with a 1 €cent-coin as scale (c). [P23]

In the first step to demonstrate the feasibility of this concept, the WLEs themselves were designed (Figure 5.3). While the general design of WLEs, comprised of an LED, an induction coil and a capacitor, housed in a polymer shell, was already established for the application in algae cultivation^[280]. However, in several aspects it had to be adapted for the use in photocatalysis, namely the use of UVA-LEDs and corresponding UVA-transparent shell. Since the polymer itself is susceptible to degradation a multi-layer coating was developed consisting of an oxygen plasma treatment to functionalize the polymer, followed by sputtering thin layers of SiO₂ and TiO₂ (Figure 5.3b,c). [P23] These layers serve to protect the polymer from the reaction medium which may consist of strong solvents, acids and bases and also from the photocatalyst which may generate highly oxidizing species. Additionally, it improves the adhesion of the photocatalyst, which is subsequently deposited *via* dip-coating.

These coated WLEs were subsequently used for three model reactions, the generation of hydrogen peroxide from water and molecular oxygen, the decolouration of methylene blue and the reduction of nitrobenzene to aniline. All of these reactions proceeded with photonic efficiencies at least as good as published references, in the case of nitrobenzene reduction, the efficiency was even substantially higher. The reactions were performed in a standard glass flask equipped with glass frit at the bottom for gas supply. The inductive powering was achieved by copper coils mounted on a PMMA tube so it could easily be attached to or removed from the reactor (Figure 5.3a). [P23] This demonstrates that the system is broadly applicable and easily adaptable to existing equipment. Presently, studies are under way to prove the system is also well suited for performing other photochemical processes such as photoenzymatic reactions. [P21]

Also a set of equations was developed which allow the prediction of principle performance indicators such as radiant and photon flux densities in dependence of the fill factor (FF), *i.e.*, how much of the reactor volume is taken up by the WLEs (Figure 5.4). The prediction is that all relevant performance indicators increase exponentially with higher FF. This is the result of both increased light intensity and at the same time reduced reaction medium volume, indicating that tremendous intensification potential exists for the system. Indeed, the onset of this predicted behavior could be observed for photocatalytic H₂O₂-generation when the fill factor was increased up to 27% (Figure 5.4). Theoretically, up to 74% are possible in a closest packing configuration. [P23]

The calculated numbers are quite substantial, given that the achieved radiant flux of 8 mW per WLE was still relatively low. As a result of the resonant inductive coupling and lack of a rectifier in the WLE, the LEDs are driven with alternating current and are therefore only active

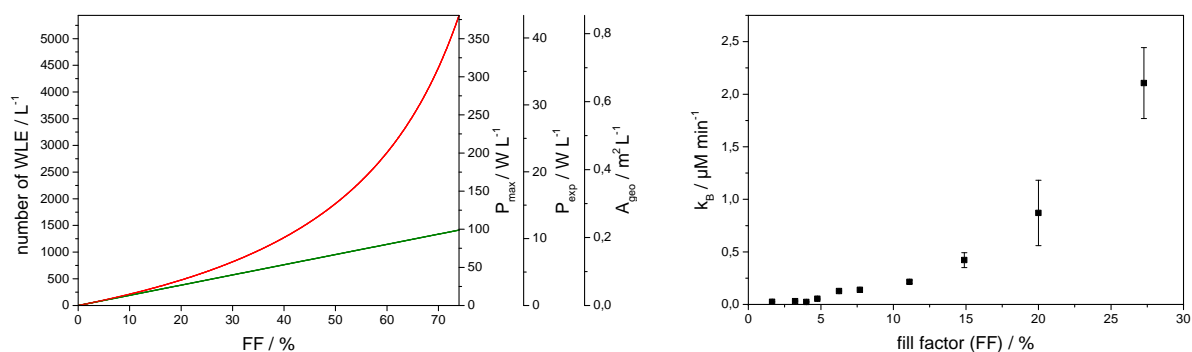


Figure 5.4: Left: The principle performance indicators radiant flux density, assuming maximum rated (P_{max}) or experimentally determined output of the used LEDs (P_{exp}), and geometric catalyst surface (A_{geo}) as a function of fill factor (FF). Shown are the values related to reactor volume (green line) and reaction medium volume (red line). Right: Experimentally determined H_2O_2 formation rates (k_B) using an increasing number of WLEs, expressed as the fill factor. [P23]

for a maximum of half of the time. Also, the strength of the electric field was not yet optimized for the WLE. In future, the WLEs could either be equipped with more than one LED or with a simple rectifier to allow a higher radiant flux. Also, optimizing the electric field with respect to maximum power transfer will undoubtedly increase the light output. [P23] The extremely rapid development in the LED sector has now made high-power LEDs with radiant fluxes upwards of 1 W per unit available. With these, radiant flux densities upwards of 1 kW L^{-1} are possible with the WLE system, which results in a tremendous intensification potential.

By distributing the light sources nearly homogeneously throughout the reaction medium, this system could solve of principal dilemma of achieving highly efficient photocatalytic reactions at scale. From detailed analysis of the kinetic model described in section 4.3 we know that the required activity of the employed photocatalyst in order to prevent efficiency losses is directly proportional to the maximum photon flux density or irradiance encountered at any point in the reaction system, usually at the very surface facing the light source.

In contrast to other photoreactors, the maximum irradiance at any point in the reactor is purely determined by the power of the individual emitter in the WLE system, not by the overall power density. For instance, a WLE of the abovementioned type with 1 cm diameter and a light output of 314 mW has an irradiance of approximately 100 mW cm^{-2} at the outer surface of the half-sphere. At maximum FF, a system employing these devices can have a theoretical power density of up to 1707 W L^{-1} without exceeding the abovementioned irradiance at any point. These calculations assume that the reaction medium is strongly absorbing so that residual light from one WLE does not increase the photon flux observed above others. However, given that typically employed photocatalyst suspensions have light penetration depths of less than a millimeter, this will usually be the case.

In contrast to the WLE system, a tubular reactor with 1 L volume, irradiated through a flat bottom with an area of 50 cm^2 could only achieve a power density of 5 W L^{-1} using the same irradiance limit. To achieve the same maximum power density, an irradiance of 34 W cm^{-2} would be required, more than 300 times the value of the WLE system. Consequently, also the employed catalyst would require a higher activity by the same factor in order to prevent efficiency losses. This demonstrates that the WLE system is vastly superior in achieving scalable efficient reactions at high photon flux.

5.5 Future prospects

For applications with medium to high value products, *e.g.*, in the pharmaceutical or specialties industries, where the energy costs to power the lamps are not critical for the overall process feasibility, concepts such as the abovementioned WLE system will allow readily scalable, efficient and fast photocatalytic reactions. For the production of lower volumes even the currently very popular flow chemistry systems employing transparent tubing are quite feasible.^[298]

Improved systems will likely feature higher power densities to further intensify the processes. However, this needs to be done with care, keeping kinetic limitations in mind to prevent efficiency losses. Also, if power densities in the excess of kW L^{-1} are employed, thermal management will increasingly be an issue. Specific challenges that need to be addressed here in future are to develop improved coatings which are more robust towards abrasion losses during operation. This is a non-trivial task since the device contains electronics and polymers which may not be subjected to high-temperature annealing conditions. Also, the materials used should be carefully re-evaluated while keeping chemical resistance in mind if the technology is applied to syntheses requiring very strong solvents, acids or bases. Finally, the price of the devices should be significantly reduced to facilitate wide-spread usage, considering that for intensified conditions there need to be hundreds to thousands of devices per liter. However, the latter will likely come naturally with larger numbers produced due to the immense scaling effects for polymer and electronics manufacturing.

On the other hand, the generation of low value commodity chemicals (*e.g.* around 1 €/kg) will be challenging even with highly efficient catalysts and reactors. The reason here are the high energy costs for powering the lamps that due to the extremely high heat of reaction (see section 5.3) will usually push the process out of feasibility if the generated heat cannot be exploited.

One way to solve this problem is by utilizing solar light instead of artificial light sources. This can significantly reduce the energy costs for the process but comes at the expense of intensification on account of sunlight having relatively low intensity (approximately 1000 W m^{-2} at 1.5x air mass) and temporal fluctuations. Also, while the sunlight is essentially free of charge, it would still be inefficient to let all the heat generated in the process go to waste.

A much more efficient way to realize these reactions would therefore be to run them at elevated temperature (at least 100°C) in order to use the excess heat from the reaction and light energy in a secondary process such as water desalination or steam generation. This will at least to some extent counter-balance the catastrophic energy balance of these reactions which would otherwise make the reactions economically unfeasible. As a secondary effect, the use of high temperature will also dramatically increase mass-transfer rates and the kinetics of the photocatalyst, enabling faster, more intensified processes.

In terms of employed reactors, internal illumination like with the WLE system are unlikely to succeed as the higher process temperatures are incompatible with the electronics of the LEDs. Nonetheless, there is technically the option of using pseudo-internal illumination with optical fibers.^[299,300] Alternatively, thin slit fixed-bed reactors can be employed, where one wall is coated with the photocatalyst and the other one is transparent, with the light source as surface irradiator behind.^[234] Given that irradiances of up to about 10 W cm^{-2} are possible with current LED technology, conversion rates comparable to industrial electrolyzers (which kind of share the same geometry) can be envisioned. Since the latter have successfully been implemented at scale in the chemical industry for more than a century, this illustrates that from a reaction engineering perspective there are no fundamental problems that prevent the implementation of photocatalytic processes in a similar fashion to produce even commodity chemicals at large scale and finally make Giacomo Ciamician's vision from 1912 reality.^[1]

6 Publications

This chapter lists the author's articles which are the basis of this work. Copies of said articles are reprinted at the end of this thesis in chapter 9 in the order they appear in this list.

- [P1] Bloh, J. Z. Refined Model for the Optimal Metal Content in Semiconductor Photocatalysts. *J. Phys. Chem. C* **2017**, *121*, 844–851, DOI: 10.1021/acs.jpcc.6b09808.
- [P2] Patzsch, J.; Spencer, J. N.; Folli, A.; Bloh, J. Z. Grafted iron(III) ions significantly enhance NO₂ oxidation rate and selectivity of TiO₂ for photocatalytic NO_x abatement. *RSC Adv.* **2018**, *8*, 27674–27685, DOI: 10.1039/C8RA05017A.
- [P3] Bloh, J. Z.; Folli, A.; Macphee, D. E. Photocatalytic NO_x Abatement: Why the Selectivity Matters. *RSC Adv.* **2014**, *4*, 45726–45734, DOI: 10.1039/C4RA07916G.
- [P4] Patzsch, J.; Folli, A.; Macphee, D. E.; Bloh, J. Z. On the underlying mechanisms of the low observed nitrate selectivity in photocatalytic NO_x abatement and the importance of the oxygen reduction reaction. *Phys. Chem. Chem. Phys.* **2017**, *19*, 32678–32686, DOI: 10.1039/C7CP05960D.
- [P5] Folli, A.; Bloh, J. Z.; Strøm, M.; Pilegaard Madsen, T.; Henriksen, T.; Macphee, D. E. Efficiency of Solar-Light-Driven TiO₂ Photocatalysis at Different Latitudes and Seasons. Where and When Does TiO₂ Really Work? *J. Phys. Chem. Lett.* **2014**, *5*, 830–832, DOI: 10.1021/jz402704n.
- [P6] Folli, A.; Bloh, J. Z.; Beukes, E.-P.; Howe, R. F.; Macphee, D. E. Photogenerated Charge Carriers and Paramagnetic Species in (W,N)-Codoped TiO₂ Photocatalysts under Visible-Light Irradiation: An EPR Study. *J. Phys. Chem. C* **2013**, *117*, 22149–22155, DOI: 10.1021/jp408181r.
- [P7] Bloh, J. Z.; Folli, A.; Macphee, D. E. Adjusting Nitrogen Doping Level in Titanium Dioxide by Codoping with Tungsten: Properties and Band Structure of the Resulting Materials. *J. Phys. Chem. C* **2014**, *118*, 21281–21292, DOI: 10.1021/jp507264g.
- [P8] Folli, A.; Bloh, J. Z.; Lecaplain, A.; Walker, R.; Macphee, D. E. Properties and photochemistry of valence-induced-Ti³⁺ enriched (Nb,N)-codoped anatase TiO₂ semiconductors. *Phys. Chem. Chem. Phys.* **2015**, *17*, 4849–4853, DOI: 10.1039/C4CP05521G.
- [P9] Folli, A.; Bloh, J. Z.; Armstrong, K.; Richards, E.; Murphy, D. M.; Lu, L.; Kiely, C. J.; Morgan, D. J.; Smith, R. I.; McLaughlin, A. C.; Macphee, D. E. Improving the Selectivity of Photocatalytic NO_x Abatement through Improved O₂ Reduction Pathways Using Ti_{0.909}W_{0.091}O₂N_x Semiconductor Nanoparticles: From Characterization to Photocatalytic Performance. *ACS Catal.* **2018**, *8*, 6927–6938, DOI: 10.1021/acscatal.8b00521.
- [P10] Folli, A.; Bloh, J. Z.; Macphee, D. Band structure and charge carrier dynamics in (W,N)-codoped TiO₂ resolved by electrochemical impedance spectroscopy combined with UV-vis and EPR spectroscopies. *J. Electroanal. Chem.* **2016**, *780*, 367–372, DOI: 10.1016/j.jelechem.2015.10.033.

- [P11] Patzsch, J.; Bloh, J. Z. Improved photocatalytic ozone abatement over transition metal-grafted titanium dioxide. *Catal. Today* **2018**, *300*, 2–11, DOI: 10.1016/j.cattod.2017.07.010.
- [P12] van Schie, M. M. C. H.; Zhang, W.; Tieves, F.; Choi, D. S.; Park, C. B.; Burek, B. O.; Bloh, J. Z.; Arends, I. W. C. E.; Paul, C. E.; Alcalde, M.; Hollmann, F. Cascading g-C₃N₄ and Peroxygenases for Selective Oxyfunctionalization Reactions. *ACS Catal.* **2019**, *9*, 7409–7417, DOI: 10.1021/acscatal.9b01341.
- [P13] Zhang, W.; Burek, B. O.; Fernández-Fueyo, E.; Alcalde, M.; Bloh, J. Z.; Hollmann, F. Selective Activation of C-H Bonds in a Cascade Process Combining Photochemistry and Biocatalysis. *Angew. Chem. Int. Ed.* **2017**, *56*, 15451–15455, DOI: 10.1002/anie.201708668.
- [P14] Burek, B. O.; de Boer, S. R.; Tieves, F.; Zhang, W.; van Schie, M.; Bormann, S.; Alcalde, M.; Holtmann, D.; Hollmann, F.; Bahnemann, D. W.; Bloh, J. Z. Photoenzymatic Hydroxylation of Ethylbenzene Catalyzed by Unspecific Peroxygenase: Origin of Enzyme Inactivation and the Impact of Light Intensity and Temperature. *ChemCatChem* **2019**, *11*, 3093–3100, DOI: 10.1002/cctc.201900610.
- [P15] Burek, B. O.; Bahnemann, D. W.; Bloh, J. Z. Modeling and Optimization of the Photocatalytic Reduction of Molecular Oxygen to Hydrogen Peroxide over Titanium Dioxide. *ACS Catal.* **2019**, *9*, 25–37, DOI: 10.1021/acscatal.8b03638.
- [P16] Burek, B. O.; Timm, J.; Bahnemann, D. W.; Bloh, J. Z. Kinetic effects and oxidation pathways of sacrificial electron donors on the example of the photocatalytic reduction of molecular oxygen to hydrogen peroxide over illuminated titanium dioxide. *Catal. Today* **2019**, *335*, 354–364, DOI: 10.1016/j.cattod.2018.12.044.
- [P17] Rath, T.; Bloh, J. Z.; Lücken, A.; Ollegott, K.; Muhler, M. Model-Based Analysis of the Photocatalytic HCl Oxidation Kinetics over TiO₂. *Ind. Eng. Chem. Res.* **2020**, *59*, 4265–4272, DOI: 10.1021/acs.iecr.9b05820.
- [P18] Burek, B. O.; Bormann, S.; Hollmann, F.; Bloh, J. Z.; Holtmann, D. Hydrogen peroxide driven biocatalysis. *Green Chem.* **2019**, *21*, 3232–3249, DOI: 10.1039/C9GC00633H.
- [P19] Bloh, J. Z. A Holistic Approach to Model the Kinetics of Photocatalytic Reactions. *Front. Chem.* **2019**, *7*, 128–140, DOI: 10.3389/fchem.2019.00128.
- [P20] Patzsch, J.; Berg, B.; Bloh, J. Z. Kinetics and Optimization of the Photocatalytic Reduction of Nitrobenzene. *Front. Chem.* **2019**, *7*, 289–298, DOI: 10.3389/fchem.2019.00289.
- [P21] Zhang, W.; Ma, M.; Huijbers, M. M. E.; Filonenko, G. A.; Pidko, E. A.; van Schie, M.; de Boer, S.; Burek, B. O.; Bloh, J. Z.; van Berkel, W. J. H.; Smith, W. A.; Hollmann, F. Hydrocarbon Synthesis via Photoenzymatic Decarboxylation of Carboxylic Acids. *J. Am. Chem. Soc.* **2019**, *141*, 3116–3120, DOI: 10.1021/jacs.8b12282.
- [P22] Bloh, J. Z.; Marschall, R. Heterogeneous Photoredox Catalysis: Reactions, Materials, and Reaction Engineering. *European J. Org. Chem.* **2017**, *2017*, 2085–2094, DOI: 10.1002/ejoc.201601591.
- [P23] Burek, B. O.; Sutor, A.; Bahnemann, D. W.; Bloh, J. Z. Completely integrated wirelessly-powered photocatalyst-coated spheres as a novel means to perform heterogeneous photocatalytic reactions. *Catal. Sci. Technol.* **2017**, *7*, 4977–4983, DOI: 10.1039/C7CY01537B.

7 References

- [1] Ciamician, G. The Photochemistry of the Future. *Science (80-.)*. **1912**, *36*, 385–394.
- [2] Anastas, P.; Eghbali, N. Green chemistry: principles and practice. *Chem. Soc. Rev.* **2010**, *39*, 301–312.
- [3] Ravelli, D.; Dondi, D.; Fagnoni, M.; Albini, A. Photocatalysis. A multi-faceted concept for green chemistry. *Chem. Soc. Rev.* **2009**, *38*, 1999–2011.
- [4] Michelin, C.; Hoffmann, N. Photosensitization and Photocatalysis - Perspectives in Organic Synthesis. *ACS Catal.* **2018**, *8*, 12046–12055.
- [5] Kisch, H. Semiconductor Photocatalysis-Mechanistic and Synthetic Aspects. *Angew. Chem. Int. Ed.* **2013**, *52*, 812–847.
- [6] Palmisano, G.; Augugliaro, V.; Pagliaro, M.; Palmisano, L. Photocatalysis: a promising route for 21st century organic chemistry. *Chem. Commun.* **2007**, 3425–3437.
- [7] Zuo, Z.; Ahneman, D. T.; Chu, L.; Terrett, J. A.; Doyle, A. G.; MacMillan, D. W. C. Merging photoredox with nickel catalysis: Coupling of α -carboxyl sp³-carbons with aryl halides. *Science (80-.)*. **2014**, *345*, 437–440.
- [8] Romero, N. A.; Nicewicz, D. A. Organic Photoredox Catalysis. *Chem. Rev.* **2016**, *116*, 10075–10166.
- [9] Twilton, J.; Le, C.; Zhang, P.; Shaw, M. H.; Evans, R. W.; MacMillan, D. W. C. The merger of transition metal and photocatalysis. *Nat. Rev. Chem.* **2017**, *1*, 52–69.
- [10] Cherevatskaya, M.; König, B. Heterogeneous photocatalysts in organic synthesis. *Russ. Chem. Rev.* **2014**, *83*, 183–195.
- [11] Friedmann, D.; Hakki, A.; Kim, H.; Choi, W.; Bahnemann, D. Heterogeneous photocatalytic organic synthesis: state-of-the-art and future perspectives. *Green Chem.* **2016**, *18*, 5391–5411.
- [12] Ghosh, I.; Khamrai, J.; Savateev, A.; Shlapakov, N.; Antonietti, M.; König, B. Organic semiconductor photocatalyst can bifunctionalize arenes and heteroarenes. *Science (80-.)*. **2019**, *365*, 360–366.
- [13] Bahnemann, D. Photocatalytic water treatment: solar energy applications. *Sol. Energy* **2004**, *77*, 445–459.
- [14] Malato, S.; Fernández-Ibáñez, P.; Maldonado, M.; Blanco, J.; Gernjak, W. Decontamination and disinfection of water by solar photocatalysis: Recent overview and trends. *Catal. Today* **2009**, *147*, 1–59.
- [15] Chong, M. N.; Jin, B.; Chow, C. W.; Saint, C. Recent developments in photocatalytic water treatment technology: A review. *Water Res.* **2010**, *44*, 2997–3027.

- [16] Ballari, M.; Hunger, M.; Hüsken, G.; Brouwers, H. NO_x photocatalytic degradation employing concrete pavement containing titanium dioxide. *Appl. Catal. B Environ.* **2010**, *95*, 245–254.
- [17] Ângelo, J.; Andrade, L.; Mendes, A. Highly active photocatalytic paint for NO_x abatement under real-outdoor conditions. *Appl. Catal. A Gen.* **2014**, *484*, 17–25.
- [18] Bianchi, C. L.; Pirola, C.; Galli, F.; Vitali, S.; Minguzzi, A.; Stucchi, M.; Manenti, F.; Capucci, V. NO_x degradation in a continuous large-scale reactor using full-size industrial photocatalytic tiles. *Catal. Sci. Technol.* **2016**, *6*, 2261–2267.
- [19] Fan, W.; Chan, K. Y.; Zhang, C.; Zhang, K.; Ning, Z.; Leung, M. K. Solar photocatalytic asphalt for removal of vehicular NO_x: A feasibility study. *Appl. Energy* **2018**, *225*, 535–541.
- [20] Schneider, J.; Matsuoka, M.; Takeuchi, M.; Zhang, J.; Horiuchi, Y.; Anpo, M.; Bahnemann, D. W. Understanding TiO₂ Photocatalysis: Mechanisms and Materials. *Chem. Rev.* **2014**, *114*, 9919–9986.
- [21] Fujishima, A.; Rao, T. N.; Tryk, D. A. Titanium dioxide photocatalysis. *J. Photochem. Photobiol. C Photochem. Rev.* **2000**, *1*, 1–21.
- [22] Balzani, V.; Bergamini, G.; Ceroni, P. Light: A Very Peculiar Reactant and Product. *Angew. Chem. Int. Ed.* **2015**, *54*, 11320–11337.
- [23] Qian, R.; Zong, H.; Schneider, J.; Zhou, G.; Zhao, T.; Li, Y.; Yang, J.; Bahnemann, D. W.; Pan, J. H. Charge carrier trapping, recombination and transfer during TiO₂ photocatalysis: An overview. *Catal. Today* **2019**, *335*, 78–90.
- [24] Zhai, Q.; Xie, S.; Fan, W.; Zhang, Q.; Wang, Y.; Deng, W.; Wang, Y. Photocatalytic conversion of carbon dioxide with water into methane: Platinum and Copper(I) oxide co-catalysts with a core-shell structure. *Angew. Chem. Int. Ed.* **2013**, *52*, 5776–5779.
- [25] Busser, G. W.; Mei, B.; Pougin, A.; Strunk, J.; Gutkowski, R.; Schuhmann, W.; Willinger, M. G.; Schlögl, R.; Muhler, M. Photodeposition of copper and chromia on gallium oxide: The role of co-catalysts in photocatalytic water splitting. *ChemSusChem* **2014**, *7*, 1030–1034.
- [26] Lüken, A.; Muhler, M.; Strunk, J. On the role of gold nanoparticles in the selective photooxidation of 2-propanol over Au/TiO₂. *Phys. Chem. Chem. Phys.* **2015**, *17*, 10391–10397.
- [27] Li Puma, G.; Brucato, A. Dimensionless analysis of slurry photocatalytic reactors using two-flux and six-flux radiation absorption-scattering models. *Catal. Today* **2007**, *122*, 78–90.
- [28] Camera-Roda, G.; Loddo, V.; Palmisano, L.; Parrino, F. Guidelines for the assessment of the rate law of slurry photocatalytic reactions. *Catal. Today* **2016**, *281*, 221–230.
- [29] Camera-Roda, G.; Augugliaro, V.; a.G. Cardillo,; Loddo, V.; Palmisano, L.; Parrino, F.; Santarelli, F. A reaction engineering approach to kinetic analysis of photocatalytic reactions in slurry systems. *Catal. Today* **2015**, *259*, 87–96.
- [30] Sagawe, G.; Satuf, M. L.; Brandi, R. J.; Muschner, J. P.; Federer, C.; Alfano, O. M.; Bahnemann, D.; Cassano, A. E. Analysis of photocatalytic reactors employing the photonic efficiency and the removal efficiency parameters: Degradation of radiation absorbing and nonabsorbing pollutants. *Ind. Eng. Chem. Res.* **2010**, *49*, 6898–6908.

-
- [31] Minero, C.; Vione, D. A quantitative evaluation of the photocatalytic performance of TiO₂ slurries. *Appl. Catal. B Environ.* **2006**, *67*, 257–269.
- [32] Cassano, A. E.; Martin, C. A.; Brandi, R. J.; Alfano, O. M. Photoreactor Analysis and Design: Fundamentals and Applications. *Ind. Eng. Chem. Res.* **1996**, *34*, 2155–2201.
- [33] Ziegenbalg, D.; Wriedt, B.; Kreisel, G.; Kralisch, D. Investigation of Photon Fluxes within Microstructured Photoreactors Revealing Great Optimization Potentials. *Chem. Eng. Technol.* **2016**, *39*, 123–134.
- [34] Mendive, C. B.; Hansmann, D.; Bahnemann, D. W.; Bredow, T. New Insights into the Mechanism of TiO₂ Photocatalysis: Thermal Processes beyond the Electron-Hole Creation. *J. Phys. Chem. C* **2011**, *115*, 19676–19685.
- [35] Choi, W.; Termin, A.; Hoffmann, M. R. The Role of Metal Ion Dopants in Quantum-Sized TiO₂: Correlation between Photoreactivity and Charge Carrier Recombination Dynamics. *J. Phys. Chem.* **1994**, *98*, 13669–13679.
- [36] Bloh, J. Z.; Dillert, R.; Bahnemann, D. W. Zinc Oxide Photocatalysis: Influence of Iron and Titanium Doping and Origin of the Optimal Doping Ratio. *ChemCatChem* **2013**, *5*, 774–778.
- [37] Zhou, M.; Yu, J.; Cheng, B. Effects of Fe-doping on the Photocatalytic Activity of Mesoporous TiO₂ Powders Prepared by an Ultrasonic Method. *J. Hazard. Mater.* **2006**, *137*, 1838–1847.
- [38] Tahiri, H.; Serpone, N.; Le van Mao, R. Application of Concept of Relative Photonic Efficiencies and Surface Characterization of a New Titania Photocatalyst Designed for Environmental Remediation. *J. Photochem. Photobiol. A Chem.* **1996**, *93*, 199–203.
- [39] Bloh, J. Z.; Dillert, R.; Bahnemann, D. W. Transition Metal Modified Zinc Oxides for UV and Visible Light Photocatalysis. *Environ. Sci. Pollut. Res.* **2012**, *19*, 3688–3695.
- [40] Zhang, Z.; Wang, C.-C.; Zakaria, R.; Ying, J. Y. Role of Particle Size in Nanocrystalline TiO₂-Based Photocatalysts. *J. Phys. Chem. B* **1998**, *102*, 10871–10878.
- [41] Bloh, J. Z.; Dillert, R.; Bahnemann, D. W. Designing Optimal Metal-Doped Photocatalysts: Correlation between Photocatalytic Activity, Doping Ratio, and Particle Size. *J. Phys. Chem. C* **2012**, *116*, 25558–25562.
- [42] Tong, T.; Zhang, J.; Tian, B.; Chen, F.; He, D. Preparation of Fe³⁺-doped TiO₂ Catalysts by Controlled Hydrolysis of Titanium Alkoxide and Study on their Photocatalytic Activity for Methyl Orange Degradation. *J. Hazard. Mater.* **2008**, *155*, 572–579.
- [43] Liqiang, J.; Xiaojun, S.; Baifu, X.; Baiqi, W.; Weimin, C.; Honggang, F. The Preparation and Characterization of La Doped TiO₂ Nanoparticles and their Photocatalytic Activity. *J. Solid State Chem.* **2004**, *177*, 3375–3382.
- [44] Deng, Q.; Xia, X.; Guo, M.; Gao, Y.; Shao, G. Mn-doped TiO₂ Nanopowders with Remarkable Visible Light Photocatalytic Activity. *Mater. Lett.* **2011**, *65*, 2051–2054.
- [45] Zhu, J.; Deng, Z.; Chen, F.; Zhang, J.; Chen, H.; Anpo, M.; Huang, J.; Zhang, L. Hydrothermal Doping Method for Preparation of Cr³⁺-TiO₂ Photocatalysts with Concentration Gradient Distribution of Cr³⁺. *Appl. Catal. B Environ.* **2006**, *62*, 329–335.

- [46] Houšková, V.; Štengl, V.; Bakardjieva, S.; Murafa, N.; Tyrpekl, V. Efficient Gas Phase Photodecomposition of Acetone by Ru-doped Titania. *Appl. Catal. B Environ.* **2009**, *89*, 613–619.
- [47] Chen, C.; Wang, Z.; Ruan, S.; Zou, B.; Zhao, M.; Wu, F. Photocatalytic Degradation of C.I. Acid Orange 52 in the Presence of Zn-doped TiO₂ Prepared by a Stearic Acid Gel Method. *Dye. Pigment.* **2008**, *77*, 204–209.
- [48] Neubert, S.; Pulisova, P.; Wiktor, C.; Weide, P.; Mei, B.; Guschin, D. A.; Fischer, R. A.; Muhler, M.; Beranek, R. Enhanced Photocatalytic Degradation Rates at Rutile TiO₂ Photocatalysts Modified with Redox Co-Catalysts. *Catal. Today* **2014**, *230*, 97–103.
- [49] Yu, H.; Irie, H.; Shimodaira, Y.; Hosogi, Y.; Kuroda, Y.; Miyauchi, M.; Hashimoto, K. An Efficient Visible-Light-Sensitive Fe(III)-Grafted TiO₂ Photocatalyst. *J. Phys. Chem. C* **2010**, *114*, 16481–16487.
- [50] Nosaka, Y.; Takahashi, S.; Sakamoto, H.; Nosaka, A. Y. Reaction Mechanism of Cu(II)-Grafted Visible-Light Responsive TiO₂ and WO₃ Photocatalysts Studied by Means of ESR Spectroscopy and Chemiluminescence Photometry. *J. Phys. Chem. C* **2011**, *115*, 21283–21290.
- [51] Irie, H.; Miura, S.; Kamiya, K.; Hashimoto, K. Efficient Visible Light-sensitive Photocatalysts: Grafting Cu(II) Ions onto TiO₂ and WO₃ Photocatalysts. *Chem. Phys. Lett.* **2008**, *457*, 202–205.
- [52] Ji, D.-l.; Zhu, J.; Ji, M.; Leng, Y. Enhanced photocatalytic reduction of Cr(VI) by manganese-doped anatase titanium dioxide. *Res. Chem. Intermed.* **2016**, *42*, 5413–5429.
- [53] Zhou, J.; Zhang, Y.; Zhao, X. S.; Ray, A. K. Photodegradation of Benzoic Acid over Metal-Doped TiO₂. *Ind. & Eng. Chem. Res.* **2006**, *45*, 3503–3511.
- [54] Christoforidis, K. C.; Fernández-García, M. Photoactivity and Charge Trapping Sites in Copper and Vanadium Doped Anatase TiO₂ Nano-materials. *Catal. Sci. Technol.* **2016**, *6*, 1094–1105.
- [55] Houšková, V.; Štengl, V.; Bakardjieva, S.; Murafa, N.; Tyrpekl, V. Photocatalytic Properties of Ru-doped Titania Prepared by Homogeneous Hydrolysis. *Cent. Eur. J. Chem.* **2009**, *7*, 259–266.
- [56] Ruggieri, F.; Di Camillo, D.; Maccarone, L.; Santucci, S.; Lozzi, L. Electrospun Cu-, W- and Fe-doped TiO₂ nanofibres for photocatalytic degradation of rhodamine 6G. *J. Nanoparticle Res.* **2013**, *15*, 1982–1992.
- [57] Behnajady, M. A.; Taba, H.; Modirshahla, N.; Shokri, M. Photocatalytic activity of Cu doped TiO₂ nanoparticles and comparison of two main doping procedures. *Micro & Nano Lett.* **2013**, *8*, 345–348.
- [58] Kuncewicz, J.; Ohtani, B. Titania Photocatalysis Through Two-photon Band-gap Excitation with Built-in Rhodium Redox Mediator. *Chem. Commun.* **2015**, *51*, 298–301.
- [59] Nelder, J. A. Inverse Polynomials, a Useful Group of Multi-Factor Response Functions. *Biometrics* **1966**, *22*, 128–141.

-
- [60] Chang, S.-m.; Liu, W.-s. The Roles of Surface-doped Metal Ions (V, Mn, Fe, Cu, Ce, and W) in the Interfacial Behavior of TiO₂ Photocatalysts. *Appl. Catal. B Environ.* **2014**, *156-157*, 466–475.
- [61] Chang, S.-m.; Liu, W.-s. Surface Doping is More Beneficial than Bulk Doping to the Photocatalytic Activity of Vanadium-doped TiO₂. *Appl. Catal. B Environ.* **2011**, *101*, 333–342.
- [62] Hu, S.; Shaner, M. R.; Beardslee, J. A.; Lichterman, M.; Brunschwig, B. S.; Lewis, N. S. Amorphous TiO₂ Coatings Stabilize Si, GaAs, and GaP Photoanodes for Efficient Water Oxidation. *Science (80-.)*. **2014**, *344*, 1005–1009.
- [63] Neubert, S.; Mitoraj, D.; Shevlin, S. A.; Pulisova, P.; Heimann, M.; Du, Y.; Goh, G. K. L.; Pacia, M.; Kruczala, K.; Turner, S.; Macyk, W.; Guo, Z. X.; Hocking, R. K.; Beranek, R. Highly Efficient Rutile TiO₂ Photocatalysts with Single Cu(II) and Fe(III) Surface Catalytic Sites. *J. Mater. Chem. A* **2016**, *4*, 3127–3138.
- [64] Neubert, S.; Ramakrishnan, A.; Strunk, J.; Shi, H.; Mei, B.; Wang, L.; Bledowski, M.; Guschin, D. A.; Kauer, M.; Wang, Y.; Muhler, M.; Beranek, R. Surface-Modified TiO₂ Photocatalysts Prepared by a Photosynthetic Route: Mechanism, Enhancement, and Limits. *Chempluschem* **2014**, *79*, 163–170.
- [65] Towle, S. N.; Brown, G. E.; Parks, G. A. Sorption of Co(II) on Metal Oxide Surfaces. *J. Colloid Interface Sci.* **1999**, *217*, 299–311.
- [66] Jin, Q.; Fujishima, M.; Nolan, M.; Iwaszuk, A.; Tada, H. Photocatalytic Activities of Tin(IV) Oxide Surface-Modified Titanium(IV) Dioxide Show a Strong Sensitivity to the TiO₂ Crystal Form. *J. Phys. Chem. C* **2012**, *116*, 12621–12626.
- [67] Jin, Q.; Fujishima, M.; Iwaszuk, A.; Nolan, M.; Tada, H. Loading Effect in Copper(II) Oxide Cluster-Surface-Modified Titanium(IV) Oxide on Visible- and UV-Light Activities. *J. Phys. Chem. C* **2013**, *117*, 23848–23857.
- [68] Chu, S.; Becerikli, A. E.; Kortewille, B.; Oropeza, F. E.; Strunk, J. Tin-grafted TiO₂ with Enhanced Activity for Photocatalytic Hydrogen Generation from Aqueous Methanol Solutions. *Int. J. Hydrogen Energy* **2014**, *39*, 18784–18792.
- [69] Kurtenbach, R.; Kleffmann, J.; Niedojadlo, A.; Wiesen, P. Primary NO₂ emissions and their impact on air quality in traffic environments in Germany. *Environ. Sci. Eur.* **2012**, *24*, 21–28.
- [70] Guerreiro, C. B. B.; Foltescu, V.; de Leeuw, F. Air quality status and trends in Europe. *Atmos. Environ.* **2014**, *98*, 376–384.
- [71] Malley, C. S.; von Schneidmesser, E.; Moller, S.; Braban, C. F.; Hicks, W. K.; Heal, M. R. Analysis of the distributions of hourly NO₂ concentrations contributing to annual average NO₂ concentrations across the European monitoring network between 2000 and 2014. *Atmos. Chem. Phys. Discuss.* **2017**, 1–43.
- [72] Williams, M. L.; Carslaw, D. C. New Directions: Science and policy - Out of step on NO_x and NO₂? *Atmos. Environ.* **2011**, *45*, 3911–3912.
- [73] Lelieveld, J.; Evans, J. S.; Fnais, M.; Giannadaki, D.; Pozzer, A. The contribution of outdoor air pollution sources to premature mortality on a global scale. *Nature* **2015**, *525*, 367–71.

- [74] European Environment Agency, Air quality in Europe — 2017 report. **2017**.
- [75] Skalska, K.; Miller, J. S.; Ledakowicz, S. Trends in NO_x abatement: A review. *Sci. Total Environ.* **2010**, *408*, 3976–89.
- [76] Franco, V.; Sánchez, F. P.; German, J.; Mock, P. The International Council on Clean Transportation: Real-World Exhaust Emissions From Modern Diesel Cars. **2014**.
- [77] Koppenol, W. H.; Bounds, P. L.; Nauser, T.; Kissner, R.; Rügger, H. Peroxynitrous acid: Controversy and consensus surrounding an enigmatic oxidant. *Dalt. Trans.* **2012**, *41*, 13779–13787.
- [78] Mothes, F.; Ifang, S.; Gallus, M.; Golly, B.; Boréave, A.; Kurtenbach, R.; Kleffmann, J.; George, C.; Herrmann, H. Bed flow photoreactor experiments to assess the photocatalytic nitrogen oxides abatement under simulated atmospheric conditions. *Appl. Catal. B Environ.* **2018**, *231*, 161–172.
- [79] Gandolfo, A.; Bartolomei, V.; Gomez Alvarez, E.; Tlili, S.; Gligorovski, S.; Kleffmann, J.; Wortham, H. The effectiveness of indoor photocatalytic paints on NO_x and HONO levels. *Appl. Catal. B Environ.* **2015**, *166-167*, 84–90.
- [80] Laufs, S.; Burgeth, G.; Duttlinger, W.; Kurtenbach, R.; Maban, M.; Thomas, C.; Wiesen, P.; Kleffmann, J. Conversion of nitrogen oxides on commercial photocatalytic dispersion paints. *Atmos. Environ.* **2010**, *44*, 2341–2349.
- [81] Dillert, R.; Engel, A.; Große, J.; Lindner, P.; Bahnemann, D. W. Light intensity dependence of the kinetics of the photocatalytic oxidation of nitrogen(II) oxide at the surface of TiO₂. *Phys. Chem. Chem. Phys.* **2013**, *15*, 20876–20886.
- [82] Ohko, Y.; Nakamura, Y.; Fukuda, A.; Matsuzawa, S.; Takeuchi, K. Photocatalytic oxidation of nitrogen dioxide with TiO₂ thin films under continuous UV-light illumination. *J. Phys. Chem. C* **2008**, *112*, 10502–10508.
- [83] Monge, M. E.; D’Anna, B.; George, C. Nitrogen dioxide removal and nitrous acid formation on titanium oxide surfaces—an air quality remediation process? *Phys. Chem. Chem. Phys.* **2010**, *12*, 8991–8998.
- [84] Bloh, J. Z.; Dillert, R.; Bahnemann, D. W. Ruthenium-modified zinc oxide, a highly active vis-photocatalyst: the nature and reactivity of photoactive centres. *Phys. Chem. Chem. Phys.* **2014**, *16*, 5833–5845.
- [85] Sambale, F.; Stahl, F.; Bahnemann, D.; Scheper, T. In vitro toxicological nanoparticle studies under flow exposure. *J. Nanoparticle Res.* **2015**, *17*, 1–12.
- [86] Balayeva, N. O.; Fleisch, M.; Bahnemann, D. W. Surface-grafted WO₃/TiO₂ photocatalysts: Enhanced visible-light activity towards indoor air purification. *Catal. Today* **2018**, *313*, 63–71.
- [87] Wang, X.; Blechert, S.; Antonietti, M. Polymeric graphitic carbon nitride for heterogeneous photocatalysis. *ACS Catal.* **2012**, *2*, 1596–1606.
- [88] Nikokavoura, A.; Trapalis, C. Graphene and g-C₃N₄ based photocatalysts for NO_x removal: A review. *Appl. Surf. Sci.* **2018**, *430*, 18–52.

-
- [89] Papailias, I.; Todorova, N.; Giannakopoulou, T.; Yu, J.; Dimotikali, D.; Trapalis, C. Photocatalytic activity of modified g-C₃N₄/TiO₂ nanocomposites for NO_x removal. *Catal. Today* **2016**, 4–11.
- [90] Giannakopoulou, T.; Papailias, I.; Todorova, N.; Boukos, N.; Liu, Y.; Yu, J.; Trapalis, C. Tailoring the energy band gap and edges' potentials of g-C₃N₄/TiO₂ composite photocatalysts for NO_x removal. *Chem. Eng. J.* **2017**, *310*, 571–580.
- [91] Papailias, I.; Todorova, N.; Giannakopoulou, T.; Karapati, S.; Boukos, N.; Dimotikali, D.; Trapalis, C. Enhanced NO₂ abatement by alkaline-earth modified g-C₃N₄ nanocomposites for efficient air purification. *Appl. Surf. Sci.* **2018**, *430*, 225–233.
- [92] Rehman, S.; Ullah, R.; Butt, A. M.; Gohar, N. D. Strategies of Making TiO₂ and ZnO Visible Light Active. *J. Hazard. Mater.* **2009**, *170*, 560–569.
- [93] Etacheri, V.; Di Valentin, C.; Schneider, J.; Bahnemann, D.; Pillai, S. C. Visible-light activation of TiO₂ photocatalysts: Advances in theory and experiments. *J. Photochem. Photobiol. C Photochem. Rev.* **2015**, *25*, 1–29.
- [94] Morikawa, T.; Asahi, R.; Ohwaki, T.; Aoki, K.; Taga, Y. Band-Gap Narrowing of Titanium Dioxide by Nitrogen Doping. *Jpn. J. Appl. Phys.* **2001**, *40*, L561–L563.
- [95] Asahi, R.; Morikawa, T. Nitrogen complex species and its chemical nature in TiO₂ for visible-light sensitized photocatalysis. *Chem. Phys.* **2007**, *339*, 57–63.
- [96] Burda, C.; Lou, Y.; Chen, X.; Samia, A. C. S.; Stout, J.; Gole, J. L. Enhanced Nitrogen Doping in TiO₂ Nanoparticles. *Nano Lett.* **2003**, *3*, 1049–1051.
- [97] Di Valentin, C.; Finazzi, E.; Pacchioni, G.; Selloni, A.; Livraghi, S.; Paganini, M. C.; Giamello, E. N-Doped TiO₂: Theory and Experiment. *Chem. Phys.* **2007**, *339*, 44–56.
- [98] Livraghi, S.; Pelaez, M.; Biedrzycki, J.; Corazzari, I.; Giamello, E.; Dionysiou, D. Influence of the Chemical Synthesis on the Physicochemical Properties of N-TiO₂ Nanoparticles. *Catal. Today* **2013**, *209*, 54–59.
- [99] Livraghi, S.; Paganini, M. C.; Giamello, E.; Selloni, A.; Di Valentin, C.; Pacchioni, G. Origin of Photoactivity of Nitrogen-Doped Titanium Dioxide under Visible Light. *J. Am. Chem. Soc.* **2006**, *128*, 15666–15671.
- [100] Livraghi, S.; Czoska, A.; Paganini, M.; Giamello, E. Preparation and Spectroscopic Characterization of Visible Light Sensitized N Doped TiO₂ (Rutile). *J. Solid State Chem.* **2009**, *182*, 160–164.
- [101] Livraghi, S.; Chierotti, M. R.; Giamello, E.; Magnacca, G.; Paganini, M. C.; Cappelletti, G.; Bianchi, C. L. Nitrogen-Doped Titanium Dioxide Active in Photocatalytic Reactions with Visible Light: A Multi-Technique Characterization of Differently Prepared Materials. *J. Phys. Chem. C* **2008**, *112*, 17244–17252.
- [102] Márquez, A.; Plata, J.; Ortega, Y.; Sanz, J.; Colón, G.; Kubacka, A.; Fernández-García, M. Making Photo-Selective TiO₂ Materials by Cation-Anion Codoping: From Structure and Electronic Properties to Photoactivity. *J. Phys. Chem. C* **2012**, 18759–18767.
- [103] Morrow, P. E. Toxicological data on NO_x: an overview. *J. Toxicol. Environ. Health* **1984**, *13*, 205–227.

- [104] Mohsenin, V. Human exposure to oxides of nitrogen at ambient and supra-ambient concentrations. *Toxicology* **1994**, *89*, 301–312.
- [105] Lewis, R. J.; Sax, N. I. *Sax's Dangerous Properties of Industrial Materials*, 9th ed.; Van Nostrand Reinhold, New York, **1996**.
- [106] International Organization for Standardization, ISO 22197-1: Fine ceramics (advanced ceramics, advanced technical ceramics) - Test method for air-purification performance of semiconducting photocatalytic materials - Part 1 : Removal of nitric oxide. **2007**.
- [107] Sivachandiran, L.; Thevenet, F.; Gravejat, P.; Rousseau, A. Investigation of NO and NO₂ adsorption mechanisms on TiO₂ at room temperature. *Appl. Catal. B Environ.* **2013**, *142-143*, 196–204.
- [108] Monge, M. E.; George, C.; D'Anna, B.; Doussin, J.-F.; Jammoul, A.; Wang, J.; Eyglunent, G.; Solignac, G.; Daële, V.; Mellouki, A. Ozone formation from illuminated titanium dioxide surfaces. *J. Am. Chem. Soc.* **2010**, *132*, 8234–8235.
- [109] Gerischer, H.; Heller, A. The Role of Oxygen in Photooxidation of Organic Molecules on Semiconductor Particles. *J. Phys. Chem.* **1991**, *95*, 5261–5267.
- [110] Vanýsek, P. Electrochemical Series. In *Handb. Chem. & Physics, 91th Ed.*; CRC Press, **2010**.
- [111] Wardman, P. Reduction Potentials of One-Electron Couples Involving Free Radicals in Aqueous Solution. *J. Phys. Chem. Ref. Data* **1989**, *18*, 1637–1755.
- [112] Kandiel, T. A.; Feldhoff, A.; Robben, L.; Dillert, R.; Bahnemann, D. W. Tailored Titanium Dioxide Nanomaterials: Anatase Nanoparticles and Brookite Nanorods as Highly Active Photocatalysts. *Chem. Mater.* **2010**, *22*, 2050–2060.
- [113] Mills, A.; Le Hunte, S. An Overview of Semiconductor Photocatalysis. *J. Photochem. Photobiol. A Chem.* **1997**, *108*, 1–35.
- [114] Li, F. B.; Li, X. Z. The enhancement of photodegradation efficiency using Pt-TiO₂ catalyst. *Chemosphere* **2002**, *48*, 1103–1111.
- [115] Lee, S. K.; Mills, A. Platinum and palladium in semiconductor photocatalytic systems. *Platin. Met. Rev.* **2003**, *47*, 61–72.
- [116] Bahnemann, D. W.; Mönig, J.; Chapman, R. Efficient Photocatalysis of the Irreversible One-Electron and Two-Electron Reduction of Halothane on Platinized Colloidal Titanium Dioxide in Aqueous Suspension. *J. Phys. Chem.* **1987**, *91*, 3782–3788.
- [117] Hu, Y.; Song, X.; Jiang, S.; Wei, C. Enhanced photocatalytic activity of Pt-doped TiO₂ for NO_x oxidation both under UV and visible light irradiation: A synergistic effect of lattice Pt⁴⁺ and surface PtO. *Chem. Eng. J.* **2015**, *274*, 102–112.
- [118] Fujiwara, K.; Müller, U.; Pratsinis, S. E. Pd Subnano-Clusters on TiO₂ for Solar-Light Removal of NO. *ACS Catal.* **2016**, *6*, 1887–1893.
- [119] Shao, M. Palladium-based electrocatalysts for hydrogen oxidation and oxygen reduction reactions. *J. Power Sources* **2011**, *196*, 2433–2444.
- [120] Vesborg, P. C. K.; Jaramillo, T. F. Addressing the terawatt challenge: scalability in the supply of chemical elements for renewable energy. *RSC Adv.* **2012**, *2*, 7933–7947.

-
- [121] Nishikawa, M.; Takanami, R.; Nakagoshi, F.; Suizu, H.; Nagai, H.; Nosaka, Y. Dominated factors for high performance of Fe³⁺ grafted metal doped TiO₂ based photocatalysts. *Appl. Catal. B Environ.* **2014**, *160-161*, 722–729.
- [122] Nishikawa, M.; Mitani, Y.; Nosaka, Y. Photocatalytic Reaction Mechanism of Fe(III)-Grafted TiO₂ Studied by Means of ESR Spectroscopy and Chemiluminescence Photometry. *J. Phys. Chem. C* **2012**, *116*, 14900–14907.
- [123] Herold, S.; Exner, M.; Nauser, T. Kinetic and mechanistic studies of the NO-mediated oxidation of oxymyoglobin and oxyhemoglobin. *Biochemistry* **2001**, *40*, 3385–3395.
- [124] Herold, S.; Rehmann, F.-J. K. Kinetics of the reactions of nitrogen monoxide and nitrite with ferryl hemoglobin. *Free Radic. Biol. Med.* **2003**, *34*, 531–545.
- [125] Jensen, M. P.; Riley, D. P. Peroxynitrite decomposition activity of iron porphyrin complexes. *Inorg. Chem.* **2002**, *41*, 4788–4797.
- [126] Sharma, S. K.; Schaefer, A. W.; Lim, H.; Matsumura, H.; Moënne-Loccoz, P.; Hedman, B.; Hodgson, K. O.; Solomon, E. I.; Karlin, K. D. A Six-Coordinate Peroxynitrite Low-Spin Iron(III) Porphyrinate Complex-The Product of the Reaction of Nitrogen Monoxide ($\cdot\text{NO}$ (g)) with a Ferric-Superoxide Species. *J. Am. Chem. Soc.* **2017**, *139*, 17421–17430.
- [127] Sadanaga, Y.; Matsumoto, J.; Kajii, Y. Photochemical reactions in the urban air: Recent understandings of radical chemistry. *J. Photochem. Photobiol. C Photochem. Rev.* **2003**, *4*, 85–104.
- [128] González-Elipe, A. R.; Soria, J.; Munuera, G. Photo-decomposition of Ozone on TiO₂. *Zeitschrift für Phys. Chemie* **1981**, *126*, 251–257.
- [129] Mills, A.; Lee, S.-K.; Lepre, A. Photodecomposition of ozone sensitised by a film of titanium dioxide on glass. *J. Photochem. Photobiol. A Chem.* **2003**, *155*, 199–205.
- [130] Wang, X.; Tan, X.; Yu, T. Kinetic Study of Ozone Photocatalytic Decomposition Using a Thin Film of TiO₂ Coated on a Glass Plate and the CFD Modeling Approach. *Ind. & Eng. Chem. Res.* **2014**, *53*, 7902–7909.
- [131] Radhakrishnan, R.; Oyama, S. Ozone Decomposition over Manganese Oxide Supported on ZrO₂ and TiO₂: A Kinetic Study Using in Situ Laser Raman Spectroscopy. *J. Catal.* **2001**, *199*, 282–290.
- [132] Dhandapani, B.; Oyama, S. T. Kinetics and Mechanism of Ozone Decomposition on a Manganese Oxide Catalyst. *Chem. Lett.* **1995**, *24*, 413–414.
- [133] Batakliiev, T.; Georgiev, V.; Anachkov, M.; Rakovsky, S.; Rakovsky, S. Ozone decomposition. *Interdiscip. Toxicol.* **2014**, *7*, 47–59.
- [134] Loegager, T.; Holcman, J.; Sehested, K.; Pedersen, T. Oxidation of ferrous ions by ozone in acidic solutions. *Inorg. Chem.* **1992**, *31*, 3523–3529.
- [135] Pestovsky, O.; Stoian, S.; Bominaar, E. L.; Shan, X.; Münck, E.; Que, L.; Bakac, A. Aqueous Fe^{IV}=O: Spectroscopic Identification and Oxo-Group Exchange. *Angew. Chem. Int. Ed.* **2005**, *44*, 6871–6874.
- [136] Bolte, G.; Flassak, T. Numerische Simulation der Wirksamkeit photokatalytisch aktiver Betonoberflächen. *Proc. 18th Int. Conf. Build. Mater. (ibausil), Weimar* **2012**,

- [137] Serpone, N. Heterogeneous Photocatalysis and Prospects of TiO₂-Based Photocatalytic DeNO_xing the Atmospheric Environment. *Catalysts* **2018**, *8*, 553–650.
- [138] Maggos, T.; Bartzis, J. G.; Liakou, M.; Gobin, C. Photocatalytic degradation of NO_x gases using TiO₂-containing paint: a real scale study. *J. Hazard. Mater.* **2007**, *146*, 668–673.
- [139] Maggos, T.; Plassais, A.; Bartzis, J. G.; Vasilakos, C.; Moussiopoulos, N.; Bonafous, L. Photocatalytic degradation of NO_x in a pilot street canyon configuration using TiO₂-mortar panels. *Environ. Monit. Assess.* **2008**, *136*, 35–44.
- [140] Guerrini, G. L. Photocatalytic performances in a city tunnel in Rome: NO_x monitoring results. *Constr. Build. Mater.* **2012**, *27*, 165–175.
- [141] Gallus, M.; Ciuraru, R.; Mothes, F.; Akylas, V.; Barmpas, F.; Beeldens, A.; Bernard, F.; Boonen, E.; Boréave, A.; Cazaunau, M.; Charbonnel, N.; Chen, H.; Daële, V.; Dupart, Y.; Gaimoz, C.; Grosselin, B.; Herrmann, H.; Ifang, S.; Kurtenbach, R.; Maille, M.; Marjanovic, I.; Michoud, V.; Mellouki, A.; Miet, K.; Moussiopoulos, N.; Poulain, L.; Zapf, P.; George, C.; Doussin, J. F.; Kleffmann, J. Photocatalytic abatement results from a model street canyon. *Environ. Sci. Pollut. Res.* **2015**, *22*, 18185–18196.
- [142] Gallus, M.; Akylas, V.; Barmpas, F.; Beeldens, a.; Boonen, E.; Boréave, a.; Cazaunau, M.; Chen, H.; Daële, V.; Doussin, J.; Dupart, Y.; Gaimoz, C.; George, C.; Grosselin, B.; Herrmann, H.; Ifang, S.; Kurtenbach, R.; Maille, M.; Mellouki, a.; Miet, K.; Mothes, F.; Moussiopoulos, N.; Poulain, L.; Rabe, R.; Zapf, P.; Kleffmann, J. Photocatalytic depollution in the Leopold II tunnel in Brussels: NO_x abatement results. *Build. Environ.* **2015**, *84*, 125–133.
- [143] Ballari, M.; Brouwers, H. Full Scale Demonstration of Air-Purifying Pavement. *J. Hazard. Mater.* **2013**, *254-255*, 406–414.
- [144] Folli, A.; Strøm, M.; Madsen, T. P.; Henriksen, T.; Lang, J.; Emenius, J.; Klevebrant, T.; Nilsson, Å. Field study of air purifying paving elements containing TiO₂. *Atmos. Environ.* **2015**, *107*, 44–51.
- [145] Hoffmann, M. R.; Martin, S. T.; Choi, W.; Bahnemann, D. W. Environmental Applications of Semiconductor Photocatalysis. *Chem. Rev.* **1995**, *95*, 69–96.
- [146] Campos-Martin, J. M.; Blanco-Brieva, G.; Fierro, J. L. G. Hydrogen peroxide synthesis: An outlook beyond the anthraquinone process. *Angew. Chem. Int. Ed.* **2006**, *45*, 6962–6984.
- [147] Bloom, R.; Davis, N. S.; Levine, S. D. Hydrogen Peroxide as a Propellant. *J. Am. Rocket Soc.* **1950**, *80*, 3–17.
- [148] Fukuzumi, S. Production of Liquid Solar Fuels and Their Use in Fuel Cells. *Joule* **2017**, *1*, 689–738.
- [149] Goor, G.; Glenneberg, J.; Jacobi, S.; Dadabhoy, J.; Candido, E. Hydrogen Peroxide. In *Ullmann's Encycl. Ind. Chem.*; Wiley-VCH Verlag GmbH & Co. KGaA: Weinheim, Germany, **2019**.
- [150] Khajornpaisan, N.; Rojanarowan, N. The Effect of Oxidized White Liquor on Pulp Brightness in Peroxide Bleaching in Pulp Mills. *Adv. Mater. Res.* **2014**, *974*, 230–234.
- [151] Dournel, P. Process for the Bleaching of Paper and Pulp. **2009**; WO 2009/144190 A1.

-
- [152] Lindhorst, A. C.; Haslinger, S.; Kühn, F. E. Molecular iron complexes as catalysts for selective C–H bond oxygenation reactions. *Chem. Commun.* **2015**, *51*, 17193–17212.
- [153] Yamada, M.; Karlin, K. D.; Fukuzumi, S. One-step selective hydroxylation of benzene to phenol with hydrogen peroxide catalysed by copper complexes incorporated into mesoporous silica–alumina. *Chem. Sci.* **2016**, *7*, 2856–2863.
- [154] Zhang, W.; Fernández-Fueyo, E.; Ni, Y.; van Schie, M.; Gacs, J.; Renirie, R.; Wever, R.; Mutti, F. G.; Rother, D.; Alcalde, M.; Hollmann, F. Selective aerobic oxidation reactions using a combination of photocatalytic water oxidation and enzymatic oxyfunctionalizations. *Nat. Catal.* **2018**, *1*, 55–62.
- [155] Oszajca, M.; Brindell, M.; Orzeł, Ł.; Dąbrowski, J. M.; Śpiewak, K.; Łabuz, P.; Pacia, M.; Stochel-Gaudyn, A.; Macyk, W.; van Eldik, R.; Stochel, G. Mechanistic studies on versatile metal-assisted hydrogen peroxide activation processes for biomedical and environmental incentives. *Coord. Chem. Rev.* **2016**, *327–328*, 143–165.
- [156] Riedl, H.-J.; Pfeiderer, G. Production of Hydrogen Peroxide. **1939**; US2158525A.
- [157] Sandelin, F.; Oinas, P.; Salmi, T.; Haario, H. Kinetics of the Catalyst Deactivation in the Recovery of Active Anthraquinones. *Stud. Surf. Sci. Catal.* **1994**, *88*, 635–640.
- [158] Dittmeyer, R.; Grunwaldt, J. D.; Pashkova, A. A review of catalyst performance and novel reaction engineering concepts in direct synthesis of hydrogen peroxide. *Catal. Today* **2015**, *248*, 149–159.
- [159] Izgorodin, A.; Izgorodina, E.; MacFarlane, D. R. Low overpotential water oxidation to hydrogen peroxide on a MnO_x catalyst. *Energy Environ. Sci.* **2012**, *5*, 9496–9501.
- [160] Reis, R. M.; Beati, A. A. G. F.; Rocha, R. S.; Assumpção, M. H. M. T.; Santos, M. C.; Bertazzoli, R.; Lanza, M. R. V. Use of gas diffusion electrode for the in situ generation of hydrogen peroxide in an electrochemical flow-by reactor. *Ind. Eng. Chem. Res.* **2012**, *51*, 649–654.
- [161] Sun, Y.; Sinev, I.; Ju, W.; Bergmann, A.; Dresch, S.; Köhl, S.; Spöri, C.; Schmies, H.; Wang, H.; Bernsmeier, D.; Paul, B.; Schmack, R.; Kraehnert, R.; Roldan Cuenya, B.; Strasser, P. Efficient Electrochemical Hydrogen Peroxide Production from Molecular Oxygen on Nitrogen-Doped Mesoporous Carbon Catalysts. *ACS Catal.* **2018**, 2844–2856.
- [162] Siahrostami, S.; Verdager-Casadevall, A.; Karamad, M.; Deiana, D.; Malacrida, P.; Wickman, B.; Escudero-Escribano, M.; Paoli, E. A.; Frydendal, R.; Hansen, T. W.; Chorkendorff, I.; Stephens, I. E. L.; Rossmeisl, J. Enabling direct H₂O₂ production through rational electrocatalyst design. *Nat. Mater.* **2013**, *12*, 1137–1143.
- [163] Lu, Z.; Chen, G.; Siahrostami, S.; Chen, Z.; Liu, K.; Xie, J.; Liao, L.; Wu, T.; Lin, D.; Liu, Y.; Jaramillo, T. F.; Nørskov, J. K.; Cui, Y. High-efficiency oxygen reduction to hydrogen peroxide catalysed by oxidized carbon materials. *Nat. Catal.* **2018**, *1*, 156–162.
- [164] Baur, E.; Neuweiler, C. Über photolytische Bildung von Hydroperoxyd. *Helv. Chim. Acta* **1927**, *10*, 901–907.
- [165] Sahel, K.; Elsellami, L.; Mirali, I.; Dappozze, F.; Bouhent, M.; Guillard, C. Hydrogen peroxide and photocatalysis. *Appl. Catal. B Environ.* **2016**, *188*, 106–112.

- [166] Moon, G.-h.; Kim, W.; Bokare, A. D.; Sung, N.-e.; Choi, W. Solar production of H₂O₂ on reduced graphene oxide-TiO₂ hybrid photocatalysts consisting of earth-abundant elements only. *Energy Environ. Sci.* **2014**, *7*, 4023–4028.
- [167] Hou, W. C.; Wang, Y. S. Photocatalytic Generation of H₂O₂ by Graphene Oxide in Organic Electron Donor-Free Condition under Sunlight. *ACS Sustain. Chem. Eng.* **2017**, *5*, 2994–3001.
- [168] Shiraishi, Y.; Kanazawa, S.; Sugano, Y.; Tsukamoto, D.; Sakamoto, H.; Ichikawa, S.; Hirai, T. Highly Selective Production of Hydrogen Peroxide on Graphitic Carbon Nitride (g-C₃N₄) Photocatalyst Activated by Visible Light. *ACS Catal.* **2014**, *4*, 774–780.
- [169] Moon, G.-h.; Fujitsuka, M.; Kim, S.; Majima, T.; Wang, X.; Choi, W. Eco-Friendly Photochemical Production of H₂O₂ through O Reduction over Carbon Nitride Frameworks Incorporated with Multiple Heteroelements. *ACS Catal.* **2017**, *7*, 2886–2895.
- [170] Kofuji, Y.; Ohkita, S.; Shiraishi, Y.; Sakamoto, H.; Tanaka, S.; Ichikawa, S.; Hirai, T. Graphitic Carbon Nitride Doped with Biphenyl Diimide: Efficient Photocatalyst for Hydrogen Peroxide Production from Water and Molecular Oxygen by Sunlight. *ACS Catal.* **2016**, *6*, 7021–7029.
- [171] Gogoi, S.; Karak, N. Solar-Driven Hydrogen Peroxide Production Using Polymer-Supported Carbon Dots as Heterogeneous Catalyst. *Nano-Micro Lett.* **2017**, *9*, 1–11.
- [172] Iglesias, D.; Giuliani, A.; Melchionna, M.; Marchesan, S.; Criado, A.; Nasi, L.; Bevilacqua, M.; Tavagnacco, C.; Vizza, F.; Prato, M.; Fornasiero, P. N-Doped Graphitized Carbon Nanohorns as a Forefront Electrocatalyst in Highly Selective O₂ Reduction to H₂O₂. *Chem* **2018**, *4*, 106–123.
- [173] Hirakawa, H.; Shiota, S.; Shiraishi, Y.; Sakamoto, H.; Ichikawa, S.; Hirai, T. Au Nanoparticles Supported on BiVO₄: Effective Inorganic Photocatalysts for H₂O₂ Production from Water and O₂ under Visible Light. *ACS Catal.* **2016**, *6*, 4976–4982.
- [174] Teranishi, M.; Naya, S.-i.; Tada, H. In Situ Liquid Phase Synthesis of Hydrogen Peroxide from Molecular Oxygen Using Gold Nanoparticle-Loaded Titanium(IV) Dioxide Photocatalyst. *J. Am. Chem. Soc.* **2010**, *132*, 7850–7851.
- [175] Teranishi, M.; Hoshino, R.; Naya, S.-i.; Tada, H. Gold-Nanoparticle-Loaded Carbonate-Modified Titanium(IV) Oxide Surface: Visible-Light-Driven Formation of Hydrogen Peroxide from Oxygen. *Angew. Chem. Int. Ed.* **2016**, *55*, 12773–12777.
- [176] Bahnemann, D. W.; Kormann, C.; Hoffmann, M. R. Photocatalytic Formation of Hydrogen Peroxide. *Am. Chem. Soc. Div. Pet. Chem. Prepr.* **1986**, *31*, 519–525.
- [177] Valdés, Á.; Qu, Z.-W.; Kroes, G.-J.; Rossmeisl, J.; Nørskov, J. K. Oxidation and Photo-Oxidation of Water on TiO₂ Surface. *J. Phys. Chem. C* **2008**, *112*, 9872–9879.
- [178] Muuronen, M.; Parker, S. M.; Berardo, E.; Le, A.; Zwijnenburg, M. A.; Furche, F. Mechanism of photocatalytic water oxidation on small TiO₂ nanoparticles. *Chem. Sci.* **2017**, *8*, 2179–2183.
- [179] Nosaka, Y.; Nosaka, A. Y. Generation and Detection of Reactive Oxygen Species in Photocatalysis. *Chem. Rev.* **2017**, *117*, 11302–11336.

-
- [180] Fujishima, A.; Zhang, X.; Tryk, D. A. TiO₂ photocatalysis and related surface phenomena. *Surf. Sci. Rep.* **2008**, *63*, 515–582.
- [181] Kormann, C.; Bahnemann, D. W.; Hoffmann, M. R. Photocatalytic production of hydrogen peroxides and organic peroxides in aqueous suspensions of titanium dioxide, zinc oxide, and desert sand. *Environ. Sci. Technol.* **1988**, *22*, 798–806.
- [182] Siahrostami, S.; Li, G.-L.; Viswanathan, V.; Nørskov, J. K. One- or Two-Electron Water Oxidation, Hydroxyl Radical, or H₂O₂ Evolution. *J. Phys. Chem. Lett.* **2017**, *8*, 1157–1160.
- [183] Hoffman, A. J.; Carraway, E. R.; Hoffmann, M. R. Photocatalytic production of H₂O₂ and organic peroxides on quantum- sized semiconductor colloids. *Environ. Sci. Technol.* **1994**, *28*, 776–785.
- [184] Shiraishi, Y.; Kanazawa, S.; Tsukamoto, D.; Shiro, A.; Sugano, Y.; Hirai, T. Selective Hydrogen Peroxide Formation by Titanium Dioxide Photocatalysis with Benzylic Alcohols and Molecular Oxygen in Water. *ACS Catal.* **2013**, *3*, 2222–2227.
- [185] Fraser, I. M.; MacCallum, J. R. Photocatalytic dehydrogenation of liquid propan-2-ol by TiO₂. Part 2.-Mechanism. *J. Chem. Soc. Faraday Trans. 1 Phys. Chem. Condens. Phases* **1986**, *82*, 2747.
- [186] Kormann, C.; Bahnemann, D. W.; Hoffmann, M. R. Photocatalytic production of H₂O₂ and organic peroxides in aqueous suspensions of TiO₂, ZnO, and desert sand. *Environ. Sci. Technol.* **1988**, *22*, 798–806.
- [187] Deng, Y. Developing a Langmuir-type excitation equilibrium equation to describe the effect of light intensity on the kinetics of the photocatalytic oxidation. *Chem. Eng. J.* **2018**, *337*, 220–227.
- [188] Dilla, M.; Mateblowski, A.; Ristig, S.; Strunk, J. Photocatalytic CO₂ Reduction under Continuous Flow High-Purity Conditions: Influence of Light Intensity and H₂O Concentration. *ChemCatChem* **2017**, *9*, 4345–4352.
- [189] Hykaway, N.; Sears, W. M.; Morisaki, H.; Morrison, S. R. Current-doubling reactions on titanium dioxide photoanodes. *J. Phys. Chem.* **1986**, *90*, 6663–6667.
- [190] Schneider, J.; Bahnemann, D. W. Undesired Role of Sacrificial Reagents in Photocatalysis. *J. Phys. Chem. Lett.* **2013**, *4*, 3479–3483.
- [191] Schwarz, H. A.; Dodson, R. W. Reduction potentials of CO₂⁻ and the alcohol radicals. *J. Phys. Chem.* **1989**, *93*, 409–414.
- [192] Mills, A.; Wang, J.; Ollis, D. Dependence of the kinetics of liquid-phase photocatalyzed reactions on oxygen concentration and light intensity. *J. Catal.* **2006**, *243*, 1–6.
- [193] Wang, B.; Chen, W.; Song, Y.; Li, G.; Wei, W.; Fang, J.; Sun, Y. Recent progress in the photocatalytic reduction of aqueous carbon dioxide. *Catal. Today* **2018**, *311*, 23–39.
- [194] Kawai, T.; Sakata, T. Photocatalytic hydrogen production from liquid methanol and water. *J. Chem. Soc. Chem. Commun.* **1980**, *47*, 694–695.
- [195] Lin, W.-C.; Yang, W.-D.; Huang, I.-L.; Wu, T.-S.; Chung, Z.-J. Hydrogen Production from Methanol/Water Photocatalytic Decomposition Using Pt/TiO_{2-x}N_x Catalyst. *Energy & Fuels* **2009**, *23*, 2192–2196.

- [196] Linnik, O.; Kisch, H. On the mechanism of nitrogen photofixation at nanostructured iron titanate films. *Photochem. Photobiol. Sci.* **2006**, *5*, 938–942.
- [197] Xu, W.; Raftery, D. Photocatalytic Oxidation of 2-Propanol on TiO₂ Powder and TiO₂ Monolayer Catalysts Studied by Solid-State NMR. *J. Phys. Chem. B* **2001**, *105*, 4343–4349.
- [198] Ahmed, A. Y.; Kandiel, T. A.; Ivanova, I.; Bahnemann, D. Photocatalytic and photoelectrochemical oxidation mechanisms of methanol on TiO₂ in aqueous solution. *Appl. Surf. Sci.* **2014**, *319*, 44–49.
- [199] Carraway, E. R.; Hoffman, a. J.; Hoffmann, M. R. Photocatalytic oxidation of organic acids on quantum-sized semiconductor colloids. *Environ. Sci. Technol.* **1994**, *28*, 786–793.
- [200] Bideau, M.; Claudel, B.; Otterbein, M. Photocatalysis of formic acid oxidation by oxygen in an aqueous medium. *J. Photochem.* **1980**, *14*, 291–302.
- [201] Janusz, J. M.; Berson, J. A. Heterogeneous Photocatalytic Synthesis of Methane from Acetic Acid—New Kolbe Reaction Pathway. *J. Am. Chem. Soc.* **1978**, *100*, 2239–2240.
- [202] Koppenol, W. H.; Rush, J. D. Reduction potential of the carbon dioxide/carbon dioxide radical anion: a comparison with other C1 radicals. *J. Phys. Chem.* **1987**, *91*, 4429–4430.
- [203] Bianchi, C. L.; Gatto, S.; Pirola, C.; Naldoni, A.; Di Michele, A.; Cerrato, G.; Crocellà, V.; Capucci, V. Photocatalytic degradation of acetone, acetaldehyde and toluene in gas-phase: Comparison between nano and micro-sized TiO₂. *Appl. Catal. B Environ.* **2014**, *146*, 123–130.
- [204] Raillard, C.; Héquet, V.; Le Cloirec, P.; Legrand, J. Photocatalytic oxidation of methyl ethyl ketone over sol-gel and commercial TiO₂ for the improvement of indoor air. *Water Sci. Technol.* **2006**, *53*, 107–115.
- [205] Ohtani, B.; Nishimoto, S.-i. Effect of surface adsorptions of aliphatic alcohols and silver ion on the photocatalytic activity of titania suspended in aqueous solutions. *J. Phys. Chem.* **1993**, *97*, 920–926.
- [206] Walker, A.; Formenti, M.; Meriaudeau, P.; Teichner, S. J. Heterogeneous photocatalysis: Photo-oxidation of methylbutanols. *J. Catal.* **1977**, *50*, 237–243.
- [207] Seddigi, Z. S.; Ahmed, S. A.; Bumajdad, A.; Gonadal, M. A.; Ekram, Y.; Shawky, A. M.; Yarkandi, N. H. Desalination and Water Treatment Photocatalytic degradation of tert-butyl alcohol and tert-butyl formate using palladium-doped zinc oxide nanoparticles with UV irradiation. *Desalin. Water Treat.* **2015**, 37–41.
- [208] Mills, A.; O'Rourke, C.; Moore, K. Powder semiconductor photocatalysis in aqueous solution: An overview of kinetics-based reaction mechanisms. *J. Photochem. Photobiol. A Chem.* **2015**, *310*, 66–105.
- [209] Alfano, O. M.; Cabrera, M. I.; Cassano, A. E. Photocatalytic reactions involving hydroxyl radical attack: I. Reaction kinetics formulation with explicit photon absorption effects. *J. Catal.* **1997**, *172*, 370–379.
- [210] Grčić, I.; Li Puma, G. Six-flux absorption-scattering models for photocatalysis under wide-spectrum irradiation sources in annular and flat reactors using catalysts with different optical properties. *Appl. Catal. B Environ.* **2017**, *211*, 222–234.

-
- [211] Motegh, M.; Cen, J.; Appel, P. W.; van Ommen, J. R.; Kreutzer, M. T. Photocatalytic-reactor efficiencies and simplified expressions to assess their relevance in kinetic experiments. *Chem. Eng. J.* **2012**, *207-208*, 607–615.
- [212] Sagawe, G.; J. Brandi, R.; Bahnemann, D.; E. Cassano, A. Photocatalytic reactors for treating water pollution with solar illumination. II: A simplified analysis for flow reactors. *Chem. Eng. Sci.* **2003**, *58*, 2601–2615.
- [213] Sagawe, G.; J. Brandi, R.; Bahnemann, D.; Cassano, A. E. Photocatalytic reactors for treating water pollution with solar illumination. I: A simplified analysis for batch reactors. *Chem. Eng. Sci.* **2003**, *58*, 2587–2599.
- [214] Sagawe, G.; Brandi, R. J.; Bahnemann, D.; Cassano, A. E. Photocatalytic reactors for treating water pollution with solar illumination: A simplified analysis for n-steps flow reactors with recirculation. *Sol. Energy* **2005**, *79*, 262–269.
- [215] Sagawe, G.; Brandi, R. J.; Bahnemann, D.; Cassano, A. E. Photocatalytic reactors for treating water pollution with solar illumination. III: A simplified analysis for recirculating reactors. *Sol. Energy* **2004**, *77*, 471–489.
- [216] Camera-Roda, G.; Santarelli, F.; Martin, C. A. Design of photocatalytic reactors made easy by considering the photons as immaterial reactants. *Sol. Energy* **2005**, *79*, 343–352.
- [217] Dillert, R.; Stötzner, J.; Engel, A.; Bahnemann, D. W. Influence of inlet concentration and light intensity on the photocatalytic oxidation of nitrogen(II) oxide at the surface of Aeroxide® TiO₂ P25. *J. Hazard. Mater.* **2012**, *211-212*, 240–246.
- [218] Ollis, D. F. Kinetics of liquid phase photocatalyzed reactions: An illuminating approach. *J. Phys. Chem. B* **2005**, *109*, 2439–2444.
- [219] Herrmann, J. Heterogeneous photocatalysis: fundamentals and applications to the removal of various types of aqueous pollutants. *Catal. Today* **1999**, *53*, 115–129.
- [220] Gaya, U.; Abdullah, A. Heterogeneous photocatalytic degradation of organic contaminants over titanium dioxide: A review of fundamentals, progress and problems. *J. Photochem. Photobiol. C Photochem. Rev.* **2008**, *9*, 1–12.
- [221] Carp, O.; Huisman, C.; Reller, A. Photoinduced reactivity of titanium dioxide. *Prog. Solid State Chem.* **2004**, *32*, 33–177.
- [222] Al-Sayyed, G.; D'Oliveira, J. C.; Pichat, P. Semiconductor-sensitized photodegradation of 4-chlorophenol in water. *J. Photochem. Photobiol. A Chem.* **1991**, *58*, 99–114.
- [223] Soares, E. T.; Lansarin, M. A.; Moro, C. C. A study of process variables for the photocatalytic degradation of rhodamine B. *Brazilian J. Chem. Eng.* **2007**, *24*, 29–36.
- [224] Hu, Q.; Liu, B.; Zhang, Z.; Song, M.; Zhao, X. Temperature effect on the photocatalytic degradation of methyl orange under UV-vis light irradiation. *J. Wuhan Univ. Technol. Sci. Ed.* **2010**, *25*, 210–213.
- [225] Costacurta, S.; Maso, G. D.; Gallo, R.; Guglielmi, M.; Brusatin, G.; Falcaro, P. Influence of Temperature on the Photocatalytic Activity of Sol-Gel TiO₂ Films. *ACS Appl. Mater. Interfaces* **2010**, *2*, 1294–1298.

- [226] Hirakawa, T.; Whitesell, J. K.; Fox, M. A. Effect of Temperature and Pressure in the Photocatalytic Oxidation of *n*-Octanol on Partially Desilvanized Hydrophobic TiO₂ Suspended in Aerated Supercritical CO₂. *J. Phys. Chem. B* **2004**, *108*, 10213–10218.
- [227] Megatiff, L.; Dillert, R.; Bahnemann, D. W. Reaction Rate Study of the Photocatalytic Degradation of Dichloroacetic Acid in a Black Body Reactor. *Catalysts* **2019**, *9*, 635–651.
- [228] Hakki, A.; Dillert, R.; Bahnemann, D. Photocatalytic conversion of nitroaromatic compounds in the presence of TiO₂. *Catal. Today* **2009**, *144*, 154–159.
- [229] Flores, S. O.; Rios-Bernij, O.; Valenzuela, M. A.; Córdova, I.; Gómez, R.; Gutiérrez, R. Photocatalytic reduction of nitrobenzene over titanium dioxide: by-product identification and possible pathways. *Top. Catal.* **2007**, *44*, 507–511.
- [230] Selvam, K.; Swaminathan, M. One-pot photocatalytic synthesis of quinaldines from nitroarenes with Au loaded TiO₂ nanoparticles. *Catal. Commun.* **2011**, *12*, 389–393.
- [231] Hakki, A.; Dillert, R.; Bahnemann, D. W. Arenesulfonic Acid-Functionalized Mesoporous Silica Decorated with Titania: A Heterogeneous Catalyst for the One-Pot Photocatalytic Synthesis of Quinolines from Nitroaromatic Compounds and Alcohols. *ACS Catal.* **2013**, *3*, 565–572.
- [232] Hakki, A.; Dillert, R.; Bahnemann, D. W. Factors Affecting the Selectivity of the Photocatalytic Conversion of Nitroaromatic Compounds over TiO₂ to Valuable Nitrogen-containing Organic Compounds. *Phys. Chem. Chem. Phys.* **2013**, *15*, 2992–3002.
- [233] Hirakawa, H.; Katayama, M.; Shiraishi, Y.; Sakamoto, H.; Wang, K.; Ohtani, B.; Ichikawa, S.; Tanaka, S.; Hirai, T. One-pot synthesis of imines from nitroaromatics and alcohols by tandem photocatalytic and catalytic reactions on degussa (Evonik) P25 titanium dioxide. *ACS Appl. Mater. Interfaces* **2015**, *7*, 3797–3806.
- [234] Rath, T.; Urich, A.; Lüken, A.; Zhao, G.; Rittermeier, A.; Muhler, M. Cl₂ Production by Photocatalytic Oxidation of HCl over TiO₂. *ChemSusChem* **2019**, *12*, 2725–2731.
- [235] Seel, C. J.; Gulder, T. Biocatalysis Fueled by Light: On the Versatile Combination of Photocatalysis and Enzymes. *ChemBioChem* **2019**, *20*, 1871–1897.
- [236] Filatov, M.; Harris, N.; Shaik, S. On the "Rebound" Mechanism of Alkane Hydroxylation by Cytochrome P450: Electronic Structure of the Intermediate and the Electron Transfer Character in the Rebound Step. *Angew. Chem. Int. Ed.* **1999**, *38*, 3510–3512.
- [237] Tuynman, A.; Vink, M. K.; Dekker, H. L.; Schoemaker, H. E.; Wever, R. The sulphoxidation of thioanisole catalysed by lactoperoxidase and Coprinus cinereus peroxidase: evidence for an oxygen-rebound mechanism. *Eur. J. Biochem.* **1998**, *258*, 906–913.
- [238] Stone, K. L.; Behan, R. K.; Green, M. T. Resonance Raman spectroscopy of chloroperoxidase compound II provides direct evidence for the existence of an iron(IV)-hydroxide. *Proc. Natl. Acad. Sci.* **2006**, *103*, 12307–12310.
- [239] Peter, S.; Kinne, M.; Wang, X.; Ullrich, R.; Kayser, G.; Groves, J. T.; Hofrichter, M. Selective hydroxylation of alkanes by an extracellular fungal peroxygenase. *FEBS J.* **2011**, *278*, 3667–3675.

-
- [240] Karich, A.; Scheibner, K.; Ullrich, R.; Hofrichter, M. Exploring the catalase activity of unspecific peroxygenases and the mechanism of peroxide-dependent heme destruction. *J. Mol. Catal. B Enzym.* **2016**, *134*, 238–246.
- [241] Bankar, S. B.; Bule, M. V.; Singhal, R. S.; Ananthanarayan, L. Glucose oxidase — An overview. *Biotechnol. Adv.* **2009**, *27*, 489–501.
- [242] Ni, Y.; Fernández-Fueyo, E.; Baraibar, A. G.; Ullrich, R.; Hofrichter, M.; Yanase, H.; Alcalde, M.; van Berkel, W. J. H.; Hollmann, F. Peroxygenase-Catalyzed Oxyfunctionalization Reactions Promoted by the Complete Oxidation of Methanol. *Angew. Chem. Int. Ed.* **2016**, *55*, 798–801.
- [243] Okrasa, K.; Falcimaigne, A.; Guibe, E. Enantioselective synthesis of sulfoxides catalysed by an oxidase – peroxidase bienzymatic system. *Tetrahedron: Asymmetry* **2002**, *13*, 519–522.
- [244] Pesic, M.; Willot, S. J.-p.; Fernández-fueyo, E.; Tieves, F.; Alcalde, M. Multienzymatic in situ hydrogen peroxide generation cascade for peroxygenase-catalysed oxyfunctionalisation reactions. **2018**, 1–4.
- [245] Holtmann, D.; Krieg, T.; Getrey, L.; Schrader, J. Electroenzymatic process to overcome enzyme instabilities. *Catal. Commun.* **2014**, *51*, 82–85.
- [246] Getrey, L.; Krieg, T.; Hollmann, F.; Schrader, J.; Holtmann, D. Enzymatic halogenation of the phenolic monoterpenes thymol and carvacrol with chloroperoxidase. *Green Chem.* **2014**, *16*, 1104–1108.
- [247] Lütz, S.; Steckhan, E.; Liese, A. First asymmetric electroenzymatic oxidation catalyzed by a peroxidase. *Electrochem. commun.* **2004**, *6*, 583–587.
- [248] Horst, A.; Bormann, S.; Meyer, J.; Steinhagen, M.; Ludwig, R.; Drews, A.; Ansorge-Schumacher, M.; Holtmann, D. Electro-enzymatic hydroxylation of ethylbenzene by the evolved unspecific peroxygenase of *Agroclybe aegerita*. *J. Mol. Catal. B Enzym.* **2016**, *133*, S137–S142.
- [249] Krieg, T.; Hüttmann, S.; Mangold, K.-M.; Schrader, J.; Holtmann, D. Gas diffusion electrode as novel reaction system for an electro-enzymatic process with chloroperoxidase. *Green Chem.* **2011**, *13*, 2686–2689.
- [250] Kohlmann, C.; Lütz, S. Electroenzymatic Synthesis of Chiral Sulfoxides. *Eng. Life Sci.* **2006**, *6*, 170–174.
- [251] Freakley, S. J.; Kochius, S.; van Marwijk, J.; Fenner, C.; Lewis, R. J.; Baldenius, K.; Marais, S. S.; Opperman, D. J.; Harrison, S. T. L.; Alcalde, M.; Smit, M. S.; Hutchings, G. J. A chemo-enzymatic oxidation cascade to activate C–H bonds with in situ generated H₂O₂. *Nat. Commun.* **2019**, *10*, 4178–4185.
- [252] Karmee, S. K.; Roosen, C.; Kohlmann, C.; Lütz, S.; Greiner, L.; Leitner, W. Chemo-enzymatic cascade oxidation in supercritical carbon dioxide/water biphasic media. *Green Chem.* **2009**, *11*, 1052–1055.
- [253] Zhang, W.; Fernández-Fueyo, E.; Ni, Y.; van Schie, M.; Gacs, J.; Renirie, R.; Wever, R.; Mutti, F. G.; Rother, D.; Alcalde, M.; Hollmann, F. Selective aerobic oxidation reactions using a combination of photocatalytic water oxidation and enzymatic oxyfunctionalizations. *Nat. Catal.* **2018**, *1*, 55–62.

- [254] Heining, M.; Buchholz, R. Photobioreactors with internal illumination - A survey and comparison. *Biotechnol. J.* **2015**, *10*, 1131–1137.
- [255] Sender, M.; Ziegenbalg, D. Light Sources for Photochemical Processes - Estimation of Technological Potentials. *Chemie Ing. Tech.* **2017**, *89*, 1159–1173.
- [256] Le, C. C.; Wismer, M. K.; Shi, Z. C.; Zhang, R.; Conway, D. V.; Li, G.; Vachal, P.; Davies, I. W.; MacMillan, D. W. A General Small-Scale Reactor to Enable Standardization and Acceleration of Photocatalytic Reactions. *ACS Cent. Sci.* **2017**, *3*, 647–653.
- [257] Cambié, D.; Dobbelaar, J.; Riente, P.; Vanderspikken, J.; Shen, C.; Seeberger, P. H.; Gilmore, K.; Debije, M. G.; Noël, T. Energy-Efficient Solar Photochemistry with Luminescent Solar Concentrator Based Photomicroreactors. *Angew. Chem. Int. Ed.* **2019**, *58*, 14374–14378.
- [258] Ziegenbalg, D.; Kreisel, G.; Weiß, D.; Kralisch, D. OLEDs as prospective light sources for microstructured photoreactors. *Photochem. Photobiol. Sci.* **2014**, *13*, 1005–15.
- [259] Rehm, T. H.; Gros, S.; Löb, P.; Renken, A. Photonic contacting of gas–liquid phases in a falling film microreactor for continuous-flow photochemical catalysis with visible light. *React. Chem. Eng.* **2016**, *i*.
- [260] Loubière, K.; Oelgemöller, M.; Aillet, T.; Dechy-Cabaret, O.; Prat, L. Continuous-flow photochemistry: A need for chemical engineering. *Chem. Eng. Process. Process Intensif.* **2016**, *104*, 120–132.
- [261] Gilmore, K.; Seeberger, P. H. Continuous Flow Photochemistry. *Chem. Rec.* **2014**, *14*, 410–418.
- [262] Cambié, D.; Bottecchia, C.; Straathof, N. J. W.; Hessel, V.; Noël, T. Applications of Continuous-Flow Photochemistry in Organic Synthesis, Material Science, and Water Treatment. *Chem. Rev.* **2016**, *116*, 10276–10341.
- [263] Straathof, N. J.; Su, Y.; Hessel, V.; Noël, T. Accelerated gas-liquid visible light photoredox catalysis with continuous-flow photochemical microreactors. *Nat. Protoc.* **2016**, *11*, 10–21.
- [264] Teoh, W. Y.; Scott, J. A.; Amal, R. Progress in heterogeneous photocatalysis: From classical radical chemistry to engineering nanomaterials and solar reactors. *J. Phys. Chem. Lett.* **2012**, *3*, 629–639.
- [265] Kuijpers, K. P.; Van Dijk, M. A.; Rumeur, Q. G.; Hessel, V.; Su, Y.; Noël, T. A sensitivity analysis of a numbered-up photomicroreactor system. *React. Chem. Eng.* **2017**, *2*, 109–115.
- [266] Zhao, F.; Cambié, D.; Janse, J.; Wieland, E. W.; Kuijpers, K. P. L.; Hessel, V.; Debije, M. G.; Noël, T. Scale-up of a Luminescent Solar Concentrator-Based Photomicroreactor via Numbering-up. *ACS Sustain. Chem. & Eng.* **2018**, *6*, 422–429.
- [267] Ray, A. K.; Beenackers, A. A. Development of a new photocatalytic reactor for water purification. *Catal. Today* **1998**, *40*, 73–83.
- [268] Ibrahim, H.; De Lasa, H. Novel photocatalytic reactor for the destruction of airborne pollutants reaction kinetics and quantum yields. *Ind. Eng. Chem. Res.* **1999**, *38*, 3211–3217.
- [269] Hofstadler, K.; Bauer, R.; Novalic, S.; Heisler, G. New Reactor Design for Photocatalytic Wastewater Treatment with TiO₂ Immobilized on Fused-Silica Glass Fibers: Photomineralization of 4-Chlorophenol. *Environ. Sci. Technol.* **1994**, *28*, 670–674.

-
- [270] Hayashi, N.; Yasutomi, R.; Kasai, E. Development of dispersed-type sonophotocatalytic process using piezoelectric effect caused by ultrasonic resonance. *Ultrason. Sonochem.* **2010**, *17*, 884–891.
- [271] Hong, J.; Sun, C.; Yang, S.; Liu, Y. Photocatalytic degradation of methylene blue in TiO₂ aqueous suspensions using microwave powered electrodeless discharge lamps. *J. Hazard. Mater.* **2006**, *133*, 162–166.
- [272] Církva, V.; Žabová, H.; Hájek, M. Microwave photocatalysis of mono-chloroacetic acid over nanoporous titanium(IV) oxide thin films using mercury electrodeless discharge lamps. *J. Photochem. Photobiol. A Chem.* **2008**, *198*, 13–17.
- [273] Sutor, A.; Heining, M.; Lindenberger, C.; Buchholz, R. Method for Optimizing the Field Coils of Internally Illuminated Photobioreactors. *IEEE Trans. Magn.* **2014**, *50*, 1–4.
- [274] Kuipers, J.; Bruning, H.; Bakker, S.; Rijnaarts, H. Near field resonant inductive coupling to power electronic devices dispersed in water. *Sensors Actuators, A Phys.* **2012**, *178*, 217–222.
- [275] Kuipers, J.; Bruning, H.; Yntema, D.; Bakker, S.; Rijnaarts, H. Self-Capacitance and Resistive Losses of Saline-Water-Filled Inductors. *IEEE Trans. Ind. Electron.* **2014**, *61*, 2356–2361.
- [276] Casanova, J.; Zhen Ning Low,.; Jenshan Lin, A Loosely Coupled Planar Wireless Power System for Multiple Receivers. *IEEE Trans. Ind. Electron.* **2009**, *56*, 3060–3068.
- [277] Carta, R.; Tortora, G.; Thoné, J.; Lenaerts, B.; Valdastrì, P.; Menciacchi, A.; Dario, P.; Puers, R. Wireless powering for a self-propelled and steerable endoscopic capsule for stomach inspection. *Biosens. Bioelectron.* **2009**, *25*, 845–851.
- [278] de Boeij, J.; Lomonova, E.; Duarte, J.; Vandenput, A. Contactless power supply for moving sensors and actuators in high-precision mechatronic systems with long-stroke power transfer capability in x-y plane. *Sensors Actuators A Phys.* **2008**, *148*, 319–328.
- [279] Lucklum, F.; Jakoby, B. Novel magnetic-acoustic resonator sensors for remote liquid phase measurement and mass detection. *Sensors Actuators A Phys.* **2008**, *145-146*, 44–51.
- [280] Heining, M.; Sutor, A.; Stute, S. C.; Lindenberger, C. P.; Buchholz, R. Internal illumination of photobioreactors via wireless light emitters: a proof of concept. *J. Appl. Phycol.* **2015**, *27*, 59–66.
- [281] Kuipers, J.; Bruning, H.; Yntema, D.; Rijnaarts, H. Wirelessly powered ultraviolet light emitting diodes for photocatalytic oxidation. *J. Photochem. Photobiol. A Chem.* **2015**, *299*, 25–30.
- [282] Zhao, F.; Cambié, D.; Hessel, V.; Debije, M. G.; Noël, T. Real-time reaction control for solar production of chemicals under fluctuating irradiance. *Green Chem.* **2018**, *20*, 2459–2464.
- [283] Shockley, W.; Queisser, H. J. Detailed Balance Limit of Efficiency of p-n Junction Solar Cells. *J. Appl. Phys.* **1961**, *32*, 510–519.
- [284] Vesborg, P. C. K.; Seger, B. Performance Limits of Photoelectrochemical CO₂ Reduction Based on Known Electrocatalysts and the Case for Two-Electron Reduction Products. *Chem. Mater.* **2016**, *28*, 8844–8850.

- [285] Chen, Y.; Sun, K.; Audesirk, H.; Xiang, C.; Lewis, N. S. A quantitative analysis of the efficiency of solar-driven water-splitting device designs based on tandem photoabsorbers patterned with islands of metallic electrocatalysts. *Energy Environ. Sci.* **2015**, *8*, 1736–1747.
- [286] Haussener, S.; Hu, S.; Xiang, C.; Weber, A. Z.; Lewis, N. S. Simulations of the irradiation and temperature dependence of the efficiency of tandem photoelectrochemical water-splitting systems. *Energy Environ. Sci.* **2013**, *6*, 3605–3618.
- [287] Zhao, Y.; Meek, G. a.; Levine, B. G.; Lunt, R. R. Near-infrared harvesting transparent luminescent solar concentrators. *Adv. Opt. Mater.* **2014**, *2*, 606–611.
- [288] Haussener, S.; Levêque, G.; Bader, R.; Lipin, W. High-flux optical systems for solar thermochemistry. **2017**, *156*, 133–148.
- [289] Cambié, D.; Noël, T. Solar Photochemistry in Flow. *Top. Curr. Chem.* **2018**, *376*, 1–27.
- [290] Cho, J.; Park, J. H.; Kim, J. K.; Schubert, E. F. White light-emitting diodes: History, progress, and future. *Laser Photon. Rev.* **2017**, *11*, 1600147.
- [291] Haitz’s law. *Nat. Photonics* **2007**, *1*, 23–23.
- [292] Moore, G. E. Cramming more components onto integrated circuits. *Electronics* **1965**, *38*, 114–117.
- [293] Auf der Maur, M.; Pecchia, A.; Penazzi, G.; Rodrigues, W.; Di Carlo, A. Unraveling the “Green Gap” problem: The role of random alloy fluctuations in InGa_N/Ga_N light emitting diodes. *Phys. Rev. Lett.* **2016**, *116*, 027401.
- [294] Xue, J. Towards the efficiency limit of visible light-emitting diodes. Master Thesis. Massachusetts Institute of Technology, **2017**.
- [295] Gao, M.; Peh, C. K. N.; Ho, G. W. Plasmonic Photothermic Directed Broadband Sunlight Harnessing for Seawater Catalysis and Desalination. *Energy Environ. Sci.* **2016**, *9*, 3151–3160.
- [296] Li, Y.; Peng, Y.-K.; Hu, L.; Zheng, J.; Prabhakaran, D.; Wu, S.; Puchtler, T. J.; Li, M.; Wong, K.-Y.; Taylor, R. A.; Tsang, S. C. E. Photocatalytic water splitting by N-TiO₂ on MgO (111) with exceptional quantum efficiencies at elevated temperatures. *Nat. Commun.* **2019**, *10*, 4421–4429.
- [297] Westrich, T. A.; Dahlberg, K. A.; Kaviany, M.; Schwank, J. W. High-temperature photocatalytic ethylene oxidation over TiO₂. *J. Phys. Chem. C* **2011**, *115*, 16537–16543.
- [298] Noël, T. A personal perspective on the future of flow photochemistry. *J. Flow Chem.* **2017**, *7*, 87–93.
- [299] Liou, P. Y.; Chen, S. C.; Wu, J. C. S.; Liu, D.; MacKintosh, S.; Maroto-Valer, M.; Linforth, R. Photocatalytic CO₂ reduction using an internally illuminated monolith photoreactor. *Energy Environ. Sci.* **2011**, *4*, 1487–1494.
- [300] Khan, A. A.; Tahir, M. Recent advancements in engineering approach towards design of photo-reactors for selective photocatalytic CO₂ reduction to renewable fuels. *J. CO₂ Util.* **2019**, *29*, 205–239.

8 About the author

8.1 Curriculum Vitae

Dr. rer. nat. Jonathan Zacharias Bloh,

born 17.09.1983 in Vesbeck, Neustadt am Rübenberge (Lower Saxony, Germany).

- | | |
|-----------------------|---|
| Oct. 2003 – July 2006 | Study of Life Science at the Leibniz Universität Hannover, Germany. Graduation with Bachelor of Science (A-excellent). |
| Oct. 2006 – Nov. 2008 | Study of Life Science at the Leibniz Universität Hannover, Germany. Graduation with Master of Science (A-excellent), master thesis <i>Investigations of the Cytotoxicity of Photocatalytically Active Titanium Dioxide Nanoparticles</i> under the supervision of Prof. Dr. Thomas Scheper and Prof. Dr. Detlef W. Bahnemann. |
| Jan. 2006 – Oct. 2012 | PhD student under the supervision of Prof. Dr. Detlef W. Bahnemann at the Institut für Technische Chemie, Leibniz Universität Hannover, Germany. Graduation with Dr. rer. nat. (<i>summa cum laude</i>) with the thesis <i>Development of Zinc Oxide Photocatalysts for the Abatement of Air Pollutants</i> . |
| Oct. 2012 – Mar. 2014 | Postdoctorial Research Fellow at the Department of Chemistry, University of Aberdeen, United Kingdom, research group Prof. Dr. Donald E. Macphee. |
| since Apr. 2014 | Head of the Chemical Technology research group at the DECHEMA-Forschungsinstitut, Frankfurt am Main, Germany. |

8.2 List of teaching activities

Winter semester 2011/2012

Leibniz Universität Hannover, Naturwissenschaftliche Fakultät
“Technische Chemie II: Übungen zur Vorlesung *Grundoperationen der Chem. Industrie*” (9 hours)
and “Vorlesung *Funktionsprinzipien ausgewählter Festkörpermateriale*” (4 hours)

Winter semester 2013/2014

University of Aberdeen, Department of Chemistry
“Lecture *Advanced Chemistry 1 (CM4025)*” (6 hours)
and “Seminar *Impedance Spectroscopy*” (4 hours)

Winter semester 2016/2017

Leibniz Universität Hannover, Naturwissenschaftliche Fakultät
“Vorlesung *Funktionsprinzipien ausgewählter Festkörpermateriale*” (10 hours)

Winter semester 2017/2018

Leibniz Universität Hannover, Naturwissenschaftliche Fakultät
“Vorlesung *Katalyse und Reaktionsmechanismen*” (10 hours)

Winter semester 2018/2019

Leibniz Universität Hannover, Naturwissenschaftliche Fakultät
“Vorlesung *Katalyse und Reaktionsmechanismen*” (15 hours)

Winter semester 2019/2020

Leibniz Universität Hannover, Naturwissenschaftliche Fakultät
“Vorlesung *Katalyse und Reaktionsmechanismen*” (15 hours)

8.3 List of publications

8.3.1 Peer-reviewed articles

- (1) Bloh, J.Z.; Wagner, S.; Bahnemann, D.W.; Scheper, T.; Kasper, C. Untersuchungen zur Zytotoxizität von photokatalytisch aktiven Titandioxid-Nanopartikeln. *Chem. Ing. Tech.* **2009**, *82*, 335-341, DOI: 10.1002/cite.200900057.
- (2) Wagner, S.; Bloh, J.Z.; Kasper, C.; Bahnemann, D.W. Toxicological Issues of Nanoparticles Employed in Photocatalysis. *Green* **2011**, *1*, 171-188, DOI: 10.1515/green.2011.013.
- (3) Baumanis, C.; Bloh, J.Z.; Dillert, R.; Bahnemann, D.W. Hematite Photocatalysis: Dechlorination of 2,6-Dichloroindophenol and Oxidation of Water. *The J. Phys. Chem. C* **2011**, *115*, 25442-25450, DOI: 10.1021/jp210279r.
- (4) Bloh, J.Z.; Dillert, R.; Bahnemann, D.W. Transition Metal Modified Zinc Oxide for UV and Visible Light Photocatalysis. *Enviro. Sci. Poll. Res.* **2012**, *19*, 3688-3695, DOI: 10.1007/s11356-012-0932-y.
- (5) Bloh, J.Z.; Dillert, R.; Bahnemann, D.W. Zinc oxide photocatalysis: Influence of iron- and titanium-doping and origin of optimal doping ratio. *ChemCatChem* **2013**, *5*, 774-778, DOI: 10.1002/cctc.201200558.
- (6) Bloh, J.Z.; Dillert, R.; Bahnemann, D.W. Designing Optimal Metal-Doped Photocatalysts - Correlation Between Photocatalytic Activity, Doping Ratio and Particle Size. *J. Phys. Chem. C* **2013**, *116*, 25558-25562, DOI: 10.1021/jp307313z.
- (7) Folli, A.; Bloh, J.Z.; Beukes, E.-P.; Howe, R.F.; Macphee, D.E. Photo-Generated Charge Carriers and Paramagnetic Species in (W,N) Codoped TiO₂ Photocatalysts Under Visible Light Irradiation: An EPR Study. *J. Phys. Chem. C* **2013**, *117*, 22149-22155, DOI: 10.1021/jp408181r.
- (8) Bloh, J.Z.; Dillert, R.; Bahnemann, D.W. Ruthenium-modified Zinc Oxide, a Highly Active Vis-Photocatalyst: Nature and Reactivity of Photoactive Centres. *Phys. Chem. Chem. Phys.* **2014**, *16*, 5833-5845, DOI: 10.1039/c3cp55136a.
- (9) Folli, A.; Bloh, J.Z.; Strøm, M.; Pilegaard Madsen, T.; Henriksen T.; Macphee, D.E. Efficiency of Solar-Light-Driven TiO₂ Photocatalysis at Different Latitudes and Seasons. Where and When Does TiO₂ Really Work? *J. Phys. Chem. Lett.* **2014**, *5*, 830-832, DOI: 10.1021/jz402704n.
- (10) Bloh, J.Z.; Folli, A.; Macphee, D.E. Adjusting the Nitrogen Doping Level in Titanium Dioxide by Codoping with Tungsten: Properties and Band Structure of the Resulting Materials. *J. Phys. Chem. C* **2014**, *118*, 21281-21292, DOI: 10.1021/jp507264g.
- (11) Bloh, J.Z.; Folli, A.; Macphee, D.E. Photocatalytic NO_x abatement: Why the selectivity matters. *RSC Adv.* **2014**, *4*, 45726-45734, DOI: 10.1039/c4ra07916g.
- (12) Folli, A.; Bloh, J.Z.; Lecaplain, A.; Walker, R.; Macphee, D.E. Mechanism of the crystal defect-driven enhanced Ti³⁺ formation in (Nb,N)-codoped TiO₂ semiconductors revealed by EPR spectroscopy. *Phys. Chem. Chem. Phys.* **2015**, *17*, 4849-4853, DOI: 10.1039/c4cp05521g.
- (13) Folli, A.; Bloh, J.Z.; Macphee, D.E. Band Structure and Charge Carrier Dynamics in (W,N)-codoped TiO₂ resolved by Electrochemical Impedance Spectroscopy combined

- with UV-vis and EPR spectroscopies. *J. Electroanal. Chem.* **2016**, *780*, 367-372, DOI: 10.1016/j.jelechem.2015.10.033.
- (14) Hopper, H.A.; Le, J.-B.; Cheng, J.; Weller, T.; Marschall, R.; Bloh, J.Z.; Macphee, D.E.; Folli, A.; McLaughlin, A. An Investigation of the Optical Properties and Water Splitting Potential of the Coloured Metallic Perovskites $\text{Sr}_{1-x}\text{Ba}_x\text{MoO}_3$. *J. Solid State Chem.* **2016**, *234*, 87-92, DOI: 10.1016/j.jssc.2015.12.002.
- (15) Bloh, J.Z. Refined Model for the Optimal Metal Content in Semiconductor Photocatalysts. *J. Phys. Chem. C* **2017**, *121*, 844-851, DOI: 10.1021/acs.jpcc.6b09808.
- (16) Bloh, J.Z.; Marschall, R. Heterogeneous Photoredox Catalysis: Reactions, Materials, and Reaction Engineering, *European J. Org. Chem.* **2017**, *15*, 2085-2094, DOI: 10.1002/ejoc.201601591.
- (17) Burek, B.O.; Sutor, A.; Bahnemann, D.W.; Bloh, J.Z. Completely integrated wirelessly-powered photocatalyst-coated spheres as a novel means to perform heterogeneous photocatalytic reactions. *Cat. Sci. Technol.* **2017**, *7*, 4977-4983, DOI: 10.1039/c7cy01537b.
- (18) Zhang, W.; Burek, B.O.; Fernández-Fueyo, E.; Alcalde, M.; Bloh, J.Z.; Hollmann, F. Selective activation of C-H bonds by cascading photochemistry with biocatalysis. *Angew. Chem. Int. Ed.* **2017**, *56*, 15451-15455, DOI: 10.1002/ange.201708668.
- (19) Patzsch, J.; Folli, A.; Macphee, D.E.; Bloh, J.Z. On the underlying mechanisms of the low observed nitrate selectivity in photocatalytic NO_x abatement and the importance of the oxygen reduction reaction. *Phys. Chem. Chem. Phys.* **2017**, *19*, 32678-32686, DOI: 10.1039/C7CP05960D.
- (20) Patzsch, J.; Bloh, J.Z. Improved photocatalytic ozone abatement over transition metal-grafted titanium dioxide. *Catal. Today* **2018**, *300*, 2-11, DOI: 10.1016/j.cattod.2017.07.010.
- (21) Folli, A.; Bloh, J.Z.; Armstrong, K.L.; Richards, E.; Murphy, D.M.; Lu, L.; Kiely, C.; Morgan, D.J.; Smith, R.I.; McLaughlin, A.C.; Macphee, D.E. Improving the selectivity of photocatalytic NO_x abatement through improved O₂ reduction pathways using $\text{Ti}_{0.909}\text{W}_{0.091}\text{O}_2\text{N}_x$ semiconductor nanoparticles: from characterisation to photocatalytic performance. *ACS Catal.* **2018**, *8*, 6927-6938, DOI: 10.1021/acscatal.8b00521.
- (22) Patzsch, J.; Spencer, J.N.; Folli, A.; Macphee, D.E.; Bloh, J.Z. Grafted iron(III) ions significantly enhance NO₂ oxidation rate and selectivity of TiO₂ for photocatalytic NO_x abatement. *RSC Adv.* **2018**, *8*, 27674-27685, DOI: 10.1039/C8RA05017A.
- (23) Burek, B.O.; Bahnemann, D.W.; Bloh, J.Z. Modeling and Optimization of Photocatalytic Hydrogen Peroxide Production over Titanium Dioxide. *ACS Catal.* **2019**, *9*, 25-37, DOI: 10.1021/acscatal.8b03638.
- (24) Burek, B.O.; Timm, J.; Bahnemann, D.W.; Bloh, J.Z. Kinetic Effects of Sacrificial Electron Donors in Photocatalytic Hydrogen Peroxide Production over illuminated Titanium Dioxide. *Catal. Today* **2019**, *335*, 354-364, DOI: 10.1016/j.cattod.2018.12.044.
- (25) Milker, S.; Pätzold, M.; Bloh, J.Z.; Holtmann, D. Comparison of deep eutectic solvents and solvent-free reaction conditions for aldol production. *Mol. Catal.* **2019**, *466*, 70-74, DOI: 10.1016/j.mcat.2019.01.012.
- (26) Zhang, W.; Ma, M.; Huijbers M.M.E.; Filonenko, G.A.; Pidko, E.A.; van Schie, M.; de Boer, S.R.; Burek, B.O.; Bloh, J.Z.; van Berkel, W.J.H.; Smith, W.A; Hollmann, F. Selective

- photoenzymatic synthesis of light hydrocarbons. *J. Am. Chem. Soc.* **2019**, *141*, 3116-3120, DOI: 10.1021/jacs.8b12282.
- (27) Bloh, J.Z. A Holistic Approach to Model the Kinetics of Photocatalytic Reactions. *Front. Chem. (Rising Stars Collection)* **2019**, *7*, 128-140, DOI: 10.3389/fchem.2019.00128.
- (28) Pätzold, M.; Burek, B.O.; Bloh, J.Z.; Liese, A.; Holtmann, D. Product recovery of an enzymatically synthesized (-)-menthol ester in a deep eutectic solvent. *Bioproc. Biosyst. Eng.* **2019**, *42*, 1385-1389, DOI: 10.1007/s00449-019-02125-6.
- (29) Patzsch, J.; Berg, B.; Bloh, J.Z. Kinetics and Optimization of the Photocatalytic Reduction of Nitrobenzene. *Front. Chem.* **2019**, *7*, 289-298, DOI: 10.3389/fchem.2019.00289.
- (30) Burek, B.O.; Bormann, S.; Hollmann, F.; Bloh, J.Z.; Holtmann, D. Hydrogen peroxide driven biocatalysis. *Green Chem.* **2019**, *21*, 3232-3249, DOI: 10.1039/c9gc00633h.
- (31) Burek, B.O.; de Boer, S.R.; Tieves, F.; Zhang, W.; van Schie, M.; Bormann, S.; Alcalde, M.; Holtmann, D.; Hollmann, F.; Bahnemann, D.W.; Bloh, J.Z. Photoenzymatic Hydroxylation of Ethylbenzene catalyzed by Unspecific Peroxygenase: Origin of Enzyme Inactivation and the Impact of Light Intensity and Temperature. *ChemCatChem* **2019**, *11*, 3093-3100, DOI: 10.1002/cctc.201900610.
- (32) van Schie, M.M.C.H.; Zhang, W.; Tieves, F.; Choi, D.S.; Park, C.B.; Burek, B.O.; Bloh, J.Z.; Arends, I.W.C.E.; Paul, C.E.; Alcalde, M.; Hollmann, F. Cascading g-C₃N₄ and Peroxygenases for Selective Oxyfunctionalization Reactions. *ACS Catal.* **2019**, *9*, 7409-7417, DOI: 10.1021/acscatal.9b01341.
- (33) Özgen, F.F.; Runda, M.E.; Burek, B.O.; Wied, P.; Bloh, J.Z.; Kourist, R.; Schmidt, S. Artificial light-harvesting complexes enable Rieske oxygenase-catalyzed hydroxylations in non-photosynthetic cells. *Angew. Chem. Int. Ed.* **2020**, *59*, 3982-3987, DOI: 10.1002/anie.201914519.
- (34) Rath, T.; Bloh, J. Z.; Lüken, A.; Ollegott, K.; Muhler, M. Model-Based Analysis of the Photocatalytic HCl Oxidation Kinetics over TiO₂. *Ind. Eng. Chem. Res.* **2020**, *59*, 4265-4272, DOI: 10.1021/acs.iecr.9b05820.

8.3.2 Other articles

- (1) Bloh, J.Z.; Mangold, K.-M. Trendbericht Technische Chemie 2015. *Nachrichten aus der Chemie* **2016**, *64*, 348-350, DOI: 10.1002/nadc.20164047842.
- (2) Bloh, J.Z. Photocatalytic NO_x abatement - Theory, applications, current research, and limitations. *Gefahrstoffe - Reinhaltung der Luft* **2017**, *77*, 27-30.

8.3.3 Patents filed

- (1) Macphee, D.E.; Bloh, J.Z.; Folli, A.; Greenhalgh, D.J. A Method of Photocatalytically Oxidising Nitrogen Oxides. **2014**, *WO 2016/005760 A1*.
- (2) Bloh, J.Z.; Weidlich, C. Durch Licht aufladbare Redox-Flow-Batterie. **2014**, *DE 10 2015 119 159 A1*.
- (3) Bloh, J.Z.; Burek, B.O.; Mangold, K.-M.; Ravichandran, S.; Schuster, J.; Weidlich, C. Redox-Flow-Batterie. **2016**, *DE 10 2016 116 154.3*.

- (4) Bauer, J.; Bloh, J.Z.; Braun, M.; Depentori, F.; Fürbeth, W.; Galetz, M.; Montero, X.; Schütze, M. Langzeitstabiler, lagerfähiger Schlicker für umweltfreundliche Diffusionsbeschichtungen. **2017**, *DE 10 2016 009 854*.
- (5) Burek, B.O.; Bloh, J.Z. Drahtlos betreibbare Leuchte zur Anregung lichtgetriebener chemischer Reaktionen in einem Reaktionsgefäß, Verfahren zu deren Herstellung und Vorrichtung mit einer solchen Leuchte. **2017**, *DE 10 2017 109 687.6*.

9 Publication reprints

On the following pages, this chapter contains electronic reprints of the publications listed in chapter 6, which are the basis of this thesis.

For copyright reasons, this chapter is not available in the online version of this thesis. In this case, the relevant publications can be found and accessed directly *via* the respective publishers using the DOIs given in chapter 6.